

A Large Recurrent Action Model: xLSTM Enables Fast Inference for Robotics Tasks

Thomas Schmied¹ Thomas Adler¹ Vihang Patil¹ Maximilian Beck^{1,2} Korbinian Pöppel^{1,2}
Johannes Brandstetter^{1,2} Günter Klambauer^{1,2} Razvan Pascanu^{3,4} Sepp Hochreiter^{1,2}

Abstract

In recent years, there has been a trend in the field of Reinforcement Learning (RL) towards large action models trained offline on large-scale datasets via sequence modeling. Existing models are primarily based on the Transformer architecture, which results in powerful agents. However, due to slow inference times, Transformer-based approaches are impractical for real-time applications, such as robotics. Recently, modern recurrent architectures, such as xLSTM and Mamba, have been proposed that exhibit parallelization benefits during training similar to the Transformer architecture while offering fast inference. In this work, we study the aptitude of these modern recurrent architectures for large action models. Consequently, we propose a Large Recurrent Action Model (LRAM) with an xLSTM at its core that comes with linear-time inference complexity and natural sequence length extrapolation abilities. Experiments on 432 tasks from 6 domains show that LRAM compares favorably to Transformers in terms of performance and speed.

1. Introduction

Reinforcement Learning (RL) has been responsible for impressive success stories such as game-playing (Silver et al., 2016; Vinyals et al., 2019; Berner et al., 2019; Patil et al., 2022), plasma control for fusion (Degraeve et al., 2022), or navigation of stratospheric balloons (Bellemare et al., 2020). While these successes were based on classical RL approaches, in which agents have been trained online with RL objectives, recently there has been a trend towards offline RL settings (Levine et al., 2020; Schweighofer et al., 2022)

and sequence models trained via behavior cloning (Chen et al., 2021; Janner et al., 2021). Such approaches, in which agents are trained on large-scale offline datasets with causal sequence modeling objectives, have been driven by the proliferation of Transformer-based architectures and gave rise to what we refer to as *Large Action Models* (LAMs) to highlight their similarity to large language models (LLMs) (Radford et al., 2018). LAM approaches can also be used in multi-task settings to develop generalist agents such as Gato (Reed et al., 2022).

Existing LAMs are primarily based on the Transformer (Vaswani et al., 2017) architecture. Because of their powerful predictive performance, robotics has become an emergent application area for large models (Brohan et al., 2023b;a; Octo Model Team et al., 2024; Gu et al., 2023; Wang et al., 2023), and a number of large multi-task datasets were collected (Jia et al., 2024; Embodiment Collaboration et al., 2024; Jiang et al., 2023; Mandlekar et al., 2023). This development bears the potential to produce robotics agents that learn to master complex tasks in a wide range of environments and even different embodiments. For example, recently it has been demonstrated, albeit in restricted settings, that sequence models trained on multi-episodic contexts can perform in-context learning (ICL) (Laskin et al., 2020; Lee et al., 2023). One potential application of ICL can be to learn new related tasks in robotics without the need for re-training or fine-tuning.

One of the key reasons for the success of Transformer-based models is their ability to scale to large datasets through their efficient parallelization during training. However, despite numerous success stories in RL, language modeling (Brown et al., 2020) or computer vision (Dosovitskiy et al., 2021; He et al., 2022), a persistent drawback of Transformer-based architectures is their high inference cost in terms of both speed and memory (Kim et al., 2023). Consequently, deploying Transformer-based models in resource-constrained scenarios, such as on devices with limited hardware capacity and/or real-time constraints, e.g., robots or smartphones, is prohibitive because of the required fast inference times (Firoozi et al., 2023; Hu et al., 2023). A basic principle of control theory is that the controller sample rate should be in the order of magnitude of the sample rate of the sensors

¹ELLIS Unit, LIT AI Lab, Institute for Machine Learning, JKU Linz, Austria ²NXAI GmbH, Linz, Austria ³Google DeepMind ⁴Mila - Québec AI Institute.

Proceedings of the 42nd International Conference on Machine Learning, Vancouver, Canada. PMLR 267, 2025. Copyright 2025 by the author(s).

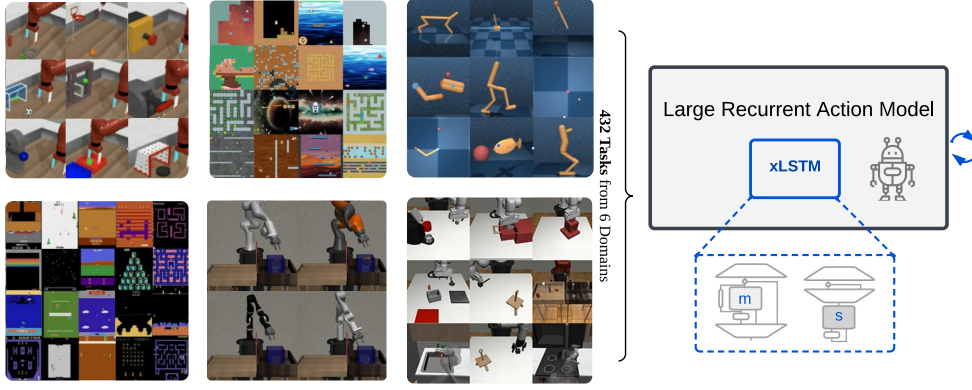


Figure 1. Illustration of our **Large Recurrent Action Model (LRAM)** with an xLSTM (Beck et al., 2024) at its core.

(Franklin et al., 1998, Ch. 11). To illustrate this, for typical robots such as drones or industrial robot arms, rates of 100Hz-1000Hz are required to keep the system stable (Salzmann et al., 2023; El-Hussieny, 2024; Hu et al., 2023; Chignoli et al., 2021). This implies inference times of less than 10ms. At 1000Hz, a 15-second movement of the agent corresponds to a sequence of 15K steps (El-Hussieny, 2024), resulting in long context lengths even without ICL. While there exists a range of techniques to make large models faster, such as quantization (Frantar et al., 2023), distillation (Hinton et al., 2015), or pruning (LeCun et al., 1989), the quadratic-time complexity of self attention still remains.

Recently, *modern recurrent architectures* have been proposed, which exhibit similar parallelization properties during training as the Transformer architecture while offering linear-time inference complexity. These modern recurrent architectures include xLSTM (Beck et al., 2024) and state-space models (SSMs), such as Mamba (Gu & Dao, 2023; Dao & Gu, 2024) and Griffin/Hawk (De et al., 2024), and have challenged the dominance of the Transformer in language modeling but also in other domains such as computer vision (Alkin et al., 2024; Zhu et al., 2024), and biomedicine (Schmidinger et al., 2024). More importantly, their linear-time inference makes them suitable for deployment in scenarios with limited compute, large context sizes, and real-time requirements, such as robotics.

In this work, we assess the aptitude of modern recurrent architectures, such as xLSTM and Mamba, as large action models. To this end, we introduce a Large Recurrent Action Model (LRAM) with an xLSTM at its core (see Figure 1). We train our agents on 432 tasks from 6 domains using a supervised learning setting similar to that of the Decision Transformer (Chen et al., 2021, DT). We use data collected during online-RL training of single-task specialist agents and compile these trajectories alongside other expert demonstrations into a large-scale multi-domain dataset comprising 894M transitions. Due to their parallelization properties,

the modern recurrent architectures considered in this work can process this large-scale training set as efficiently as the Transformer, while being faster at inference. Experiments across 4 model sizes with our multi-task models indicate that LRAM compares favorably to Transformers in terms of both performance and speed. In addition, we study the effect of modern recurrent architectures on fine-tuning performance and in-context learning abilities, and find that they exhibit strong performance in both dimensions.

The main purpose of this paper is to test the hypothesis that *modern recurrent model architectures are better suited for building LAMs than Transformers*. Hereby, we make the following **contributions**.

- We propose a Large Recurrent Action Model (LRAM) with an xLSTM at its core that enables efficient inference.
- We assess the aptitude of modern recurrent architectures as backbones for large-action models with respect to their efficiency at inference time and overall performance in multi-task, fine-tuning, and in-context learning settings.
- To foster further research on large action models, we release our data preparation pipeline and our datasets.¹

2. Related work

Sequence Models in RL. LSTM (Hochreiter & Schmidhuber, 1997) is the dominant backbone architecture for partially observable online RL problems and has been behind achievements such as mastering Starcraft II (Vinyals et al., 2019), Dota 2 (Berner et al., 2019), and Atari (Espeholt et al., 2018; Kapturowski et al., 2019). After the success of the Transformer in NLP (Devlin et al., 2019; Radford et al., 2019; Brown et al., 2020), computer vision (Dosovitskiy

¹GitHub: <https://github.com/ml-jku/LRAM>

et al., 2021; He et al., 2022; Radford et al., 2021; Fürst et al., 2022) and speech recognition (Radford et al., 2022; Baevski et al., 2020), the architecture has found its way into RL. Chen et al. (2021) proposed the Decision Transformer (DT), a GPT-style model (Radford et al., 2018), that learns to predict actions from offline trajectories via behavior cloning. Trajectory Transformer (Janner et al., 2021) predicts actions along with states and rewards, which allows for dynamics modeling. Other follow-up works build on the DT (Zheng et al., 2022; Wang et al., 2022; Shang et al., 2022; Meng et al., 2021; Siebenborn et al., 2022; Schmied et al., 2024a) or replace the Transformer with Mamba (Ota, 2024; Dai et al., 2024). Furthermore, sequence models trained to predict the next action were found to exhibit ICL if conditioned on previous trajectories (Laskin et al., 2022; Lee et al., 2022; Kirsch et al., 2023), albeit in limited scenarios.

Large Action Models (LAMs). LAMs, such as the Decision Transformer, are well-suited for multi-task settings. Lee et al. (2022) found that a multi-game DT can learn to play 46 Atari games. Reed et al. (2022) introduced a generalist agent trained on over 600 tasks from different domains, ranging from Atari to manipulation of a robot arm. Jiang et al. (2022) a Transformer for robot manipulation based on multi-modal prompts, that allow to steer the model to perform new tasks. Recently, Raad et al. (2024) introduced an agent instructable via language to play a variety of commercial video games. Since then, robotics has become an emergent area for developing LAMs (Brohan et al., 2023b;a; Octo Model Team et al., 2024; Gu et al., 2023; Wang et al., 2023; Kim et al., 2024), also due to the availability of large-scale datasets (Jia et al., 2024; Embodiment Collaboration et al., 2024; Jiang et al., 2023; Mandlekar et al., 2023).

Next-generation Sequence Modeling Architectures. Linear recurrent models, such as state-space models (SSM, Gu et al., 2021; 2022b; Smith et al., 2023; Orvieto et al., 2023) have challenged the dominance of the Transformer (Vaswani et al., 2017) architecture on long-range tasks (Tay et al., 2020). The key insight of those linear RNNs was to diagonalize the recurrent state matrix and enforce stable training via an exponential parameterization (Gu et al., 2022a; Orvieto et al., 2023). Since then, there have been efforts to include features such as gating from RNNs (Elman, 1990; Jordan, 1990; Hochreiter & Schmidhuber, 1997; Cho et al., 2014). Non-linear gates are believed to have higher expressivity, but are harder to train. Griffin (De et al., 2024) mixes gated linear recurrences with local attention to achieve more training data efficiency than Llama-2 (Touvron et al., 2023) and better sequence extrapolation. Mamba (Gu & Dao, 2023) introduces a selection mechanism similar to gating into SSMs, which makes its state and input matrix time-dependent. This is similar to the gating mechanism of RNNs but also bears resemblance to approaches like fast weights (Schmidhuber, 1992) and Linear Atten-

tion (Katharopoulos et al., 2020). Mamba-2 (Dao & Gu, 2024) highlights the connection between SSMs with input-dependent state and input matrices and (Gated) Linear attention variants. Most recently, the xLSTM (Beck et al., 2024) was proposed as an improvement over the classic LSTM (Hochreiter & Schmidhuber, 1997) that combines gating, linear recurrences, and recurrent weights into a single architecture for language modeling. First, xLSTM leverages exponential gating with stabilization to RNNs for stronger emphasis on important inputs. Second, xLSTM is composed of two variants, the mLSTM variant with an emphasis on memory that proves important in language modeling, and the sLSTM variant that keeps the non-diagonalized recurrent matrix to enable state-tracking (Merrill et al., 2024). State tracking is important in logic tasks and cannot be modeled fundamentally by linearized recurrent or state-space models like Mamba, Griffin, or Transformers.

3. Large Recurrent Action Models

3.1. Background

Reinforcement Learning. We assume the standard RL formulation via a Markov Decision Process (MDP) represented by a tuple of $(\mathcal{S}, \mathcal{A}, \mathcal{P}, \mathcal{R})$, where \mathcal{S} and \mathcal{A} denote state and action spaces, respectively. At every timestep t , the agent observes state $s_t \in \mathcal{S}$, predicts action $a_t \in \mathcal{A}$, and receives a scalar reward r_t . The reward is determined by the reward function $\mathcal{R}(r_t | s_t, a_t)$. $\mathcal{P}(s_{t+1} | s_t, a_t)$ defines the transition dynamics and constitutes a probability distribution over next states s_{t+1} when executing action a_t in state s_t . The goal of RL is to learn a policy $\pi(a_t | s_t)$ that predicts an action a_t in state s_t that maximizes r_t .

Decision Transformer (Chen et al., 2021) casts the RL problem setting as next action prediction task via causal sequence modeling. At training time, DT aims to learn a policy π_θ that maps future rewards to actions, which is often referred to as upside-down RL (Schmidhuber, 2019). At inference time, the DT is conditioned via a target return to emit high-reward actions. Consequently, we assume access to a dataset $\mathcal{D} = \{\tau_i\}_{i=1}^N$ containing N trajectories τ_i consisting of quadruplets $\tau_i = (s_1, \hat{R}_1, a_1, r_1, \dots, s_T, \hat{R}_T, a_T, r_T)$ of state s_t , return-to-go (RTG) $\hat{R}_t = \sum_{t'=t}^T r_{t'}$, action a_t , and reward r_t . Here, T refers to the length of the trajectory. The DT π_θ is trained to predict the ground-truth action a_t conditioned on sub-trajectories from the dataset:

$$\hat{a}_t \sim \pi_\theta(\hat{a}_t | s_{t-C}, \hat{R}_{t-C}, a_{t-C}, r_{t-C}, \dots, s_{t-1}, \hat{R}_{t-1}, a_{t-1}, r_{t-1}, s_t, \hat{R}_t) \quad (1)$$

where $C \leq T$ is the size of the context window. In fact, Equation 1 describes the setting of the multi-game DT (Lee et al., 2022), which also includes rewards in the sequence representation.

Table 1. Dataset statistics for all 432 training tasks.

Dataset	Tasks	Trajectories	Mean Trj. Length	Total Transitions	Repetitions
Atari	41	136K	2733	205M	1.03×
Composuite	240	480K	500	240M	0.87×
DMControl	11	110K	1000	110M	1.92×
Meta-World	45	450K	200	90M	2.34×
Mimicgen	83	83K	300	25M	8.5×
Procgen	12	2185K	144	224M	0.94×
Total	432	3.4M	-	894M	-

3.2. Large Recurrent Action Models (LRAMs)

Our LRAM has a modern recurrent architecture at its core (see Figure 1), which comes with a parallel training and a recurrent inference mode. We instantiate LRAM with three different variants, two different xLSTM configurations, and Mamba. We use a training protocol similar to that of Lee et al. (2022) and Reed et al. (2022) with important differences that aim to speed up inference across backbones.

Multi-modal sequence representation. To encode input from different environments with varying state and action spaces, we use separate encoders per modality that are shared across tasks and domains. For encoding images, we use a CNN similar to Espeholt et al. (2018), whereas for low-dimensional inputs we use a fully connected network. We refrain from patchifying images and tokenizing continuous states to avoid unnecessarily long sequences. Similarly, we use linear layers to encode rewards and RTGs. We omit actions in our sequence formulation, as we found that this can be detrimental to performance, in particular for continuous control tasks with smoothly changing actions (see Section 4.3). Consequently, our trajectories have the form $\tau_i = (s_1, \hat{R}_1, r_1, \dots, s_T, \hat{R}_T, r_T)$ and we train our policy π_ρ to predict the ground-truth action a_t as:

$$\hat{a}_t \sim \pi_\rho(\hat{a}_t | s_{t-C}, \hat{R}_{t-C}, r_{t-C}, \dots, s_{t-1}, \hat{R}_{t-1}, r_{t-1}, s_t, \hat{R}_t). \quad (2)$$

Shared action head. Action spaces in RL typically vary across environments. For example, in the environments we consider, there are 18 discrete actions and a maximum of 8 continuous dimensions for continuous control environments. Therefore, we employ discretization of continuous action dimensions into 256 uniformly-spaced bins, similar to Reed et al. (2022) and Brohan et al. (2023b). Unlike prior work, we leverage a shared action head to predict all discrete actions or continuous action dimensions jointly. We found that this setup significantly reduces inference time compared to using autoregressive action prediction of continuous actions.

Recurrent inference mode. At inference time, we leverage the recurrent backbone and maintain the hidden states of

the last timestep. This enables fast inference with linear-time complexity along the sequence length. In addition, the recurrent-style inference is well-suited for online fine-tuning via RL objectives, similar to LSTM-based policies in online RL. To speed up inference, we leverage custom kernels for the xLSTM backbone (see Appendix 21).

Our unified discrete action representation enables consistent training of our agents via the cross-entropy loss as training objective across all tasks and domains, similar to Reed et al. (2022). We use separate reward scales per domain and target returns per task. Furthermore, we do not make use of timestep encodings as used by Chen et al. (2021), which are detrimental when episode lengths vary. We provide additional implementation details in Appendix C.

4. Experiments

We study the aptitude of modern recurrent architectures as LAMs on 432 tasks from 6 domains: Atari (Bellemare et al., 2013), Composuite (Mendez et al., 2022), DMControl (Tassa et al., 2018), Meta-World (Yu et al., 2020b), Mimicgen (Mandlekar et al., 2023), and Procgen (Cobbe et al., 2020b). To this end, we compile a large-scale dataset containing 894 million transitions (see Section 4.1). Across all experiments, we compare four backbone variants: xLSTM [7:1], xLSTM [1:0] (Beck et al., 2024), Mamba (Gu & Dao, 2023), and the GPT-2 style Transformer employed in the DT (Chen et al., 2021). Following (Beck et al., 2024), we use the bracket notation for xLSTM, which indicates the ratio of mLSTM to sLSTM blocks. For example, xLSTM [1:0] contains only mLSTM blocks.

In Section 4.2, we conduct a scaling comparison for four model sizes ranging from 16M to 206M parameters that shows that modern recurrent architectures achieve performance comparable or favorable to the Transformer baseline across different model sizes. In Section 4.3, we study the impact of the recurrent backbones on fine-tuning performance, ICL abilities, and further analyze our trained recurrent backbones. Finally, in Section 4.4, we empirically examine the differences at inference time in terms of latency and through-

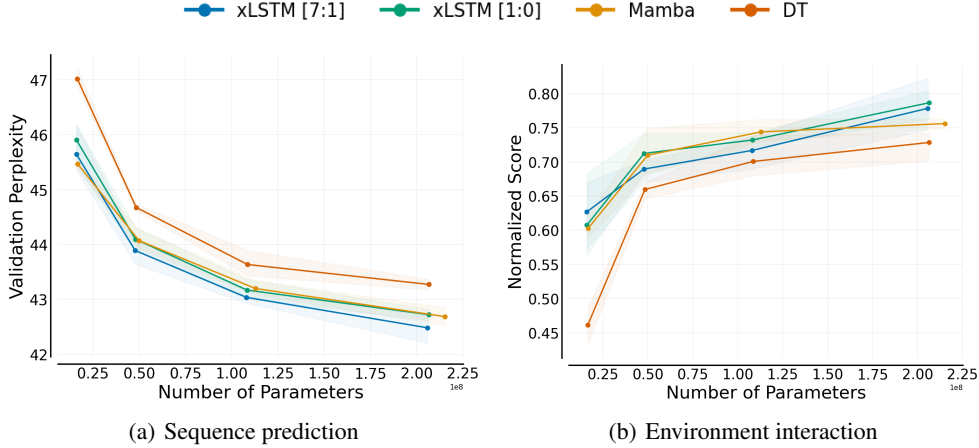


Figure 2. **Scaling comparison.** We compare xLSTM, Mamba, DT in four model sizes: 16M, 48M, 110M, and 206M parameters. We show the (a) validation perplexity on the hold-out datasets, and (b) normalized scores obtained from evaluating in the training task environments, averaged over all 6 domains.

put between xLSTM and Transformer-based agents, which indicate advantages for the recurrent backbone.

4.1. Datasets & Environments

Datasets. We compile a large-scale dataset comprising 432 tasks from six domains. We leverage datasets from prior works if available, and generate our own data otherwise. For Atari, we extract 5M transitions per task from the DQN-Replay dataset released by Agarwal et al. (2020). For Composuite, we leverage the datasets released by (Hussing et al., 2023). For Meta-World, we use 2M transitions per task released by (Schmied et al., 2024a). For DMControl, we generate 10M transitions per task using task-specific RL agents. For Mimicgen, we use the datasets for the 21 tasks released by (Mandlekar et al., 2023) and generate trajectories for the remaining 62 tasks. Finally, for Procgen, we extract 20M transitions from the datasets released by (Schmied et al., 2024b). Our final dataset contains 3.4M trajectories and in total 894M transitions (see Table 2). We reserve an additional 37 tasks from the same domains for zero-shot evaluation. To foster future research, we release our data-preparation pipeline and generated data. We provide the rationales for our specific dataset selection in Appendix B.1.

Environments. Atari and Procgen come with image observations and discrete actions. In contrast, the remaining four domains exhibit state-based observations and continuous actions. Consequently, our experiments involve a mixture of state and action spaces as well as varying episode lengths (see Table 2). Periodically evaluating the trained agents on all 432 tasks sequentially is time-consuming, and we, therefore, distributed the evaluation across GPUs and parallel processes (see Appendix C). Additional details on our datasets and environments are available in Appendix B.

4.2. Scaling comparison

To conduct our main comparisons, we train our four backbone variants on the full training task mixture of 432 tasks. For each architecture backbone, we report performance scores for four model sizes: 16M, 48M, 108M, and 206M parameters. We train all models for 200K updates with a batch size of 128 and a context length of 50 timesteps. All domains are represented with approximately equal proportion, resulting in 33K updates per domain. Additional implementation details and hyperparameters for every backbone variant and model size are available in Appendix C.

Sequence prediction performance. In Figure 2a, we report the validation set perplexity for all backbones and model sizes averaged over the individual scores from all domains. To achieve this, we maintain a hold-out set of trajectories for each training task (2.5%) and compute the perplexities after every 50K steps (see Figure 12 for training perplexities). Both recurrent backbones outperform the Transformer baseline considerably, especially as the model sizes increase.

Evaluation performance. During training, we evaluate our agents after every 50K step in all 432 training environments. In Figure 2b, we report the resulting normalized performances averaged across all six domains. The recurrent backbones outperform the Transformer one across model sizes. While xLSTM and Mamba perform similarly at smaller scales, xLSTM tends to outperform Mamba at larger scales (206M). This is an important advantage of xLSTM, as LRAM agents can strongly benefit from more data and consequently larger models. Note that Mamba has a significantly higher number of parameters than competitors. For the zero-shot evaluation performances on the 37 hold-out tasks, we refer to Figure 14 in Appendix D.2.

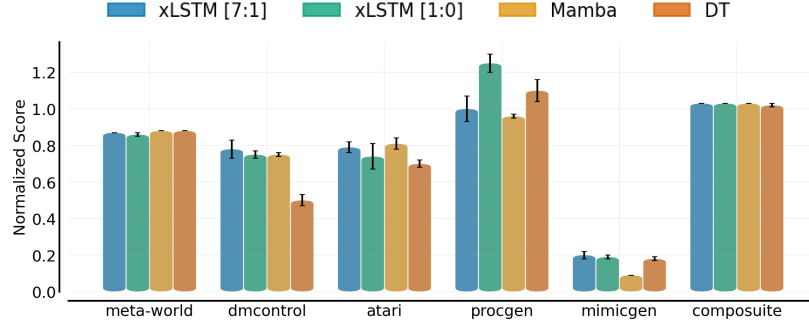


Figure 3. **Normalized scores per domain** for model size 206M. For Meta-World, DMControl, Mimicgen, Composuite, and Procgen, we report data-normalized scores, for Atari we report human-normalized scores.

Performance per domain. In Figure 3, we report the normalized scores for the 206M models attained on all six domains. For Meta-World, DMControl, Mimicgen, Composuite, and Procgen, we use data-normalized scores, as suggested by (Levine et al., 2020). For Atari, we report human-normalized scores. We observe that xLSTM outperforms competitors on three of the six domains, while they perform similarly on the remaining domains.

4.3. Analyses & Ablations

Fine-tuning. To assess the effect of the recurrent backbones on fine-tuning performance, we fine-tune our models on 37 held-out environments from all 6 domains. We evaluate the fine-tuning performance of the xLSTM architecture for the 16M pretrained models and compare it against an xLSTM trained from scratch. The pretrained LRAM outperforms the randomly initialized xLSTM model in most domains (see Figure 15). This suggests that fine-tuning performance is not affected negatively by switching the backbone.

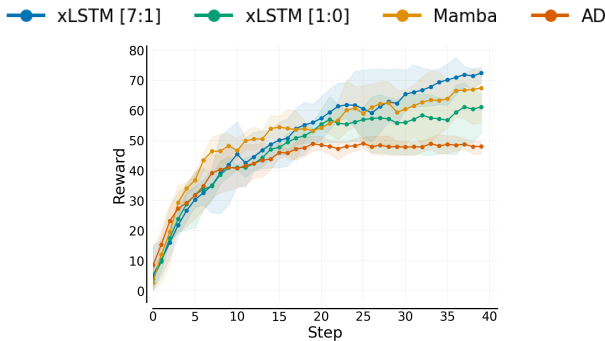


Figure 4. **In-context Learning** with modern recurrent architectures on 20 hold-out tasks for Dark-Room 10×10 .

In-context Learning. Next, we study the ICL abilities of our recurrent backbones on the Dark-Room environment considered in prior work on in-context RL (Laskin et al., 2022; Lee et al., 2023; Schmied et al., 2024b). To study ICL in isolation, we train models from scratch with a multi-

episodic context, which results in a large context length (see Appendix D.4 for details on the experiment setup). In particular, we adopt the Algorithm Distillation (AD, Laskin et al., 2022) framework and exchange the Transformer backbone architecture with modern recurrent architectures. In Figure 4, we report the ICL performance on the 20 hold-out tasks (see Figure 16 for training tasks). We find that xLSTM [7:1] attains the highest overall scores both on the 80 training and 20 hold-out tasks, which we attribute to the state-tracking abilities (Merrill et al., 2024) of sLSTM blocks.

Embedding space analysis. In Figure 5, we analyze the representations learned by our model. We sample 32 sub-trajectories from every task, extract the sequence representation at the last layer, cluster them using UMAP (McInnes et al., 2018), and color every point by its domain (see Appendix F for more details). We find that tasks from the same domain cluster together. Furthermore, xLSTM exhibits a more refined domain separation compared to DT, which may further contribute to the better downstream performance. See Appendix F for a more detailed discussion on the embedding space analysis and a comparison to Mamba.

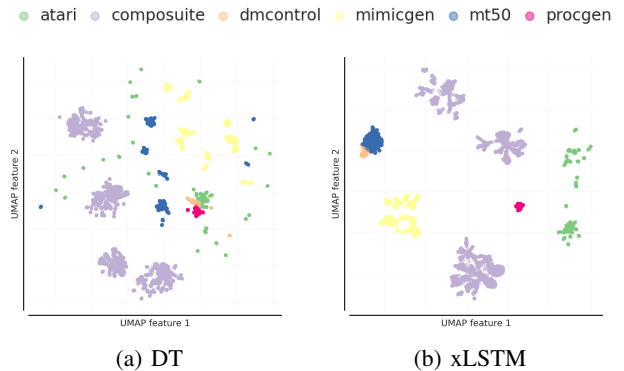


Figure 5. **Embedding space comparison.** UMAP clustering of hidden states for all tasks for 16M, colored by domain. xLSTM exhibits a better domain separation than DT.

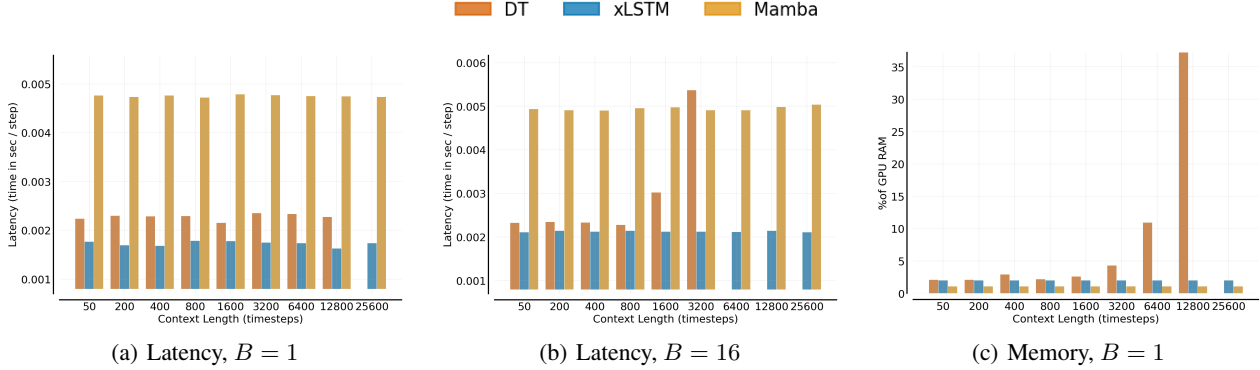


Figure 6. **Latency** comparison on A100. We report latency for varying context lengths (in timesteps) with batch sizes (a) $B = 1$ and (b) $B = 16$. In (c), we show the memory consumption in % of GPU memory with $B = 1$. We compare DT to xLSTM and Mamba with the same number of layer blocks and parameters on Atari Freeway. Missing bars for DT indicate out-of-memory (OOM).

Removing Actions & Effect of Context Length. We found that removing actions from the context results in better performance across backbones. While context lengths beyond 1 hurt performance on Meta-World and DMControl, and when training with actions, the reverse is true when training without actions (see Figures 23, 24, 26). This is in contrast to recent works, which did not benefit from longer contexts (Octo Model Team et al., 2024). While removing actions improves performance on Meta-World/DMControl, it does not affect performance on discrete control environments. For Meta-World/DMControl, we observed that the models become overly confident, which is problematic if poor initial actions are produced. This is because many robotics environments exhibit smoothly changing actions, and by observing previous actions, the agent can learn shortcuts. A similar issue has been observed by Wen et al. (2020) and termed the *copycat problem*. Removing actions from the input prevents the agent from using shortcuts and, therefore, alleviates the copycat problem. Importantly, the evaluation performance improves across domains as the sequence length increases, which indicates that the history helps to predict the next action (e.g., by observing mistakes made in the past, see Figures 25, 27).

Return-conditioning vs. Behavior Cloning. Across our experiments, we utilized a sequence representation that includes return-to-go tokens, as commonly used in DTs (Chen et al., 2021; Lee et al., 2022). However, many recent works focus on behavior cloning without return conditioning (Reed et al., 2022; Brohan et al., 2023a). Therefore, we study the effect of excluding the RTG/reward tokens from the sequence at the 206M parameter scale, to validate that our findings transfer to the behavior cloning setting. Indeed, we find that the same trends hold (see Figures 28 and 29).

mLSTM-to-sLSTM Ratio. Throughout experiments, we compare two xLSTM variants: xLSTM [7:1] and xLSTM [1:0]. These ratios were proposed by Beck et al. (2024) and

we maintain the same ratios for consistency (see Appendix C.3). While mLSTM is parallelizable, sLSTM enables state-tracking (Merrill et al., 2024). To better understand the effect of the ratio, we conduct ablation studies both on the 432 tasks and on Dark-Room (see Appendix E.3), similar to Beck et al. (2024). We find that other ratios, such as [3:1], can be effective, and highlight the importance of placing sLSTMs at lower-level layers (Figure 31). However, the effectiveness of sLSTM layers is dependent on the task at hand. Complex tasks with long horizons or partial observability, as are common in real-world applications, may benefit from the state-tracking abilities provided by sLSTM.

We present additional ablations on the effect of reducing the number of layers in xLSTM and disabling Dropout on DT in Appendix E.5 and E.4, respectively.

4.4. Inference Time Comparison

Finally, we empirically examine the difference between recurrent and Transformer-based agents at inference time. Similar to De et al. (2024), we report both latency and throughput. We focus our analysis on latency, as it is the more important dimension for real-time applications.

Setup. We conduct all inference time tests on A100s with 40GB of RAM using 206M models. For the Transformer, we use KV-caching and FlashAttention (Dao, 2023) as supported by PyTorch (Paszke et al., 2019). For xLSTM, we use recurrent-style inference using custom kernels to accelerate computations (see Figure 21 for the impact of kernel acceleration). For Mamba, we make use of the kernels introduced by Gu & Dao (2023). For DT and xLSTM, we use `torch.compile`, but not for Mamba because we found the kernels to be incompatible with compilation. The Transformer with KV-caching has a linear time complexity per step and quadratic in the sequence length. In contrast, the xLSTM and Mamba have a constant time complexity per

step and are linear in the sequence length. Therefore, we expect speed-ups especially for longer sequences and larger batch sizes, as observed by De et al. (2024). To ensure a fair comparison, we compare all backbones with the same number of layer blocks and increase the hidden size of xLSTM and Mamba to match the number of parameters of DT (see Appendix E.5 for evaluation performance of these models). We provide further details on our inference time tests in Appendix D.5.

Environment. We conduct all inference time tests on the environment that exhibited the longest average episode lengths in our experiments, the Atari game *Freeway*. Every episode in *Freeway* lasts for 8192 steps, which is equivalent to 24576 tokens (s/rtg/r). We evaluate all models for 5 episodes and preserve the KV-cache/hidden state across episode boundaries. The reported latencies and throughputs are averaged across all evaluation episodes, except for the first episode, which we discard to exclude compilation times and prefilling. We opted for measuring the inference times during environment interaction, i.e., including simulator latency, rather than mere token generation.

Latency. Similar to De et al. (2024), we measure latency by the average time (in seconds) taken to perform a single inference step with a fixed batch size B (lower is better). In Figure 6, we report the latencies for varying context lengths, $C \in [50, 25600]$ and two batch sizes $B \in \{1, 16\}$. Note that C is in time steps, and every time step contains 3 tokens (state, reward-to-go, reward). Hence, the effective sequence length for the largest C is 76800. As expected, we find that the recurrent backbones attain lower inference latencies than the Transformer one, especially for longer sequences and with a larger batch size. For $B = 1$, we find that Mamba is slower than the Transformer and xLSTM, which we believe is because of the incompatibility with `torch.compile`. Note that we expect the gap to xLSTM to be closed with compatible kernels. As the sequence length increases, DT runs out of memory due to the increasing size of the KV cache (see Figure 6c). In contrast, the inference speeds for Mamba/xLSTM are independent of the context length and therefore, enable significantly longer context lengths. This property is particularly interesting for in-context RL, which requires keeping multiple episodes in the context (Laskin et al., 2022). Nevertheless, our experiments highlight that the materialization of the complexity advantage depends on the device, model size, batch size, and the context length, which is similar to findings by De et al. (2024).

Throughput. Throughput is measured by the total number of inference steps performed per second for a model with a fixed context length. In Figure 7, we report the throughputs for varying batch sizes, $B \in [1, 128]$ for a fixed context length of $C = 1600$. Here, the batch size can be interpreted as the number of parallel environments the agent interacts

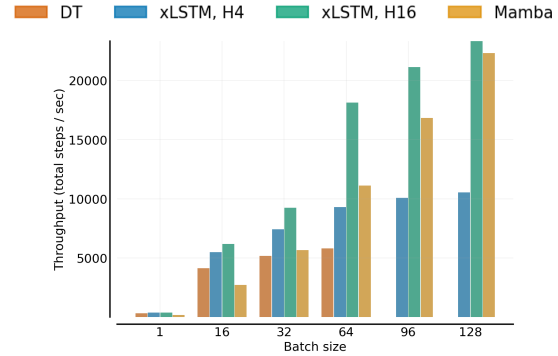


Figure 7. **Throughput** comparison on A100 for varying batch sizes with $C = 1600$ timesteps on the Atari *Freeway* environment. We compare DT, xLSTM with 4 and 16 heads, and Mamba. Missing bars for DT indicate OOM.

with. For xLSTM, we report numbers for two variants with 4 and 16 heads, respectively. We found that decreasing the head dimension (more heads, same total hidden dim) is important for xLSTM to enable high throughput. This is because a higher head dimension incurs more FLOPS (see Figure 22 in Appendix D.5.4 for an ablation on the impact of the head dimension). As expected, we find that both Mamba and xLSTM attain considerably higher throughputs than the DT. These benefits increase with larger batch sizes. While the DT with quadratic complexity in the sequence length goes OOM for batch sizes above 64, the recurrent backbones with linear complexity can easily handle larger batch sizes. This throughput advantage may be particularly relevant for online fine-tuning of agents in many parallel environments.

5. Conclusion

In this work, we study the aptitude of modern recurrent architectures as alternatives to Transformers for building LAMs. We found that our LRAM with an xLSTM or Mamba at its core compares favorably to the Transformer in terms of evaluation performance across model scales ranging from 16M to 206M parameters (see Section 4.2). Moreover, we demonstrated that LRAM exhibits higher inference speeds, especially at large context sizes (see Section 4.4). Thus, the empirical evidence suggests that recurrent backbones can be attractive alternatives for LAMs. Notably, the linear-time inference complexity of xLSTM and Mamba may enable applications that require long context lengths (e.g., ICL) and facilitate the application of large-scale agents for real-time applications, such as robotics.

Modern recurrent architectures and Transformers come with different advantages and disadvantages. xLSTM and Mamba, on the one hand, exhibit a fundamental complexity advantage over Transformers. Their linear complexity

ensures that the computational requirements increase more slowly with the sequence length, which enables more efficient inference and is particularly relevant for edge applications. While we conduct our inference time comparisons on a high-end data center GPU, applications on edge devices may have to deal with less powerful accelerators. Importantly, we found that LAMs strongly benefit from longer sequences (see Section 4.3). Their ability to efficiently handle long sequences can be beneficial for applications in real-world environments, which often exhibit long-term dependencies. Similarly, longer context can be relevant for ICL applications, which benefit from keeping multiple episodes (such as demonstrations or previous trials) in the context. Transformers, on the other hand, are effective for applications that require exact recall of tokens (such as particular locations in a grid, signs in an image) in a sequence, which can be important for decision-making (Ni et al., 2024). Finally, xLSTM in particular enables state-tracking via sLSTM blocks, which Transformers and Mamba cannot perform (Merrill et al., 2024). State tracking can be important for logic tasks or dealing with partial observability and may be a useful tool for practitioners. Given these differences, different backbones should be considered depending on the task at hand.

Limitations & Future Work. The primary target application of LAMs is robotics. While the majority of our experiments involve robotic simulations, we do not yet provide experiments for real robots. We do, however, believe that our findings translate to real-world scenarios and aim to provide further evidence in future work. Moreover, our fine-tuning experiments are limited to offline RL. We envision that an agent pre-trained on large-scale datasets can be successfully fine-tuned via online RL to explore new strategies that do not appear in the training data. Modern recurrent architectures offer both parallel and recurrent training modes, which might be the key to success for such applications. While we provide evidence for improved ICL abilities of LRAM, we only consider a grid-world setting. We aim to further investigate the ICL abilities of LRAM in more complex environments.

Impact Statement

While we conduct all our experiments in simulated environments, the primary target application of our method is robotics. We believe that our work can positively impact applications in the near future that require efficient inference, on-device processing, or have real-time constraints. However, robotics applications in the real world are not without risks. In particular, in areas where humans are involved, such as factory settings, special care is required. LAMs are trained via next-action prediction similar to LLMs. Consequently, LAMs may also suffer from hallucinations in

unknown scenarios. We therefore strongly discourage users from blindly following the predictions made by real-world LAMs without appropriate precautions regarding safety and robustness. It is essential to ensure the responsible deployment of such future technologies, and we believe that more research on the robustness of LAMs is necessary.

Acknowledgements

We acknowledge EuroHPC Joint Undertaking for awarding us access to Karolina at IT4Innovations, Czech Republic, MeluXina at LuxProvide, Luxembourg, and Leonardo at CINECA, Italy. The ELLIS Unit Linz, the LIT AI Lab, the Institute for Machine Learning, are supported by the Federal State Upper Austria. We thank the projects FWF AIRI FG 9-N (10.55776/FG9), AI4GreenHeatingGrids (FFG- 899943), Stars4Waters (HORIZON-CL6-2021-CLIMATE-01-01), FWF Bilateral Artificial Intelligence (10.55776/COE12). We thank NXAI GmbH, Audi AG, Silicon Austria Labs (SAL), Merck Healthcare KGaA, GLS (Univ. Waterloo), TÜV Holding GmbH, Software Competence Center Hagenberg GmbH, dSPACE GmbH, TRUMPF SE + Co. KG.

References

- Agarwal, R., Schuurmans, D., and Norouzi, M. An optimistic perspective on offline reinforcement learning. In *International Conference on Machine Learning*, pp. 104–114. PMLR, 2020.
- Agarwal, R., Schwarzer, M., Castro, P. S., Courville, A. C., and Bellemare, M. Deep reinforcement learning at the edge of the statistical precipice. *Advances in neural information processing systems*, 34:29304–29320, 2021.
- Alkin, B., Beck, M., Pöppel, K., Hochreiter, S., and Brandstetter, J. Vision-lstm: xlstm as generic vision backbone. *CoRR*, abs/2406.04303, 2024. doi: 10.48550/ARXIV.2406.04303. URL <https://doi.org/10.48550/arXiv.2406.04303>.
- Baevski, A., Zhou, Y., Mohamed, A., and Auli, M. wav2vec 2.0: A framework for self-supervised learning of speech representations. *Advances in Neural Information Processing Systems*, 33:12449–12460, 2020.
- Beck, M., Pöppel, K., Spanring, M., Auer, A., Prudnikova, O., Kopp, M., Klambauer, G., Brandstetter, J., and Hochreiter, S. xlstm: Extended long short-term memory. *CoRR*, abs/2405.04517, 2024. doi: 10.48550/ARXIV.2405.04517. URL <https://doi.org/10.48550/arXiv.2405.04517>.
- Bellemare, M. G., Naddaf, Y., Veness, J., and Bowling, M. The Arcade learning environment: An evaluation plat-

- form for general agents. *Journal of Artificial Intelligence Research*, 47:253–279, 2013.
- Bellemare, M. G., Candido, S., Castro, P. S., Gong, J., Machado, M. C., Moitra, S., Ponda, S. S., and Wang, Z. Autonomous navigation of stratospheric balloons using reinforcement learning. *Nature*, 588(7836):77–82, 2020.
- Berner, C., Brockman, G., Chan, B., Cheung, V., Dkebiak, P., Dennison, C., Farhi, D., Fischer, Q., Hashme, S., Hesse, C., et al. Dota 2 with large scale deep reinforcement learning. *arXiv preprint arXiv:1912.06680*, 2019.
- Brohan, A., Brown, N., Carbajal, J., Chebotar, Y., Chen, X., Choromanski, K., Ding, T., Driess, D., Dubey, A., Finn, C., et al. Rt-2: Vision-language-action models transfer web knowledge to robotic control. *arXiv preprint arXiv:2307.15818*, 2023a.
- Brohan, A., Brown, N., Carbajal, J., Chebotar, Y., Dabis, J., Finn, C., Gopalakrishnan, K., Hausman, K., Herzog, A., Hsu, J., Ibarz, J., Ichter, B., Irpan, A., Jackson, T., Jesmonth, S., Joshi, N. J., Julian, R., Kalashnikov, D., Kuang, Y., Leal, I., Lee, K., Levine, S., Lu, Y., Malla, U., Manjunath, D., Mordatch, I., Nachum, O., Parada, C., Peralta, J., Perez, E., Pertsch, K., Quiambao, J., Rao, K., Ryoo, M. S., Salazar, G., Sanketi, P. R., Sayed, K., Singh, J., Sontakke, S., Stone, A., Tan, C., Tran, H. T., Vanhoucke, V., Vega, S., Vuong, Q., Xia, F., Xiao, T., Xu, P., Xu, S., Yu, T., and Zitkovich, B. RT-1: robotics transformer for real-world control at scale. In Bekris, K. E., Hauser, K., Herbert, S. L., and Yu, J. (eds.), *Robotics: Science and Systems XIX, Daegu, Republic of Korea, July 10-14, 2023*, 2023b. doi: 10.15607/RSS.2023.XIX.025. URL <https://doi.org/10.15607/RSS.2023.XIX.025>.
- Brown, T., Mann, B., Ryder, N., Subbiah, M., Kaplan, J., Dhariwal, P., Neelakantan, A., Shyam, P., Sastry, G., Askell, A., Agarwal, S., Herbert-Voss, A., Krueger, G., Henighan, T., Child, R., Ramesh, A., Ziegler, D., Wu, J., Winter, C., Hesse, C., Chen, M., Sigler, E., Litwin, M., Gray, S., Chess, B., Clark, J., Berner, C., McCandlish, S., Radford, A., Sutskever, I., and Amodei, D. Language models are few-shot learners. In Larochelle, H., Ranzato, M., Hadsell, R., Balcan, M., and Lin, H. (eds.), *Advances in Neural Information Processing Systems*, volume 33, pp. 1877–1901. Curran Associates, Inc., 2020. URL https://proceedings.neurips.cc/paper_files/paper/2020/file/1457c0d6bfcb4967418bfb8ac142f64a-Paper.pdf.
- Chen, L., Lu, K., Rajeswaran, A., Lee, K., Grover, A., Laskin, M., Abbeel, P., Srinivas, A., and Mordatch, I. Decision transformer: Reinforcement learning via sequence modeling. *Advances in neural information processing systems*, 34:15084–15097, 2021.
- Chignoli, M., Kim, D., Stanger-Jones, E., and Kim, S. The mit humanoid robot: Design, motion planning, and control for acrobatic behaviors. In *2020 IEEE-RAS 20th International Conference on Humanoid Robots (Humanoids)*, pp. 1–8. IEEE, 2021.
- Cho, K., van Merriënboer, B., Gülçehre, Ç., Bahdanau, D., Bougares, F., Schwenk, H., and Bengio, Y. Learning phrase representations using RNN encoder-decoder for statistical machine translation. In Moschitti, A., Pang, B., and Daelemans, W. (eds.), *Proceedings of the 2014 Conference on Empirical Methods in Natural Language Processing, EMNLP 2014, October 25-29, 2014, Doha, Qatar, A meeting of SIGDAT, a Special Interest Group of the ACL*, pp. 1724–1734. ACL, 2014. doi: 10.3115/V1/D14-1179. URL <https://doi.org/10.3115/V1/D14-1179>.
- Cobbe, K., Hesse, C., Hilton, J., and Schulman, J. Leveraging procedural generation to benchmark reinforcement learning. In *International conference on machine learning*, pp. 2048–2056. PMLR, 2020a.
- Cobbe, K., Hesse, C., Hilton, J., and Schulman, J. Leveraging procedural generation to benchmark reinforcement learning. In *Proceedings of the 37th International Conference on Machine Learning, ICML 2020, 13-18 July 2020, Virtual Event*, volume 119 of *Proceedings of Machine Learning Research*, pp. 2048–2056. PMLR, 2020b. URL <http://proceedings.mlr.press/v119/cobbe20a.html>.
- Dai, Y., Ma, O., Zhang, L., Liang, X., Hu, S., Wang, M., Ji, S., Huang, J., and Shen, L. Is mamba compatible with trajectory optimization in offline reinforcement learning? *arXiv preprint arXiv:2405.12094*, 2024.
- Dao, T. Flashattention-2: Faster attention with better parallelism and work partitioning. *arXiv preprint arXiv:2307.08691*, 2023.
- Dao, T. and Gu, A. Transformers are ssms: Generalized models and efficient algorithms through structured state space duality. *arXiv preprint arXiv:2405.21060*, 2024.
- De, S., Smith, S. L., Fernando, A., Botev, A., Cristian-Muraru, G., Gu, A., Haroun, R., Berrada, L., Chen, Y., Srinivasan, S., et al. Griffin: Mixing gated linear recurrences with local attention for efficient language models. *arXiv preprint arXiv:2402.19427*, 2024.
- Degrave, J., Felici, F., Buchli, J., Neunert, M., Tracey, B., Carpanese, F., Ewalds, T., Hafner, R., Abdolmaleki, A., de Las Casas, D., et al. Magnetic control of tokamak plasmas through deep reinforcement learning. *Nature*, 602(7897):414–419, 2022.

- Devlin, J., Chang, M., Lee, K., and Toutanova, K. BERT: pre-training of deep bidirectional transformers for language understanding. In Burstein, J., Doran, C., and Solorio, T. (eds.), *Proceedings of the 2019 Conference of the North American Chapter of the Association for Computational Linguistics: Human Language Technologies, NAACL-HLT 2019, Minneapolis, MN, USA, June 2-7, 2019, Volume 1 (Long and Short Papers)*, pp. 4171–4186. Association for Computational Linguistics, 2019. doi: 10.18653/v1/n19-1423.
- Dosovitskiy, A., Beyer, L., Kolesnikov, A., Weissenborn, D., Zhai, X., Unterthiner, T., Dehghani, M., Minderer, M., Heigold, G., Gelly, S., Uszkoreit, J., and Housley, N. An image is worth 16x16 words: Transformers for image recognition at scale. In *9th International Conference on Learning Representations, ICLR 2021, Virtual Event, Austria, May 3-7, 2021*. OpenReview.net, 2021.
- El-Hussieny, H. Real-time deep learning-based model predictive control of a 3-dof biped robot leg. *Scientific Reports*, 14(1):16243, 2024.
- Elman, J. L. Finding structure in time. *Cogn. Sci.*, 14(2): 179–211, 1990. doi: 10.1207/S15516709COG1402\1. URL https://doi.org/10.1207/S15516709cog1402_1.
- Embodiment Collaboration, O’Neill, A., Rehman, A., Madhukuri, A., Gupta, A., Padalkar, A., Lee, A., Pooley, A., Gupta, A., Mandlekar, A., Jain, A., Tung, A., Bewley, A., Herzog, A., Irpan, A., Khazatsky, A., Rai, A., Gupta, A., Wang, A., Singh, A., Garg, A., Kembhavi, A., Xie, A., Brohan, A., Raffin, A., Sharma, A., Yavary, A., Jain, A., Balakrishna, A., Wahid, A., Burgess-Limerick, B., Kim, B., Schölkopf, B., Wulfe, B., Ichter, B., Lu, C., Xu, C., Le, C., Finn, C., Wang, C., Xu, C., Chi, C., Huang, C., Chan, C., Agia, C., Pan, C., Fu, C., Devin, C., Xu, D., Morton, D., Driess, D., Chen, D., Pathak, D., Shah, D., Büchler, D., Jayaraman, D., Kalashnikov, D., Sadigh, D., Johns, E., Foster, E., Liu, F., Ceola, F., Xia, F., Zhao, F., Stulp, F., Zhou, G., Sukhatme, G. S., Salhotra, G., Yan, G., Feng, G., Schiavi, G., Berseth, G., Kahn, G., Wang, G., Su, H., Fang, H., Shi, H., Bao, H., Amor, H. B., Christensen, H. I., Furuta, H., Walke, H., Fang, H., Ha, H., Mordatch, I., Radosavovic, I., Leal, I., Liang, J., Abou-Chakra, J., Kim, J., Drake, J., Peters, J., Schneider, J., Hsu, J., Bohg, J., Bingham, J., Wu, J., Gao, J., Hu, J., Wu, J., Wu, J., Tan, J., Oh, J., Wu, J., Lu, J., Yang, J., Salvador, J., Lim, J. J., Han, J., Wang, K., Rao, K., Pertsch, K., Hausman, K., Go, K., Gopalakrishnan, K., Goldberg, K., Byrne, K., Kawaharazuka, K., Black, K., Lin, K., Zhang, K., Ehsani, K., Lekkala, K., Ellis, K., Rana, K., Fang, K., Singh, K., Zeng, K., Hatch, K., Hsu, K., Itti, L., Chen, L. Y., Pinto, L., Fei-Fei, L., Tan, L., Fan, L., Ott, L., Lee, L., Weihs, L., Chen, M., Lepert, M., Memmel, M., Tomizuka, M., Itkina, M., Castro, M. G., Spero, M., Du, M., Ahn, M., Yip, M. C., Zhang, M., Ding, M., Heo, M., Srirama, M. K., Sharma, M., Kim, M. J., Kanazawa, M., Hansen, N., Heess, N., Joshi, N. J., Suenderhauf, N., Liu, N., Palo, N. D., Shafiullah, N., Mees, O., Kroemer, O., Bastani, O., Sanketi, P. R., Miller, P., Yin, P., Wohlhart, P., Xu, P., Fagan, P., Mitrano, P., Sermanet, P., Abbeel, P., Sundaresan, P., Chen, Q., Vuong, Q., Rafailov, R., Tian, R., Doshi, R., Martín-Martín, R., Baijal, R., Scalise, R., Hendrix, R., Lin, R., Qian, R., Zhang, R., Mendonca, R., Shah, R., Hoque, R., Julian, R., Bustamante, S., Kirmani, S., Levine, S., Lin, S., Moore, S., Bahl, S., Dass, S., Sonawani, S., Song, S., Xu, S., Haldar, S., Karamcheti, S., Adebola, S., Guist, S., Nasiriany, S., Schaal, S., Welker, S., Tian, S., Ramamoorthy, S., Dasari, S., Belkhal, S., Park, S., Nair, S., Mirchandani, S., Osa, T., Gupta, T., Harada, T., Matsushima, T., Xiao, T., Kollar, T., Yu, T., Ding, T., Davchev, T., Zhao, T. Z., Armstrong, T., Darrell, T., Chung, T., Jain, V., Vanhoucke, V., Zhan, W., Zhou, W., Burgard, W., Chen, X., Wang, X., Zhu, X., Geng, X., Liu, X., Liangwei, X., Li, X., Lu, Y., Ma, Y., Kim, Y., Chebotar, Y., Zhou, Y., Zhu, Y., Wu, Y., Xu, Y., Wang, Y., Bisk, Y., Cho, Y., Lee, Y., Cui, Y., Cao, Y., Wu, Y., Tang, Y., Zhu, Y., Zhang, Y., Jiang, Y., Li, Y., Li, Y., Iwasawa, Y., Matsuo, Y., Ma, Z., Xu, Z., Cui, Z., Zhang, Z., Fu, Z., and Lin, Z. Open x-embodiment: Robotic learning datasets and rt-x models, 2024.
- Espeholt, L., Soyer, H., Munos, R., Simonyan, K., Mnih, V., Ward, T., Doron, Y., Firoiu, V., Harley, T., Dunning, I., et al. Impala: Scalable distributed deep-rl with importance weighted actor-learner architectures. In *International conference on machine learning*, pp. 1407–1416. PMLR, 2018.
- Firoozi, R., Tucker, J., Tian, S., Majumdar, A., Sun, J., Liu, W., Zhu, Y., Song, S., Kapoor, A., Hausman, K., et al. Foundation models in robotics: Applications, challenges, and the future. *The International Journal of Robotics Research*, pp. 02783649241281508, 2023.
- Franklin, G. F., Powell, J. D., Workman, M. L., et al. *Digital control of dynamic systems*, volume 3. Addison-wesley Menlo Park, 1998.
- Frantar, E., Ashkboos, S., Hoeffer, T., and Alistarh, D. OPTQ: accurate quantization for generative pre-trained transformers. In *The Eleventh International Conference on Learning Representations, ICLR 2023, Kigali, Rwanda, May 1-5, 2023*. OpenReview.net, 2023. URL <https://openreview.net/forum?id=tcbBPnfwxS>.
- Fürst, A., Rumetshofer, E., Lehner, J., Tran, V., Tang, F., Ramsauer, H., Kreil, D., Kopp, M., Klambauer, G., Bitto-

- Nemling, A., and Hochreiter, S. Cloob: Modern hopfield networks with infoloob outperform clip, 2022.
- Gu, A. and Dao, T. Mamba: Linear-time sequence modeling with selective state spaces. *CoRR*, abs/2312.00752, 2023. doi: 10.48550/ARXIV.2312.00752. URL <https://doi.org/10.48550/arXiv.2312.00752>.
- Gu, A., Johnson, I., Goel, K., Saab, K., Dao, T., Rudra, A., and Ré, C. Combining recurrent, convolutional, and continuous-time models with linear state space layers. In Ranzato, M., Beygelzimer, A., Dauphin, Y. N., Liang, P., and Vaughan, J. W. (eds.), *Advances in Neural Information Processing Systems 34: Annual Conference on Neural Information Processing Systems 2021, NeurIPS 2021, December 6-14, 2021, virtual*, pp. 572–585, 2021. URL <https://proceedings.neurips.cc/paper/2021/hash/05546b0e38ab9175cd905eebcc6ebb76-Abstract.html>.
- Gu, A., Goel, K., Gupta, A., and Ré, C. On the parameterization and initialization of diagonal state space models. *Advances in Neural Information Processing Systems*, 35: 35971–35983, 2022a.
- Gu, A., Goel, K., and Ré, C. Efficiently modeling long sequences with structured state spaces. In *The Tenth International Conference on Learning Representations, ICLR 2022, Virtual Event, April 25-29, 2022*. OpenReview.net, 2022b. URL <https://openreview.net/forum?id=uYLFoz1vlAC>.
- Gu, J., Kirmani, S., Wohlhart, P., Lu, Y., Arenas, M. G., Rao, K., Yu, W., Fu, C., Gopalakrishnan, K., Xu, Z., Sundaresan, P., Xu, P., Su, H., Hausman, K., Finn, C., Vuong, Q., and Xiao, T. Rt-trajectory: Robotic task generalization via hindsight trajectory sketches, 2023.
- Gu, X., Wang, Y.-J., and Chen, J. Humanoid-gym: Reinforcement learning for humanoid robot with zero-shot sim2real transfer, 2024.
- Haarnoja, T., Zhou, A., Abbeel, P., and Levine, S. Soft actor-critic: Off-policy maximum entropy deep reinforcement learning with a stochastic actor. In Dy, J. G. and Krause, A. (eds.), *Proceedings of the 35th International Conference on Machine Learning, ICML 2018, Stockholm, Sweden, July 10-15, 2018*, volume 80 of *Proceedings of Machine Learning Research*, pp. 1856–1865. PMLR, 2018.
- Hafner, D., Lillicrap, T., Fischer, I., Villegas, R., Ha, D., Lee, H., and Davidson, J. Learning latent dynamics for planning from pixels. In *International conference on machine learning*, pp. 2555–2565. PMLR, 2019.
- He, K., Chen, X., Xie, S., Li, Y., Dollár, P., and Girshick, R. B. Masked autoencoders are scalable vision learners. In *IEEE/CVF Conference on Computer Vision and Pattern Recognition, CVPR 2022, New Orleans, LA, USA, June 18-24, 2022*, pp. 15979–15988. IEEE, 2022. doi: 10.1109/CVPR52688.2022.01553.
- Hessel, M., Modayil, J., van Hasselt, H., Schaul, T., Ostrovski, G., Dabney, W., Horgan, D., Piot, B., Azar, M. G., and Silver, D. Rainbow: Combining improvements in deep reinforcement learning. *ArXiv*, 2017.
- Hinton, G. E., Vinyals, O., and Dean, J. Distilling the knowledge in a neural network. *CoRR*, abs/1503.02531, 2015. URL <http://arxiv.org/abs/1503.02531>.
- Hochreiter, S. and Schmidhuber, J. Long short-term memory. *Neural Comput.*, 9(8):1735–1780, 1997.
- Hu, Y., Xie, Q., Jain, V., Francis, J., Patrikar, J., Keetha, N., Kim, S., Xie, Y., Zhang, T., Zhao, Z., et al. Toward general-purpose robots via foundation models: A survey and meta-analysis. *arXiv preprint arXiv:2312.08782*, 2023.
- Hussing, M., Mendez, J. A., Singrodia, A., Kent, C., and Eaton, E. Robotic manipulation datasets for offline compositional reinforcement learning. *arXiv preprint arXiv:2307.07091*, 2023.
- Janner, M., Li, Q., and Levine, S. Offline reinforcement learning as one big sequence modeling problem. *Advances in neural information processing systems*, 34: 1273–1286, 2021.
- Jia, X., Blessing, D., Jiang, X., Reuss, M., Donat, A., Lioutikov, R., and Neumann, G. Towards diverse behaviors: A benchmark for imitation learning with human demonstrations. In *The Twelfth International Conference on Learning Representations*, 2024. URL <https://openreview.net/forum?id=6pPYRXKPpw>.
- Jiang, Y., Gupta, A., Zhang, Z., Wang, G., Dou, Y., Chen, Y., Fei-Fei, L., Anandkumar, A., Zhu, Y., and Fan, L. Vima: General robot manipulation with multimodal prompts. *arXiv preprint arXiv:2210.03094*, 2022.
- Jiang, Y., Gupta, A., Zhang, Z., Wang, G., Dou, Y., Chen, Y., Fei-Fei, L., Anandkumar, A., Zhu, Y., and Fan, L. Vima: General robot manipulation with multimodal prompts, 2023.
- Jordan, M. I. *Attractor dynamics and parallelism in a connectionist sequential machine*, pp. 112–127. IEEE Press, 1990. ISBN 0818620153.

- Kapturowski, S., Ostrovski, G., Dabney, W., Quan, J., and Munos, R. Recurrent experience replay in distributed reinforcement learning. In *International Conference on Learning Representations*, 2019. URL <https://openreview.net/forum?id=r1lyTjAqYX>.
- Katharopoulos, A., Vyas, A., Pappas, N., and Fleuret, F. Transformers are rnns: Fast autoregressive transformers with linear attention. In *International conference on machine learning*, pp. 5156–5165. PMLR, 2020.
- Kim, M. J., Pertsch, K., Karamcheti, S., Xiao, T., Balakrishna, A., Nair, S., Rafailov, R., Foster, E., Lam, G., Sanketi, P., et al. Openvla: An open-source vision-language-action model. *arXiv preprint arXiv:2406.09246*, 2024.
- Kim, S., Hooper, C., Wattanawong, T., Kang, M., Yan, R., Genc, H., Dinh, G., Huang, Q., Keutzer, K., Mahoney, M. W., et al. Full stack optimization of transformer inference: a survey. *arXiv preprint arXiv:2302.14017*, 2023.
- Kirsch, L., Harrison, J., Freeman, C., Sohl-Dickstein, J., and Schmidhuber, J. Towards general-purpose in-context learning agents. In *NeurIPS 2023 Workshop on Generalization in Planning*, 2023.
- Laskin, M., Lee, K., Stooke, A., Pinto, L., Abbeel, P., and Srinivas, A. Reinforcement learning with augmented data. *ArXiv*, 2004.14990, 2020.
- Laskin, M., Wang, L., Oh, J., Parisotto, E., Spencer, S., Steigerwald, R., Strouse, D., Hansen, S., Filos, A., Brooks, E., et al. In-context reinforcement learning with algorithm distillation. *arXiv preprint arXiv:2210.14215*, 2022.
- LeCun, Y., Denker, J. S., and Solla, S. A. Optimal brain damage. In Touretzky, D. S. (ed.), *Advances in Neural Information Processing Systems 2, [NIPS Conference, Denver, Colorado, USA, November 27-30, 1989]*, pp. 598–605. Morgan Kaufmann, 1989. URL <http://papers.nips.cc/paper/250-optimal-brain-damage>.
- Lee, J. N., Xie, A., Pacchiano, A., Chandak, Y., Finn, C., Nachum, O., and Brunskill, E. Supervised pretraining can learn in-context reinforcement learning. *arXiv preprint arXiv:2306.14892*, 2023.
- Lee, K.-H., Nachum, O., Yang, M., Lee, L., Freeman, D., Xu, W., Guadarrama, S., Fischer, I., Jang, E., Michalewski, H., et al. Multi-game decision transformers. *arXiv preprint arXiv:2205.15241*, 2022.
- Levine, S., Kumar, A., Tucker, G., and Fu, J. Offline reinforcement learning: Tutorial, review, and perspectives on open problems. *arXiv preprint arXiv:2005.01643*, 2020.
- Loshchilov, I. and Hutter, F. Decoupled weight decay regularization. In *International Conference on Learning Representations*, 2018.
- Mandlekar, A., Nasiriany, S., Wen, B., Akinola, I., Narang, Y., Fan, L., Zhu, Y., and Fox, D. Mimicgen: A data generation system for scalable robot learning using human demonstrations, 2023.
- McInnes, L., Healy, J., and Melville, J. Umap: Uniform manifold approximation and projection for dimension reduction. *arXiv preprint arXiv:1802.03426*, 2018.
- Mendez, J. A., Hussing, M., Gummadi, M., and Eaton, E. Composuite: A compositional reinforcement learning benchmark. In Chandar, S., Pascanu, R., and Precup, D. (eds.), *Conference on Lifelong Learning Agents, CoLLAs 2022, 22-24 August 2022, McGill University, Montréal, Québec, Canada*, volume 199 of *Proceedings of Machine Learning Research*, pp. 982–1003. PMLR, 2022. URL <https://proceedings.mlr.press/v199/mendez22a.html>.
- Meng, L., Wen, M., Yang, Y., Le, C., Li, X., Zhang, W., Wen, Y., Zhang, H., Wang, J., and Xu, B. Offline pre-trained multi-agent decision transformer: One big sequence model conquers all starcraftii tasks. *arXiv preprint arXiv:2112.02845*, 2021.
- Merrill, W., Petty, J., and Sabharwal, A. The illusion of state in state-space models. *CoRR*, abs/2404.08819, 2024. doi: 10.48550/ARXIV.2404.08819. URL <https://doi.org/10.48550/arXiv.2404.08819>.
- Micikevicius, P., Narang, S., Alben, J., Diamos, G., Elsen, E., Garcia, D., Ginsburg, B., Houston, M., Kuchaiev, O., Venkatesh, G., et al. Mixed precision training. *arXiv preprint arXiv:1710.03740*, 2017.
- Mnih, V., Kavukcuoglu, K., Silver, D., Rusu, A. A., Veness, J., Bellemare, M. G., Graves, A., Riedmiller, M., Fidjeland, A. K., Ostrovski, G., Petersen, S., Beattie, C., Sadik, A., Antonoglou, I., King, H., Kumaran, D., Wierstra, D., Legg, S., and Hassabis, D. Human-level control through deep reinforcement learning. *Nature*, 518(7540): 529–533, 2015. doi: 10.1038/nature14236.
- Ni, T., Ma, M., Eysenbach, B., and Bacon, P.-L. When do transformers shine in rl? decoupling memory from credit assignment. *Advances in Neural Information Processing Systems*, 36, 2024.
- Octo Model Team, Ghosh, D., Walke, H., Pertsch, K., Black, K., Mees, O., Dasari, S., Hejna, J., Kreiman, T., Xu, C., Luo, J., Tan, Y. L., Sanketi, P., Vuong, Q., Xiao, T., Sadigh, D., Finn, C., and Levine, S. Octo: An open-source generalist robot policy, 2024.

- Orvieto, A., Smith, S. L., Gu, A., Fernando, A., Gülçehre, Ç., Pascanu, R., and De, S. Resurrecting recurrent neural networks for long sequences. In Krause, A., Brunskill, E., Cho, K., Engelhardt, B., Sabato, S., and Scarlett, J. (eds.), *International Conference on Machine Learning, ICML 2023, 23-29 July 2023, Honolulu, Hawaii, USA*, volume 202 of *Proceedings of Machine Learning Research*, pp. 26670–26698. PMLR, 2023. URL <https://proceedings.mlr.press/v202/orvieto23a.html>.
- Ota, T. Decision mamba: Reinforcement learning via sequence modeling with selective state spaces. *arXiv preprint arXiv:2403.19925*, 2024.
- Paszke, A., Gross, S., Massa, F., Lerer, A., Bradbury, J., Chanan, G., Killeen, T., Lin, Z., Gimelshein, N., Antiga, L., et al. Pytorch: An imperative style, high-performance deep learning library. *Advances in neural information processing systems*, 32, 2019.
- Patil, V., Hofmarcher, M., Dinu, M., Dorfer, M., Blies, P. M., Brandstetter, J., Arjona-Medina, J. A., and Hochreiter, S. Align-rudder: Learning from few demonstrations by reward redistribution. In Chaudhuri, K., Jegelka, S., Song, L., Szepesvári, C., Niu, G., and Sabato, S. (eds.), *International Conference on Machine Learning, ICML 2022, 17-23 July 2022, Baltimore, Maryland, USA*, volume 162 of *Proceedings of Machine Learning Research*, pp. 17531–17572. PMLR, 2022.
- Raad, M. A., Ahuja, A., Barros, C., Besse, F., Bolt, A., Bolton, A., Brownfield, B., Buttimore, G., Cant, M., Chakera, S., et al. Scaling instructable agents across many simulated worlds. *arXiv preprint arXiv:2404.10179*, 2024.
- Radford, A., Narasimhan, K., Salimans, T., Sutskever, I., et al. Improving language understanding by generative pre-training. 2018.
- Radford, A., Wu, J., Child, R., Luan, D., Amodei, D., Sutskever, I., et al. Language models are unsupervised multitask learners. *OpenAI blog*, 1(8):9, 2019.
- Radford, A., Kim, J. W., Hallacy, C., Ramesh, A., Goh, G., Agarwal, S., Sastry, G., Askell, A., Mishkin, P., Clark, J., Krueger, G., and Sutskever, I. Learning transferable visual models from natural language supervision. In Meila, M. and Zhang, T. (eds.), *Proceedings of the 38th International Conference on Machine Learning, ICML 2021, 18-24 July 2021, Virtual Event*, volume 139 of *Proceedings of Machine Learning Research*, pp. 8748–8763. PMLR, 2021.
- Radford, A., Kim, J. W., Xu, T., Brockman, G., McLeavey, C., and Sutskever, I. Robust speech recognition via large-scale weak supervision. *arXiv preprint arXiv:2212.04356*, 2022.
- Raparthi, S. C., Hambro, E., Kirk, R., Henaff, M., and Raileanu, R. Generalization to new sequential decision making tasks with in-context learning, 2023.
- Reed, S. E., Zolna, K., Parisotto, E., Colmenarejo, S. G., Novikov, A., Barth-Maron, G., Gimenez, M., Sulsky, Y., Kay, J., Springenberg, J. T., Eccles, T., Bruce, J., Razavi, A., Edwards, A., Heess, N., Chen, Y., Hadsell, R., Vinyals, O., Bordbar, M., and de Freitas, N. A generalist agent. *CoRR*, abs/2205.06175, 2022. doi: 10.48550/arXiv.2205.06175.
- Salzmann, T., Kaufmann, E., Arrizabalaga, J., Pavone, M., Scaramuzza, D., and Ryll, M. Real-time neural mpc: Deep learning model predictive control for quadrotors and agile robotic platforms. *IEEE Robotics and Automation Letters*, 8(4):2397–2404, 2023.
- Schmidhuber, J. Learning to control fast-weight memories: An alternative to dynamic recurrent networks. *Neural Comput.*, 4(1):131–139, 1992. doi: 10.1162/NECO.1992.4.1.131. URL <https://doi.org/10.1162/neco.1992.4.1.131>.
- Schmidhuber, J. Reinforcement learning upside down: Don’t predict rewards—just map them to actions. *arXiv preprint arXiv:1912.02875*, 2019.
- Schmidinger, N., Schneckenreiter, L., Seidl, P., Schimunek, J., Luukkonen, S., Hoedt, P.-J., Brandstetter, J., Mayr, A., Hochreiter, S., and Klambauer, G. Bio-xlstm: Generative modeling, representation and in-context learning of biological and chemical sequences. *Under reveiw*, 2024.
- Schmidt, D. and Schmied, T. Fast and data-efficient training of rainbow: an experimental study on atari. *arXiv preprint arXiv:2111.10247*, 2021.
- Schmied, T., Hofmarcher, M., Paischer, F., Pascanu, R., and Hochreiter, S. Learning to modulate pre-trained models in rl. *Advances in Neural Information Processing Systems*, 36, 2024a.
- Schmied, T., Paischer, F., Patil, V., Hofmarcher, M., Pascanu, R., and Hochreiter, S. Retrieval-augmented decision transformer: External memory for in-context rl. *arXiv preprint arXiv:2410.07071*, 2024b.
- Schulman, J., Wolski, F., Dhariwal, P., Radford, A., and Klimov, O. Proximal policy optimization algorithms. *ArXiv*, 2018.
- Schwarzer, M., Ceron, J. S. O., Courville, A., Bellemare, M. G., Agarwal, R., and Castro, P. S. Bigger, better, faster: Human-level atari with human-level efficiency.

- In *International Conference on Machine Learning*, pp. 30365–30380. PMLR, 2023.
- Schweighofer, K., Dinu, M.-c., Radler, A., Hofmarcher, M., Patil, V. P., Bitto-Nemling, A., Eghbal-zadeh, H., and Hochreiter, S. A dataset perspective on offline reinforcement learning. In *Conference on Lifelong Learning Agents*, pp. 470–517. PMLR, 2022.
- Shang, J., Kahatapitiya, K., Li, X., and Ryoo, M. S. Star-former: Transformer with state-action-reward representations for visual reinforcement learning. In *European Conference on Computer Vision*, pp. 462–479. Springer, 2022.
- Siebenborn, M., Belousov, B., Huang, J., and Peters, J. How crucial is transformer in decision transformer? *arXiv preprint arXiv:2211.14655*, 2022.
- Silver, D., Huang, A., Maddison, C. J., Guez, A., Sifre, L., van den Driessche, G., Schrittwieser, J., Antonoglou, I., Panneershelvam, V., Lanctot, M., Dieleman, S., Grewe, D., Nham, J., Kalchbrenner, N., Sutskever, I., Lillicrap, T. P., Leach, M., Kavukcuoglu, K., Graepel, T., and Hassabis, D. Mastering the game of Go with deep neural networks and tree search. *Nature*, 529(7587):484–489, 2016. doi: 10.1038/nature16961.
- Smith, J. T. H., Warrington, A., and Linderman, S. W. Simplified state space layers for sequence modeling. In *The Eleventh International Conference on Learning Representations, ICLR 2023, Kigali, Rwanda, May 1-5, 2023*. OpenReview.net, 2023. URL <https://openreview.net/forum?id=Ai8Hw3AXqks>.
- Srivastava, N., Hinton, G., Krizhevsky, A., Sutskever, I., and Salakhutdinov, R. Dropout: a simple way to prevent neural networks from overfitting. *The journal of machine learning research*, 15(1):1929–1958, 2014.
- Tassa, Y., Doron, Y., Muldal, A., Erez, T., Li, Y., de Las Casas, D., Budden, D., Abdolmaleki, A., Merel, J., Lefrancq, A., Lillicrap, T. P., and Riedmiller, M. A. Deepmind control suite. *CoRR*, abs/1801.00690, 2018.
- Tay, Y., Dehghani, M., Abnar, S., Shen, Y., Bahri, D., Pham, P., Rao, J., Yang, L., Ruder, S., and Metzler, D. Long range arena: A benchmark for efficient transformers. *arXiv preprint arXiv:2011.04006*, 2020.
- Todorov, E., Erez, T., and Tassa, Y. MuJoCo: A physics engine for model-based control. In *2012 IEEE/RSJ International Conference on Intelligent Robots and Systems*, pp. 5026–5033, October 2012a. doi: 10.1109/IROS.2012.6386109.
- Todorov, E., Erez, T., and Tassa, Y. Mujoco: A physics engine for model-based control. In *2012 IEEE/RSJ International Conference on Intelligent Robots and Systems*, pp. 5026–5033. IEEE, 2012b.
- Touvron, H., Martin, L., Stone, K., Albert, P., Almahairi, A., Babaei, Y., Bashlykov, N., Batra, S., Bhargava, P., Bhosale, S., Bikel, D., Blecher, L., Canton-Ferrer, C., Chen, M., Cucurull, G., Esiobu, D., Fernandes, J., Fu, J., Fu, W., Fuller, B., Gao, C., Goswami, V., Goyal, N., Hartshorn, A., Hosseini, S., Hou, R., Inan, H., Kardaş, M., Kerkez, V., Khabsa, M., Kloumann, I., Korenev, A., Koura, P. S., Lachaux, M., Lavril, T., Lee, J., Liskovich, D., Lu, Y., Mao, Y., Martinet, X., Mihaylov, T., Mishra, P., Molybog, I., Nie, Y., Poulton, A., Reizenstein, J., Rungta, R., Saladi, K., Schelten, A., Silva, R., Smith, E. M., Subramanian, R., Tan, X. E., Tang, B., Taylor, R., Williams, A., Kuan, J. X., Xu, P., Yan, Z., Zarov, I., Zhang, Y., Fan, A., Kambadur, M., Narang, S., Rodriguez, A., Stojnic, R., Edunov, S., and Scialom, T. Llama 2: Open foundation and fine-tuned chat models. *CoRR*, abs/2307.09288, 2023. doi: 10.48550/ARXIV.2307.09288. URL <https://doi.org/10.48550/arXiv.2307.09288>.
- Vaswani, A., Shazeer, N., Parmar, N., Uszkoreit, J., Jones, L., Gomez, A. N., Kaiser, I., and Polosukhin, I. Attention is all you need. *Advances in neural information processing systems*, 30, 2017.
- Vinyals, O., Babuschkin, I., Czarnecki, W. M., Mathieu, M., Dudzik, A., Chung, J., Choi, D. H., Powell, R., Ewalds, T., Georgiev, P., Oh, J., Horgan, D., Kroiss, M., Danihelka, I., Huang, A., Sifre, L., Cai, T., Agapiou, J. P., Jaderberg, M., Vezhnevets, A. S., Leblond, R., Pohlen, T., Dalibard, V., Budden, D., Sulsky, Y., Molloy, J., Paine, T. L., Gülçehre, Ç., Wang, Z., Pfaff, T., Wu, Y., Ring, R., Yogatama, D., Wünsch, D., McKinney, K., Smith, O., Schaul, T., Lillicrap, T. P., Kavukcuoglu, K., Hassabis, D., Apps, C., and Silver, D. Grandmaster level in starcraft II using multi-agent reinforcement learning. *Nat.*, 575(7782):350–354, 2019. doi: 10.1038/s41586-019-1724-z.
- Wang, G., Xie, Y., Jiang, Y., Mandlekar, A., Xiao, C., Zhu, Y., Fan, L., and Anandkumar, A. Voyager: An open-ended embodied agent with large language models, 2023.
- Wang, K., Zhao, H., Luo, X., Ren, K., Zhang, W., and Li, D. Bootstrapped transformer for offline reinforcement learning. *arXiv preprint arXiv:2206.08569*, 2022.
- Wen, C., Lin, J., Darrell, T., Jayaraman, D., and Gao, Y. Fighting copycat agents in behavioral cloning from observation histories. *Advances in Neural Information Processing Systems*, 33:2564–2575, 2020.
- Wolczyk, M., Zajkac, M., Pascanu, R., Kuciński, L., and Miloś, P. Continual world: A robotic benchmark for

- continual reinforcement learning. *Advances in Neural Information Processing Systems*, 34:28496–28510, 2021.
- Yu, T., Kumar, S., Gupta, A., Levine, S., Hausman, K., and Finn, C. Gradient surgery for multi-task learning. In Larochelle, H., Ranzato, M., Hadsell, R., Balcan, M., and Lin, H. (eds.), *Advances in Neural Information Processing Systems 33: Annual Conference on Neural Information Processing Systems 2020, NeurIPS 2020, December 6-12, 2020, virtual*, 2020a.
- Yu, T., Quillen, D., He, Z., Julian, R., Hausman, K., Finn, C., and Levine, S. Meta-world: A benchmark and evaluation for multi-task and meta reinforcement learning. In *Conference on robot learning*, pp. 1094–1100. PMLR, 2020b.
- Zheng, Q., Zhang, A., and Grover, A. Online decision transformer. In Chaudhuri, K., Jegelka, S., Song, L., Szepesvári, C., Niu, G., and Sabato, S. (eds.), *International Conference on Machine Learning, ICML 2022, 17-23 July 2022, Baltimore, Maryland, USA*, volume 162 of *Proceedings of Machine Learning Research*, pp. 27042–27059. PMLR, 2022.
- Zhu, G., Lin, Z., Yang, G., and Zhang, C. Episodic reinforcement learning with associative memory. In *International Conference on Learning Representations*, 2020.
- Zhu, L., Liao, B., Zhang, Q., Wang, X., Liu, W., and Wang, X. Vision mamba: Efficient visual representation learning with bidirectional state space model. *CoRR*, abs/2401.09417, 2024. doi: 10.48550/ARXIV.2401.09417. URL <https://doi.org/10.48550/arXiv.2401.09417>.

Appendix

A. Reproducibility Statement

We make the code base used for our experiments publicly available and release the datasets we generated. Both are available at: <https://github.com/ml-jku/LRAM>. We describe the environments we use for our experiments and provide dataset statistics in Appendix B. Furthermore, in Appendix C, we provide implementation details for all methods and a list of hyperparameters used for our experiments. In Appendix D, we present additional figures that accompany our results in the main text (e.g., all model sizes). Finally, in Appendices E and F, we provide further details on the conducted ablation studies and the embedding space analysis, respectively.

B. Environments & Datasets

B.1. General

We compile a large-scale dataset comprising 432 tasks from six domains, 3.4M trajectories, and 894M transitions in total (see Table 2). A key motivation behind our dataset compilation is the scarcity of suitable datasets that span many simulated tasks. To address this and to enable a robust comparison of different sequence model architectures, we aimed to assemble a collection of datasets that span as many tasks as possible. In particular, we focused on trajectories in simulated environments rather than real-world trajectories (Embodiment Collaboration et al., 2024), to enable faster iteration cycles. To facilitate usability for future works, we consider standard benchmarks that are widely adopted by the community (e.g., Atari, Meta-World).

We release our data pipeline and generated dataset, and hope that they can serve as a solid basis for future research on multi-task agents. To enable fast and targeted data-loading, every trajectory is stored in a separate `hdf5` file. We trade off some data-loading speed for disk space efficiency by compressing trajectories that contain image-based observations.

B.2. Atari

The Arcade Learning Environment (ALE) (Bellemare et al., 2013) is the standard benchmark for evaluating RL agents and consists of 57 Atari games. Input observations in Atari are RGB images, but as is standard practice, we gray-scale and crop frames ($|\mathcal{S}| = 1 \times 64 \times 64$). There are 18 discrete actions across all 57 Atari games ($|\mathcal{A}| = 18$), but individual games may use only a subset of these actions. Furthermore, we adopt the standard Atari recipe as used in prior works, including a frame skip of 4, maximum number of no-ops of 30, resetting on life loss, and reward clipping to $[-1, 1]$ (Mnih et al., 2015; Hessel et al., 2017).

Tasks. Similar to Lee et al. (2022), we assign 41 games to the training set and 5 additional tasks to the hold-out set. The 41 training tasks include:

amidar, assault, asterix, atlantis, bank-heist, battle-zone, beam-rider, boxing, breakout, carnival, centipede, chopper-command, crazy-climber, demon-attack, double-dunk, enduro, fishing-derby, freeway, frostbite, gopher, gravitar, hero, ice-hockey, jamesbond, kangaroo, krull, kung-fu-master, name-this-game, phoenix, pooyan, qbert, riverraid, road-runner, robotank, seaquest, time-pilot, up-n-down, video-pinball, wizard-of-wor, yars-revenge, zaxxon

The 5 hold-out tasks include: alien, pong, ms-pacman, space-invaders, star-gunner

Dataset. For Atari, we leverage the DQN-Replay dataset released by Agarwal et al. (2020). The dataset contains the trajectories seen over the entire training of the DQN agent (50M frames). We extract a subset of the last 5M transitions for every task, amounting to 205M transitions in total for the 41 training tasks. The number of episodes, the episode lengths, and total achieved rewards vary across tasks, as shown in Table 2.

B.3. Meta-World

The Meta-World benchmark (Yu et al., 2020a) consists of 50 manipulation tasks using a Sawyer robotic arm, ranging from opening or closing windows to pressing buttons. Meta-World is based on the MuJoCo physics engine (Todorov et al., 2012a). Observations in Meta-World are 39-dimensional continuous vectors ($|\mathcal{S}| = 1 \times 64 \times 39$), and actions are represented by 6

Table 2. Atari Dataset Statistics.

Task	# of Trajectories	Mean Length	Mean Return
amidar	1813	2753	145
pooyan	2773	1800	176
frostbite	5218	766	18
video-pinball	1023	3902	266
wizard-of-wor	3059	1314	15
chopper-command	5452	738	18
breakout	3780	1300	39
phoenix	3307	1509	49
asterix	5250	951	55
enduro	571	8720	636
kung-fu-master	1775	2812	131
hero	3022	1345	168
assault	3782	1170	77
demon-attack	1649	2431	116
qbert	3939	1138	155
jamesbond	2841	1758	11
bank-heist	4146	1204	62
up-n-down	3246	1538	99
centipede	6879	582	81
boxing	4796	1041	63
battle-zone	1933	2134	15
name-this-game	988	5049	389
zaxxon	2561	1950	12
beam-rider	1232	3248	77
time-pilot	3886	1029	11
ice-hockey	1465	3407	-6
riverraid	2645	1512	143
krull	3032	1319	528
gopher	1817	2338	185
freeway	2438	2048	33
seaquest	2807	1779	150
double-dunk	1774	2815	0
road-runner	3308	1217	135
atlantis	186	26349	1394
gravitar	6187	646	1
yars-revenge	4094	1036	96
crazy-climber	1105	3954	572
kangaroo	1787	2792	50
fishing-derby	2737	1825	0
carnival	21131	194	37
robotank	747	6652	56
Average	3321	2734	153

continuous dimensions ($|\mathcal{A}| = 18$) in range $[-1, 1]$. All tasks share a common action and state space. Following Wolczyk et al. (2021) and Schmied et al. (2024a), we limit the episode lengths to 200 interactions.

Tasks. We follow Yu et al. (2020a) and split the 50 Meta-World tasks into 45 training tasks (MT45) and 5 evaluation tasks (MT5).

The 45 training tasks are:

reach, push, pick-place, door-open, drawer-open, drawer-close, button-press-topdown, peg-insert-side, window-open, window-close, door-close, reach-wall, pick-place-wall, push-wall, button-press, button-press-topdown-wall, button-press-wall, peg-unplug-side, disassemble, hammer, plate-slide, plate-slide-side, plate-slide-back, plate-slide-back-side, handle-press, handle-pull, handle-press-side, handle-pull-side, stick-push, stick-pull, basketball, soccer, faucet-open, faucet-close, coffee-push, coffee-pull, coffee-button, sweep, sweep-into, pick-out-of-hole, assembly, shelf-place, push-back, lever-pull, dial-turn

The 5 evaluation tasks are: bin-picking, box-close, door-lock, door-unlock, hand-insert

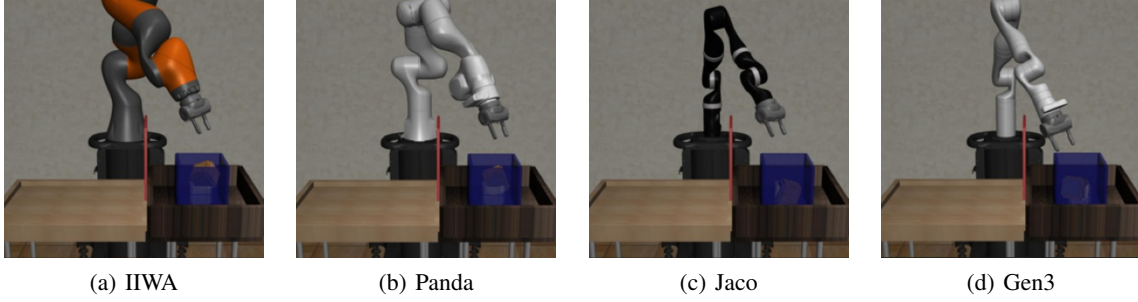


Figure 8. Illustration of the four supported robot arms in **Composuite** (Mendez et al., 2022).

Dataset. For Meta-World, we use the datasets released by (Schmied et al., 2024a), which contain 2M transitions per task and consequently 90M transitions in total for the training set. All episodes last for 200 environment interaction steps, and consequently, there are 10K episodes for every task. For detailed dataset statistics per task, we refer to their publication.

B.4. DMControl

The DMControl benchmark (Tassa et al., 2018) consists of 30 different robotic tasks. Unlike Meta-World, the benchmark contains robots with different morphologies instead of a single common Sawyer arm. Due to the different robot morphologies, the state and action spaces vary across tasks ($3 \leq |\mathcal{S}| \leq 24$, $1 \leq |\mathcal{A}| \leq 6$), with all actions in the range $[-1, 1]$.

Tasks. We do not use all 30 tasks contained in the DMControl benchmark, but select 16 of the 30 tasks that have been used in prior works (Hafner et al., 2019; Schmied et al., 2024a;b), which we refer to as DMC11 and DMC5, respectively.

The 11 training tasks are:

finger-turn_easy, fish-upright, hopper-stand, point_mass_easy, walker-stand, walker-run, ball_in_cup_catch, cartpole-swingup, cheetah-run, finger-spin, reacher_easy

The 5 evaluation tasks are:

cartpole-balance, finger-turn_hard, pendulum-swingup, reacher-hard, walker-walk

Dataset. For DMControl, we generate 10M transitions per task by training task-specific SAC (Haarnoja et al., 2018) agents, using the same setup as Schmied et al. (2024a). Episodes in all DMControl tasks last for 1000 environment steps, and per time-step a maximum reward of +1 can be achieved, which results in a maximum reward of 1000 per episode. Consequently, our training set contains 10K episodes per task, amounting to 110K episodes and 110M transitions in total across all tasks. We list the dataset statistics for all 11 tasks in Table 3.

Table 3. DMControl Data statistics.

Task	# of Trajectories	Mean Length	Mean Return
point_mass_easy	10K	1K	851
cheetah_run	10K	1K	385
walker_run	10K	1K	230
ball_in_cup_catch	10K	1K	969
hopper_stand	10K	1K	460
walker_stand	10K	1K	939
finger_turn_easy	10K	1K	954
reacher_easy	10K	1K	938
cartpole_swingup	10K	1K	817
fish_upright	10K	1K	815
finger_spin	10K	1K	966
Average	19628	152	8.2

B.5. Composuite

The Composuite benchmark (Mendez et al., 2022) is a robotics benchmark for grasping and object manipulation. The benchmark is implemented on top of `robotsuite` (Zhu et al., 2020), which in turn leverages the MuJoCo simulator under the hood (Todorov et al., 2012b). Composuite contains a mix of 4 simulated robot arms: `IIWA`, `Jaco`, `Gen3`, and `Panda` (see Figure 8). All arms share a common state and action space containing 93 continuous state dimensions and 8 continuous action dimensions, respectively ($|\mathcal{S}| = 93$, $|\mathcal{A}| = 8$).

Tasks. CompoSuite is designed as a compositional multi-task benchmark for RL, in which a particular *robot* manipulates a particular *object* given an *objective*, while avoiding *obstacles*. Overall, there are 4 robot arms, 4 objects, 4 obstacles, and 4 task objectives. This results in 256 possible robot/object/objective/obstacle combinations. For our experiments, we assign 240 tasks to the training set and use the remaining 16 tasks as a hold-out set (`Panda` and `Object_Wall`) combinations. For a list of all 256 tasks, we refer to Mendez et al. (2022).

Dataset. For Composuite, we leverage the datasets released by Hussing et al. (2023). For every task, we select 2000 episodes, which last on average for 500 steps. This amounts to 1M transitions per task, and 240M transitions across all 240 training tasks. For dataset statistics, we refer to Hussing et al. (2023).

B.6. Mimicgen

Similar to Composuite, Mimicgen (Mandlekar et al., 2023) is based on `robotsuite` and the MuJoCo simulator. Mimicgen is designed for automatically synthesizing large-scale datasets from only a handful of human demonstrations. Observations in Mimicgen can be represented as images (from multiple cameras) or low-dimensional continuous states. For our experiments, we opt for the low-dimensional state representation to simplify learning. Therefore, observations and actions are represented by 37-dimensional and 7-dimensional continuous vectors, respectively ($|\mathcal{S}| = 37$, $|\mathcal{A}| = 7$). Similar to Composuite, Mimicgen supports 4 different robot arms: `Panda`, `IIWA`, `Sawyer`, and `UR5e` (see Figure 9).

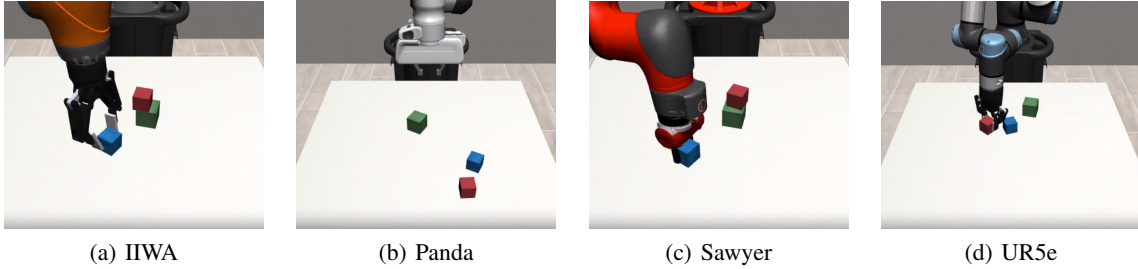


Figure 9. Illustration of the four supported robot arms in Mimicgen (Mandlekar et al., 2023) solving the `stack-three` task.

Tasks. Mimicgen consists of 24 diverse tasks, including stacking blocks, reassembling objects, and even long-horizon tasks like coffee preparation. These 24 tasks can be performed with the four supported robot arms, amounting to 96 tasks in total.

Dataset. Mandlekar et al. (2023) released datasets for the 24 tasks using the default robot arm `Panda`. To increase the dataset diversity, we additionally generated data for the remaining 3 robot arms. However, not all data generation runs produce successful trajectories, and we discard the ones with too few successful trajectories. Our final dataset for Mimicgen contains 83 training and 2 evaluation tasks. For each task, we collect 1000 successful demonstrations (we do not include unsuccessful trajectories). Episode lengths vary across tasks, ranging from 260 to 850 environment steps.

B.7. Procgen

The Procgen benchmark consists of 16 procedurally-generated video games (Cobbe et al., 2020a). Observations in Procgen are RGB images of dimension $3 \times 64 \times 64$. However, for training efficiency, we apply gray-scaling to image observations ($|\mathcal{S}| = 1 \times 64 \times 64$). All 16 environments share a common action space of 15 discrete actions ($|\mathcal{A}| = 16$). Procgen is designed to test the generalization abilities of RL agents. Consequently, procedural generation is employed to randomize background and colors, while retaining the game dynamics.

Tasks. Following prior works (Raparthi et al., 2023; Schmied et al., 2024b), we assign 12 and 4 tasks to the training and hold-out sets, respectively. The 12 training tasks are:

bigfish, bossfight, caveflyer, chaser, coinrun, dodgeball,
fruitbot, heist, leaper, maze, miner, starpilot

The 4 hold-out tasks are: climber, ninja, plunder, jumper

Dataset. We leverage the datasets released by (Schmied et al., 2024b), which contain 20M transitions per task. The datasets were generated by recording all transitions observed by training RL agents for 25M steps, followed by uniform subsampling to 20M transitions. Consequently, the dataset contains mixed quality trajectories ranging from random (beginning of training) to expert (end of training). We list the dataset statistics for all 16 tasks in Table 4.

Table 4. Progen Data statistics.

Task	# of Trajectories	Mean Length	Mean Return
bigfish	82835	230	6.251
bossfight	112459	141	1.946
caveflyer	151694	105	7.745
chaser	93612	212	3.248
coinrun	261117	51	9.473
dodgeball	144364	137	2.884
fruitbot	73653	270	16.094
heist	101361	196	8.405
leaper	296084	67	4.446
maze	482245	41	9.432
miner	288818	68	11.8
starpilot	96468	206	17.3
Average	182059	144	8.3

C. Experimental & Implementation Details

C.1. Training & Evaluation

In our experiments, we compare two variants of xLSTM, Mamba and DT. For our main experiments in Section 4.2, we train all models for 200K updates, and evaluate after every 50K update steps. We report the mean and 95% confidence intervals over three seeds in our experiments, as suggested by Agarwal et al. (2021). For every evaluation task, we take the average of 3 evaluation seeds.

We train our agents with a batch size of 128 and gradient accumulation across the 6 domains, such that every domain is represented with the same proportion. This is to compare Consequently, the effective batch size is 768. We use a learning rate of $1e^{-4}$, 4000 linear warm-up steps followed by a cosine decay to $1e^{-6}$, and train using the AdamW optimizer (Loshchilov & Hutter, 2018). In addition, we employ gradient clipping of 0.25, weight decay of 0.01 for all models. We do not employ Dropout, as is standard practice in DTs, as we found that it negatively affects performance (see Section 4.3). We use separate reward scales of 200, 100, and 20 for Meta-World, DMControl, and Atari, respectively. Furthermore, for all domains, we set the target return to the maximum return achieved for a particular task in the training datasets. This is particularly useful for domains where the maximum returns differ heavily across tasks (e.g., Atari). We list all hyperparameters in Table 5.

We want to highlight that we opt to represent every domain with approximately equal proportion in every update step. This is, because we aim to study how the different backbones perform across domains, rather than optimizing performance on specific domains. However, to better understand the impact of the data ratios on multitask capabilities, we believe it would be interesting to study other data ratios in future work. Varying the data ratios would, for example, allow studying potential interferences between the 432 tasks.

C.2. Context Lengths

By default, we train all models with a context length $C = 50$ timesteps. For every timestep, there are three tokens (s/rt/r), and consequently, the effective context length is 150. We found that performance improves for longer context lengths (see Section E.1), but limit our experiments to $C = 50$ to reduce the computational cost.

Table 5. Hyperparameters for LRAM.

Parameter	Value
Gradient steps	200K
Evaluation frequency	50K
Evaluation episodes	5
Optimizer	AdamW
Batch size	128
Gradient accumulation	6
Lr schedule	Linear warm-up + Cosine
Warm-up steps	4000
Learning rate	1e-4 \rightarrow 1e-6
Weight decay	0.01
Gradient clipping	0.25
Dropout	0.2
Context len (timesteps)	50
Reward scale	per-domain
Target return	per-task

C.3. Model Architectures

We train models across 4 model sizes: 16M, 48M, 110M, and 206M. We follow [Lee et al. \(2022\)](#) in selecting the number of layers and hidden dimensions. For xLSTM and Mamba, we use twice the number of layers blocks to match the number of parameters of the Transformer ([Beck et al., 2024](#); [Gu et al., 2024](#)) (see Table 6). For our xLSTM [7:1] variant, which contains sLSTM blocks, we strive to maintain the same ratio as proposed by [Beck et al. \(2024\)](#). Not all our model sizes are divisible by 8, and only the 16M and 110M models exhibit the exact 7:1 ratio of mLSTM to sLSTM blocks. For consistency, however, we maintain the same notation as ([Beck et al., 2024](#)). We place sLSTM blocks at positions [1], [1, 3], [1, 3], and [1, 3, 5] for the 16M, 48M, 110M, 206M, respectively.

Across backbones, we use linear layers to encode continuous states, reward returns-to-go, similar to [Chen et al. \(2021\)](#). The maximal state dimension across continuous control environments is 204 in our experiments. To use a shared linear embedding layer for continuous states, we pad states that have a lower number of dimensions to 204 dimensions using zeros. To encode image inputs on visual domains, we use the IMPALA-CNN proposed by [Espeholt et al. \(2018\)](#) and adopted by previous works on Procgen ([Cobbe et al., 2020a](#)) and Atari ([Schmidt & Schmied, 2021](#); [Schwarzer et al., 2023](#)). Consequently, we do not make use of discretization of continuous states or patchification of images. This design choice significantly reduces the sequence length to only three tokens per time-step (see Appendix C.2) and consequently results in faster inference.

For continuous actions, we make use of discretization and discretize of every action dimension into 256 uniformly-spaced bins, similar to [Reed et al. \(2022\)](#) and [Brohan et al. \(2023b\)](#). We experimented with lower/higher numbers of bins, but did not observe a benefit beyond 256 bins. Consequently, this resolution is sufficient for the environments we consider. We use a shared action head to predict the action bins of all continuous dimensions jointly. The maximum number of continuous action dimensions is 8 in our experiments, and consequently, the number of discrete action classes is 2048. In addition, there are 18 discrete actions originating from Atari and Procgen. Therefore, our action head learns to predict the correct action among the 2066 discrete classes. While different environments may have different action dimensions, the model predicts all action dimensions jointly. At inference time, the number of action dimensions of the current environment is known, and we extract the respective dimensions from the joint predictions. We opt for the shared action head representation, as this further speeds up inference and does not require autoregressive action prediction.

For the Transformer baseline, we use global positional embeddings similar to [Chen et al. \(2021\)](#). For the recurrent backbones, we do not make use of positional encodings.

Table 6. Model Sizes.

Model	Layers	Hidden Dim	Heads	Parameters
Transformer	4	512	8	16M
Transformer	6	768	12	48M
Transformer	8	1024	16	110M
Transformer	10	1280	20	206M
Mamba	8	512	-	16M
Mamba	12	768	-	48M
Mamba	16	1024	-	110M
Mamba	20	1280	-	206M
xLSTM	8	512	4	16M
xLSTM	12	768	4	48M
xLSTM	16	1024	4	110M
xLSTM	20	1280	4	206M

C.4. Hardware & Training Times

We train all our models on a server equipped with 4 A100 GPUs. We use distributed data parallel to distribute the workload, as supported in PyTorch (Paszke et al., 2019). Training times range from 5 hours for the smallest DT model to 30 hours for the largest Mamba model. Throughout all our experiments, we use mixed precision training (Micikevicius et al., 2017) as supported in PyTorch to speed up training time.

We evaluate our models after every 50K steps. However, periodically evaluating the trained agents on all 432 tasks sequentially is time-consuming. Therefore, we perform parallel evaluation with 4 processes at a time. For multi-GPU setups, we distribute the evaluation workload among the available GPUs. For example, with 4 available GPUs and 4 evaluation processes per GPU, 16 environments are evaluated simultaneously. Consequently, the total evaluation time for all 432 tasks ranges from 18 minutes for the smallest DT model to roughly 2 hours for the largest Mamba model.

D. Additional Results

D.1. Training Tasks

In Figures 10 and 11, we report the normalized scores obtained per domain and the average learning curves across tasks for all four model sizes.

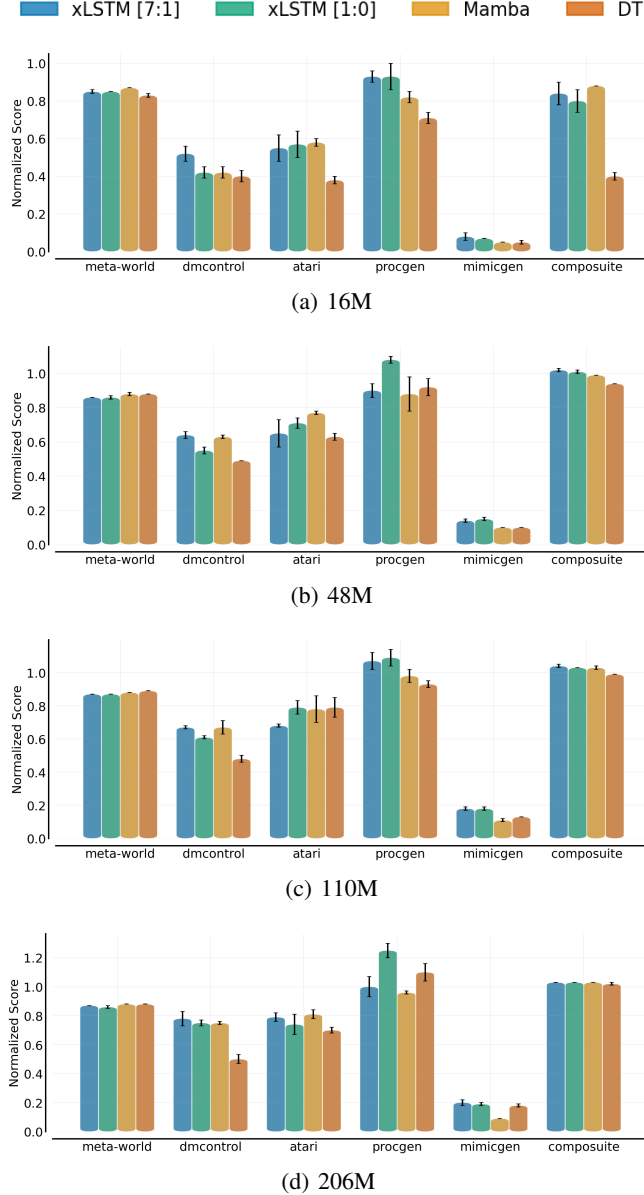


Figure 10. **Normalized scores** per-domain all four model sizes: 16M, 48M, 110M, and 206M. For Meta-World, DMControl, Mimicgen, Composite, and Procgen we report data-normalized scores, for Atari we report human-normalized scores.

In Figure 12, we report the training perplexity on the 432 training tasks over 200K updates. Here, we observe that the training perplexity behaves similarly to the validation perplexity. This is expected, as our models see most transitions only a single time (see Table 2 for the number of repetitions per domain).

Furthermore, we report the scaling curves with an additional model size of 408M parameters in Figure 13. Due to the high computational cost of the 408M models, we were currently only able to conduct a single run for this size. However, we aim to provide further empirical evidence for these model sizes in future work.

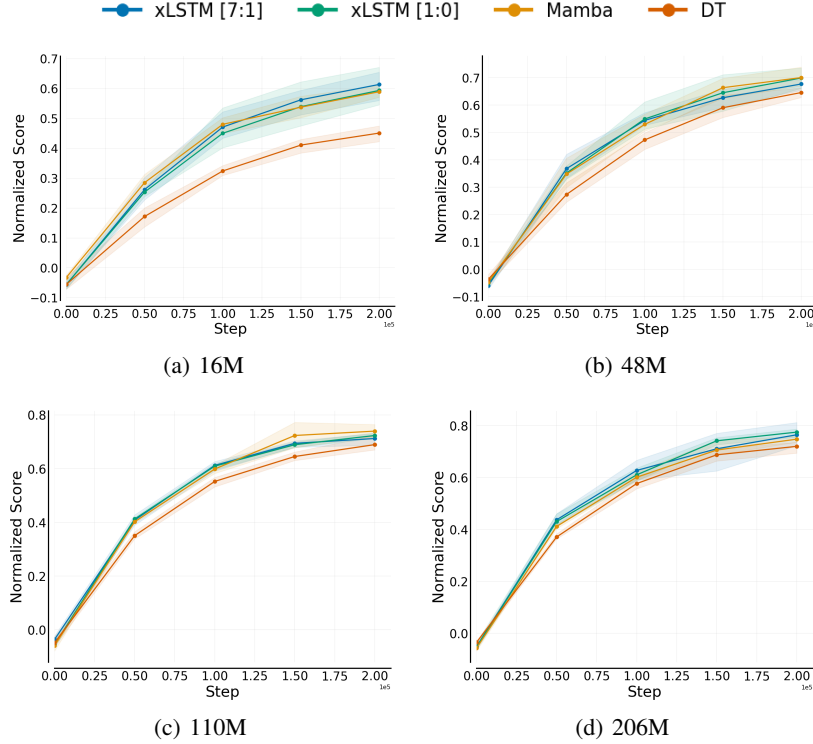


Figure 11. Learning curves for all four model sizes, 16M, 48M, 110M, and 206M, on the training tasks.

D.2. Hold-out Tasks

In Figure 14, we show the zero-shot evaluation performance on the hold-out tasks 14. We want to highlight that the performance declines for all methods and model sizes compared to performance on training tasks. This is because hold-out tasks exhibit severe shifts in state-spaces, action-spaces, and reward functions.

D.3. Fine-Tuning

In Figure 15, we present the fine-tuning evaluation performance on the held-out tasks. We compare xLSTMs trained from scratch against xLSTMs initialized with the pre-trained weights. We do observe consistent improvement of the pre-trained models over the models trained from scratch. While we train on a substantial number of environments, the total amount of data used is still only a fraction of that employed in training other large-scale models, such as LLMs. Consequently, we do not observe comparable few-shot generalization. However, we anticipate that few-shot generalization capabilities will emerge as we increase both data volume and model size.

D.4. In-context Learning

We assess the ICL abilities of modern recurrent architectures on the Dark-Room environment considered in prior works on in-context RL (Laskin et al., 2022; Lee et al., 2023; Schmied et al., 2024b). In Dark-Room, the agent is located in a dark room. The task is to navigate to an invisible goal location in that dark room. The state is partially observable, as the agent only observes its own x-y position on the grid ($|\mathcal{S}| = 2$). The action space consists of 5 discrete actions: move up, move down, move left, move right, stay ($|\mathcal{A}| = 5$). Upon reaching the goal location, the agent receives a reward of +1 for every step in the episode it resides in the goal location. Consequently, the agent first has to explore the room to find the goal. Once the goal location is found (as indicated by the positive reward), the agent can exploit this knowledge. Given a multi-episodic context, the agent should be able to exploit information contained in the previous trials (e.g., exploiting one path vs. avoiding another).

In our experiments, the Dark-Room is a 10×10 grid and episodes last for 100 steps, starting in the top left corner of the

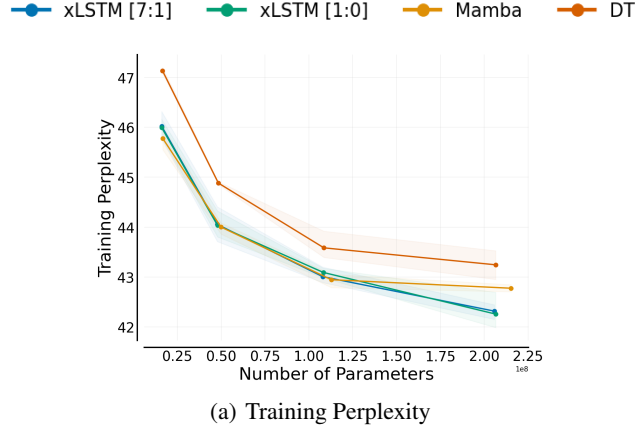


Figure 12. Scaling comparison. We compare xLSTM, Mamba, DT in four model sizes: 16M, 48M, 110M, and 206M parameters. We show the **training perplexity** on the training dataset to evaluate the sequence prediction performance.

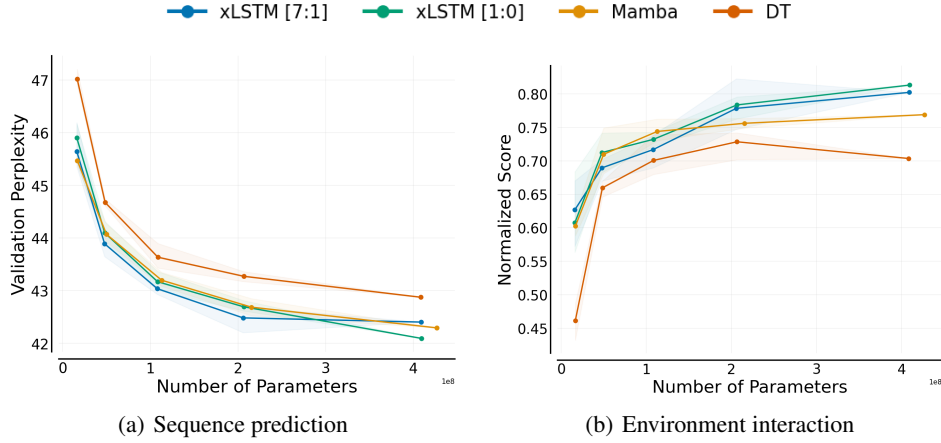


Figure 13. **Scaling comparison** with additional 408M parameter models. We show the (a) validation perplexity on the hold-out datasets, and (b) normalized scores obtained from evaluating in the training task environments, averaged over all 6 domains.

grid. We adopt the same experiment setup as [Schmied et al. \(2024b\)](#) and leverage their datasets. We train 16M parameter agents on datasets from 80 randomly selected goal locations in the grid. The datasets contain 100K transitions per task and are obtained by training task-specific PPO ([Schulman et al., 2018](#)) agents. Then, we evaluate the in-context abilities of our agents on 20 hold-out goal locations. During evaluation, the agent is given 40 episodes to interact with the environment, which we refer to as ICL-trials. Furthermore, we adopt the AD ([Laskin et al., 2022](#)) framework for training our agents with a multi-episodic context. We use the same sequence representation as used in our main experiments, consisting of states, returns-to-go (target return set to 80 during evaluation), and rewards. Note that this differs from the sequence representation used by [Laskin et al. \(2022\)](#). We set the context length for all agents to the equivalent of two episodes, which amounts to 200 timesteps in total.

In Figure 16, we report the ICL performance over the 40 ICL trials on (a) 80 training locations and (b) 20 hold-out locations for the 4 different backbones considered in this work. We observe that the recurrent backbones attain considerably higher scores than the Transformer backbone. Furthermore, we find that xLSTM [7:1] attains the highest overall scores, which we attribute to the state-tracking abilities ([Merrill et al., 2024](#)) of sLSTM blocks. We aim to explore the ICL abilities of modern recurrent backbones more in future work.

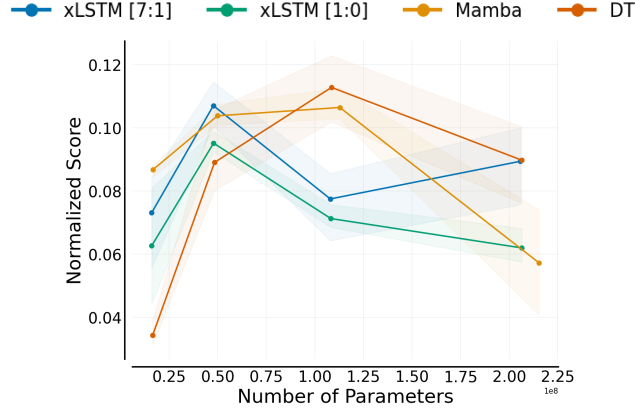


Figure 14. Scaling comparison. **Zero-shot performance on hold-out tasks** at four model sizes, 16M, 48M, 110M, and 206M. Note that performance declines for all methods and model sizes compared to performance on training tasks. This is because hold-out tasks exhibit severe shifts in state-spaces, action-spaces, and reward functions.

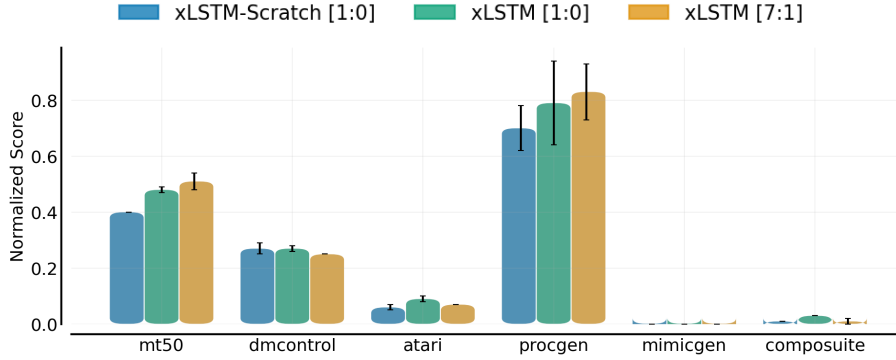


Figure 15. **Fine-tune performance on hold-out tasks.** We compare the performance of a pretrained xLSTM against an xLSTM trained from scratch, both with 16 million parameters. We select the top 5% of trajectories from our held-out tasks based on performance and use this subset to fine-tune the models. We perform 25K update steps during fine-tuning and show the normalized scores, averaged across held-out tasks from each domain.

D.5. Inference Time Comparisons

We empirically examine the difference in inference speed between of our models. Similar to [De et al. \(2024\)](#), we report both latency and throughput. For real-time applications, latency is the more important dimension, and therefore, we focus our analysis on latency.

D.5.1. LATENCY

In Figures 17 and 18, we report the latencies for DT and xLSTM with the same number of layer blocks as DT, and twice the number of layer blocks as DT, respectively. We conduct our comparison for two different batch sizes and across varying sequence lengths.

D.5.2. THROUGHPUT

In Figures 19 and 20, we similarly report the attained throughput for DT and xLSTM with the same number of layer blocks as DT, and twice the number of layer blocks as DT, respectively. We conduct our comparison for two fixed context lengths and varying batch sizes.

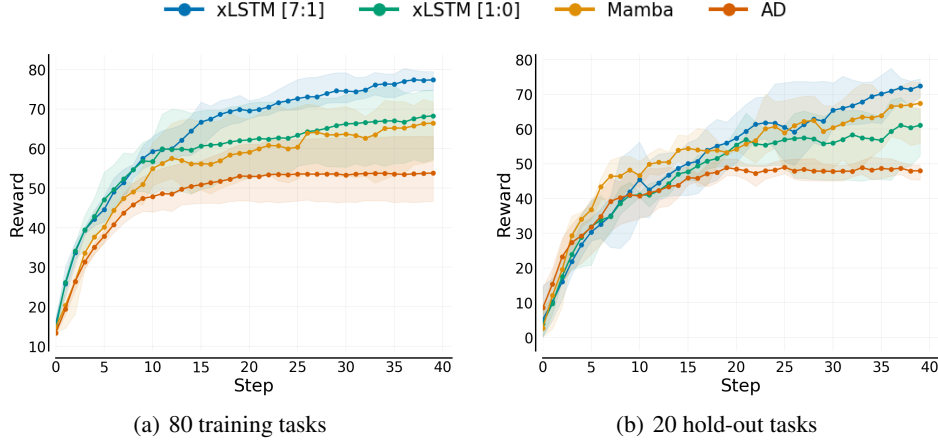


Figure 16. In-context Learning on Dark-Room 10×10 .

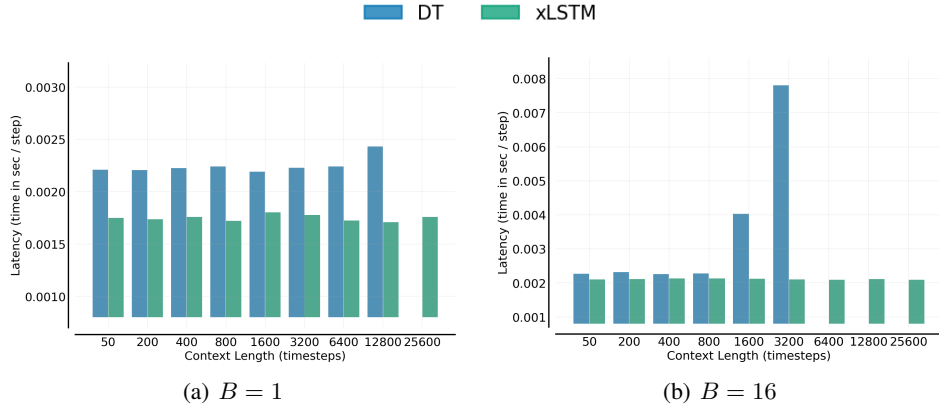


Figure 17. **Latency.** We report latency with (a) batch size of 1 and (b) batch size of 16 for DT and xLSTM with 206M parameters. For xLSTM, we use the same number of layer blocks as DT and a higher hidden dimension to match parameters.

D.5.3. xLSTM: KERNEL COMPARISONS

We leverage custom kernels for xLSTM to conduct our inference-speed comparisons. In particular, we compare 4 variants: recurrent-style inference with and without kernel acceleration, and chunkwise inference with and without kernel acceleration. In our experiments, every timestep contains 3 individual tokens. Consequently, regular recurrent-style inference requires iterating over the token sequence of length 3 in a loop, given the hidden state of the previous timestep. This requires 3 forward passes. In contrast, the chunkwise implementation operates on chunks of timesteps given a hidden state. Consequently, this only requires a single forward pass. In Figure 21, we illustrate the impact of kernel acceleration. We find that our chunkwise kernels result in considerably lower latencies. Interestingly, we find that for $B = 1$, our chunkwise implementation without kernel acceleration is faster than the recurrent-style inference with kernel acceleration. However, as the batch size increases, this trend reverses. This highlights the importance of kernel acceleration for efficient inference.

D.5.4. xLSTM: IMPACT OF HEAD DIMENSION

In our experiments, we found that choosing the appropriate head dimension is critical to enable high throughput for xLSTM. Therefore, we conduct an inference ablation with xLSTM 206M in which we vary the number of heads between 4 and 32, while keeping the total hidden dimension constant, resulting in different head dimensions. We find that throughput increases considerably when increasing the number of heads (see Figure 22). For 4 heads, and therefore the highest head dimension, the total throughput saturates at batch size 96. In contrast, when increasing the number of heads to 32 (i.e., decreasing the head dimension), the total throughput continues to increase. This is because a higher head dimension incurs more FLOPS.

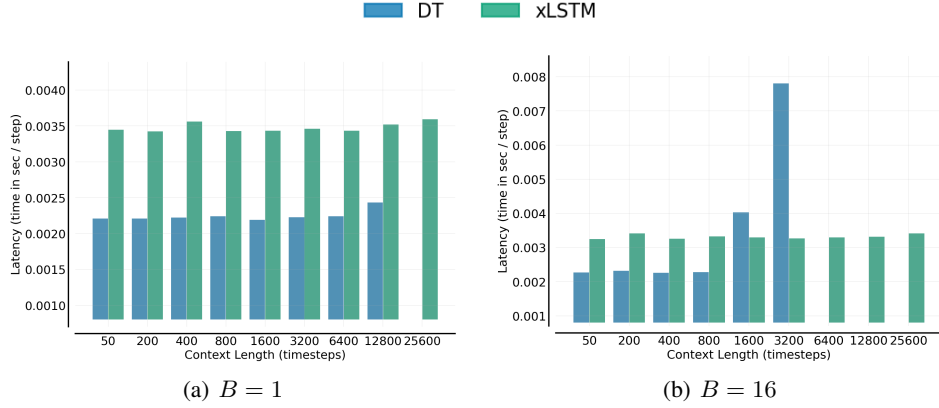


Figure 18. **Latency.** We report latency with (a) batch size of 1 and (b) batch size of 16 for DT and xLSTM with 206M parameters. For xLSTM, we use twice the number of layer blocks and the same hidden dimension as the Transformer.

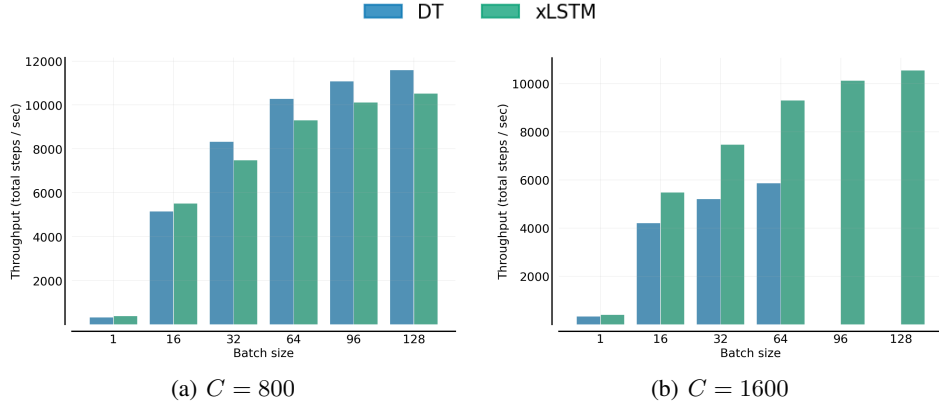


Figure 19. **Throughput.** We report throughput with (a) context size of 800, and (b) context size of 1600 timesteps for DT and xLSTM with 206M parameters. For xLSTM, we use the same number of layer blocks as DT and a higher hidden dimension to match parameters.

E. Ablations

E.1. Removing action condition

E.1.1. DT ON META-WORLD

We found that removing actions from the context results in better performance across backbones. In Figure 23, we report the learning curves over 200K updates for DT with varying context lengths on Meta-World, both with and without actions in the context. While context lengths beyond 1 hurt performance when training with actions, the reverse is true when training without actions. This is in contrast to recent works, which did not benefit from longer contexts (Octo Model Team et al., 2024). However, while removing actions improves performance on Meta-World, it does not affect performance on discrete control. On Meta-World, we observed that the models become overly confident (high action logits), which is problematic if poor initial actions are produced. We assume this is because in robotics, actions change smoothly, and by observing previous actions, the agent learns shortcuts. A similar issue has been identified by Wen et al. (2020) and termed the *copycat problem*, because the agent is incentivized to copy previous actions. Our solution is to remove actions from the input sequence. This prevents the agent from learning shortcuts and alleviates the copycat problem.

E.1.2. DT ON ALL 432 TASKS.

To further investigate the effect of removing actions from the context, we repeat this ablation on the full 432 tasks and 6 domains at the 206M model scale. In Figure 24, we report the learning curves for a DT with varying sequence lengths

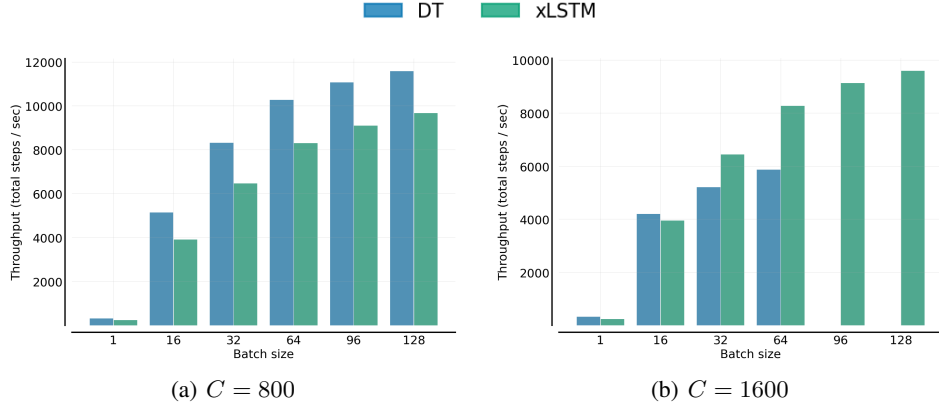


Figure 20. **Throughput.** We report throughput with (a) context size of 800, and (b) context size of 1600 timesteps for DT and xLSTM with 206M parameters. For xLSTM, we use twice the number of layer blocks and the same hidden dimension as the Transformer.

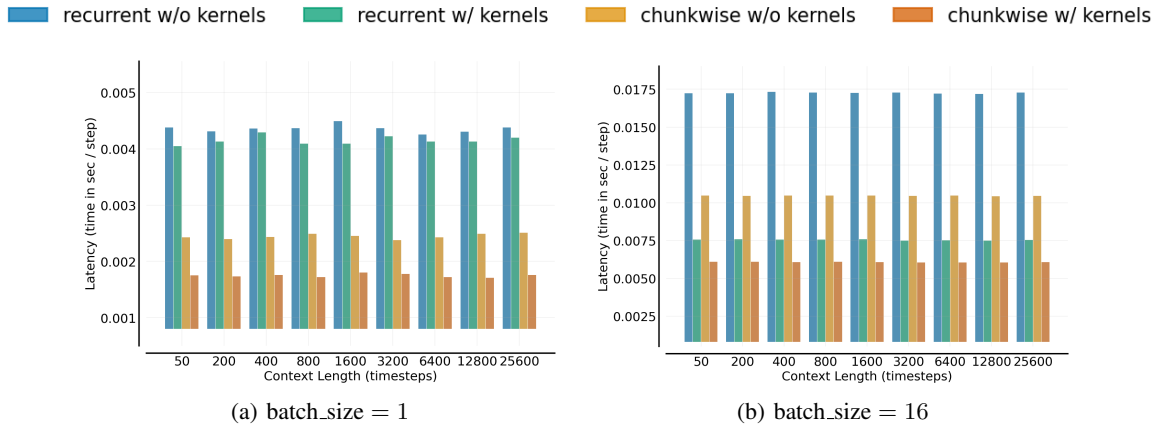


Figure 21. **Impact of kernel acceleration.** We report latency with (a) batch size of 1 and (b) batch size of 32 for DT and xLSTM with 206M parameters. For xLSTM, we use the same number of layer blocks as DT and a higher hidden dimension to match parameters.

trained (a) with and (b) without actions in the agent’s context. Similar to the single-domain study on Meta-World with smaller models, we find that providing a longer context does not improve performance, resulting in a normalized score of around 0.3 across domains. In contrast, without action in the context, we observe a consistent improvement in the evaluation performance as the sequence length increases. In fact, the normalized score increases from around 0.3 with $C = 1$ to 0.7 with $C = 50$. For computational reasons, we only report one seed per sequence length in this experiment, but we believe that the overall trends are clear.

To better understand on which domains the longer context benefits or hurts our agents, we also present the normalized score per domain in Figure 25. Without actions in the context, we find that longer context consistently benefits the performance across domains. With actions in the context, we observe that on Meta-World and DMControl, the performance deteriorates for $C > 1$. In contrast, on the discrete control domains Atari and Procgen, but also on the continuous control domain Composuite, performance tends to improve with $C > 1$. This suggests that the copycat problem is particularly present on Meta-World and DMControl. However, note that the final performances on Atari, Procgen, and Mimicgen are considerably worse when actions are present in the context compared to when they are not.

To further investigate this, we compute the MSE between subsequent actions in the training dataset (similar to Wen et al. (2020)) for the continuous control domains and report them in Table 7. Indeed, we find that Meta-World and DMControl exhibit significantly lower MSEs between subsequent actions than Composuite. While Mimicgen also exhibits a low MSE between consecutive actions, all backbones perform poorly on this challenging benchmark. Consequently, we conclude that removing actions from the agent’s context is particularly effective for domains where actions change smoothly.

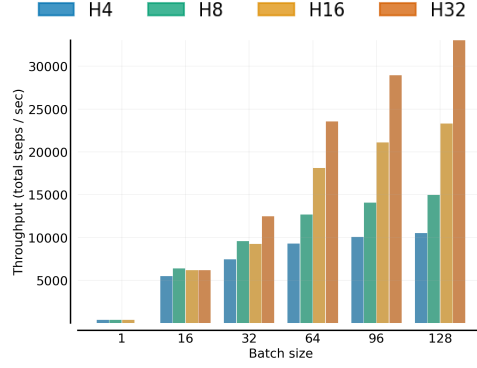


Figure 22. Throughput comparison for xLSTM 206M with varying **numbers of heads** but fixed total hidden size. By default, we used 4 heads for our experiments. Increasing the number of heads results in higher throughput.

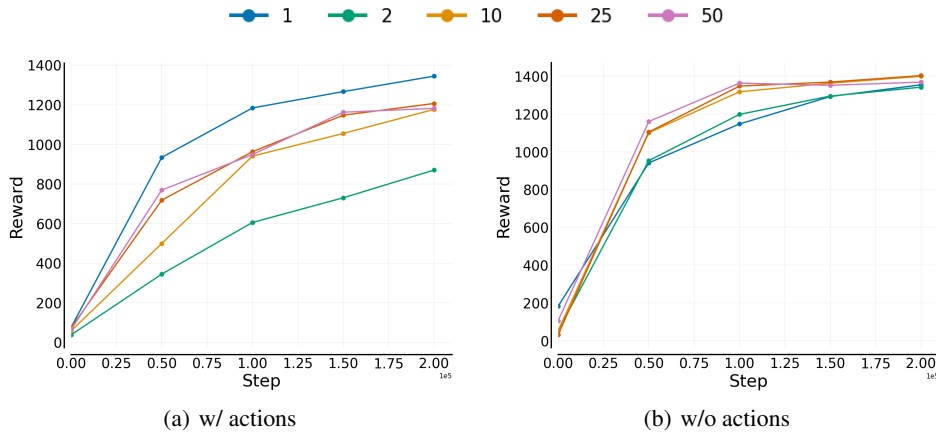


Figure 23. Ablation on removing the **action condition** for varying context lengths C . Performance of DT (a) with, and (b) without action condition on **Meta-World**. With action in the context, $C > 1$ harms performance due to overconfidence in action predictions. Without actions in the context, the performance of DT improves with increasing C .

This result highlights the fact that large action models can strongly benefit from increased context length, even on the simulated environments we consider in this work. Furthermore, we believe that this effect can be even bigger in complex real-world environments that require longer-term interactions.

E.1.3. xLSTM ON ALL 432 TASKS.

To validate that modern recurrent backbones also benefit from training with longer sequence lengths, we repeat the same ablation as presented in Appendix E.1.2 using xLSTM [1:0]. We report the learning curves, validation perplexities, and evaluation performance across all 432 tasks for varying context lengths in Figure 26. Note that the validation perplexity curves in Figure 26a, start at step 50K for readability. Again, we observe considerable improvements in the validation perplexities and the normalized scores (0.4 for $C = 1$ to 0.8 for $C = 50$) as the context length increases.

In addition, we provide the normalized scores per domain for xLSTM with varying sequence lengths in Figure 27. Across domains, we observe increasing performance with increasing C .

E.2. Return-conditioning vs. Behavior Cloning

Across experiments presented in the main text, except for the ICL experiments, we utilized a sequence representation that includes return-to-go tokens (RTG) as commonly used in the DT literature (Chen et al., 2021; Lee et al., 2022). At inference time, the RTG allows to condition the model on a high target return to produce high-quality actions. This is particularly

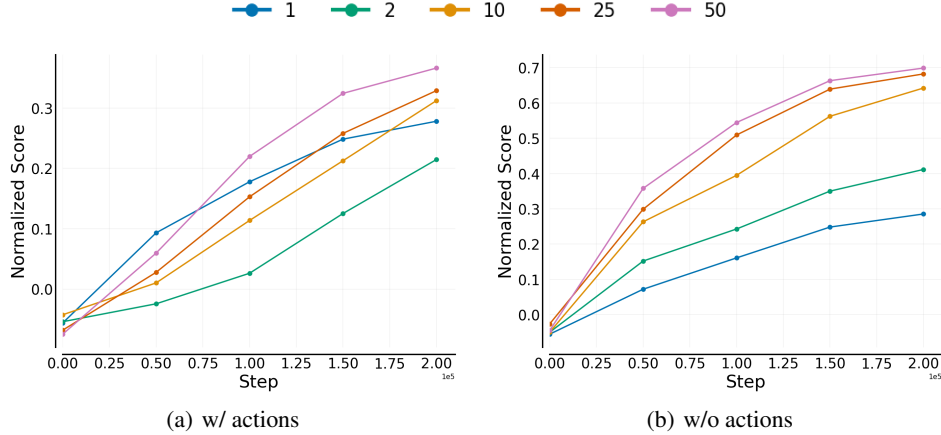


Figure 24. Ablation on removing the **action condition** for varying context lengths C . Performance of DT (a) with, and (b) without action condition on all **432 tasks**. Without actions in the context, the performance of DT improves with increasing C .

Table 7. Average MSE (\pm standard deviation) between subsequent actions in robotics datasets.

	Meta-World	DMControl	Composuite	Mimicgen
Avg. MSE	0.08 ± 0.09	0.2 ± 0.22	2.1 ± 0.3	0.015 ± 0.007

useful when the datasets contain a mixture of optimal and suboptimal trajectories. However, many recent works focus on behavior cloning without return conditioning (Brohan et al., 2023b;a; Octo Model Team et al., 2024).

To better understand whether our findings transfer to the behavior cloning setting, we conduct an ablation study in which we exclude the RTG tokens and the reward tokens from the sequence representation. This means that the sequence consists of state and reward tokens, or state-tokens only. In Figures 28 and 28, we report the (a) validation perplexities and (b) evaluation performance on the 432 task for the four considered backbones when removing RTG or RTG and reward, respectively. We retain the same training settings and datasets as reported in Appendix C (200K updates, evaluation after every 50K steps). We observe similar learning dynamics as for the 206M models that include RTG/reward tokens in the sequence representation (see Figure 2 and Figure 11). Consequently, we conclude that the same performance trends hold for training the considered backbones with and without RTG/reward condition. Note that the final performances are lower compared to the models that include the RTG condition, and that can be conditioned on a high return at inference time.

E.3. Effect of mLSTM-to-sLSTM ratio.

Throughout our experiments, we compare two xLSTM variants: xLSTM [7:1] and xLSTM [1:0]. The bracket notation was introduced by (Beck et al., 2024) and denotes the ratio of mLSTM to sLSTM blocks. For example, xLSTM [7:1] contains 1 sLSTM block for every 7 mLSTM blocks. As described in Appendix C, we aim to maintain the same ratio as proposed by Beck et al. (2024). While mLSTM blocks are fully parallelizable, sLSTM blocks are not. However, sLSTM preserves the non-diagonalized recurrent matrix to enable state-tracking (Merrill et al., 2024). As such, sLSTM can be attractive for tasks that require state-tracking (see Figure 4 in Beck et al. (2024)).

We first conduct an ablation study on the effect of the mLSTM-to-sLSTM ratio on the evaluation performance across all 432 tasks. For this experiment, we use the 16M parameter model that contains 8 xLSTM blocks in total. Consequently, we compare the following ratios [1:0] (only mLSTM), [0:1] (only sLSTM), [1:1], [1:3], [7:1]. In addition, we investigate the placement of sLSTMs across all 8 blocks. To indicate the placement, we use @ followed by the layer index (starting at 0). For example, [3:1] @ 1,3 indicates that the second and fourth layers are sLSTMs. In Figure 30, we report the validation perplexities and evaluation performance for different ratios and layer placements across the 432 tasks. For computational reasons, we conduct this experiment with only 1 seed per ratio. We find that at the 16M parameter scale, xLSTM [1:0] on average outperforms the variants that leverage sLSTM blocks. This indicates that these domains do not strongly benefit from the state tracking abilities of sLSTM.

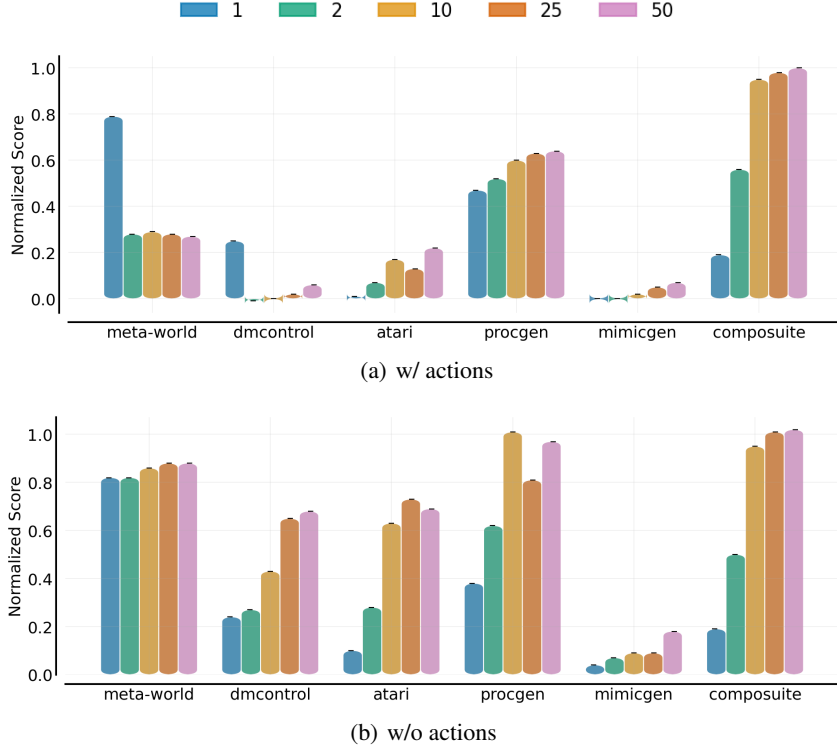


Figure 25. Ablation on removing the **action condition** for varying context lengths C . We show the normalized score **per domain** for all context lengths (a) with and (b) without actions.

Next, conduct the same analysis on Dark-Room 10×10 ICL environment as used in Appendix D.4. Unlike most of the 432 tasks used in our main experiments, Dark-Room exhibits a partially observable observation space and sparse rewards. Consequently, Dark-Room is more likely to require state tracking abilities. In fact, we already observed better performance for xLSTM [7:1] than for xLSTM [1:0] in Appendix 16. In Figure 31, we report the ICL curves for the 80 train tasks and 20 hold-out tasks. We observe that xLSTM variants that contain sLSTM blocks at lower-level positions, such as [7:1] @ 1 and [3:1] @ 1,3 outperform xLSTM [1:0]. In contrast, xLSTM variants that contain sLSTM blocks at deeper-level positions, such as [0:1] and 3:1 @ 5,7, perform poorly. This is similar to findings by Beck et al. (2024) who also place sLSTM layers at lower-level positions.

We conclude that sLSTM layers can be important building blocks for tasks that require state-tracking, such as Dark-Room. Most of the 432 tasks we consider in the main experiments of this work contain fully observable observation spaces and may not require state-tracking. However, we believe that more complex tasks with longer horizons or partial observability, as is common in real-world applications, could greatly benefit from the state-tracking abilities provided by sLSTM blocks. As such, equipping an agent with the ability to perform state-tracking by including sLSTM blocks may be a valuable option for practitioners. This is a distinguishing factor of xLSTM from Mamba, which does not exhibit state-tracking.

E.4. Effect of Dropout in DT

DTs use by default a Dropout (Srivastava et al., 2014) rate of 0.1. However, during our experiments, we found that Dropout has detrimental effects on the evaluation performance, particularly on continuous control domains like Composite. In Figure 32, we show the validation perplexities and evaluation performance for a DT trained with and without Dropout. Consequently, we remove Dropout from our DT variant.

E.5. Effect of reducing number of layers in xLSTM

In prior works, xLSTM and Mamba use twice the number of layers blocks as the Transformer baseline, while maintaining the same hidden dimension (Gu & Dao, 2023; Beck et al., 2024). For our inference-time comparisons, we therefore reduce

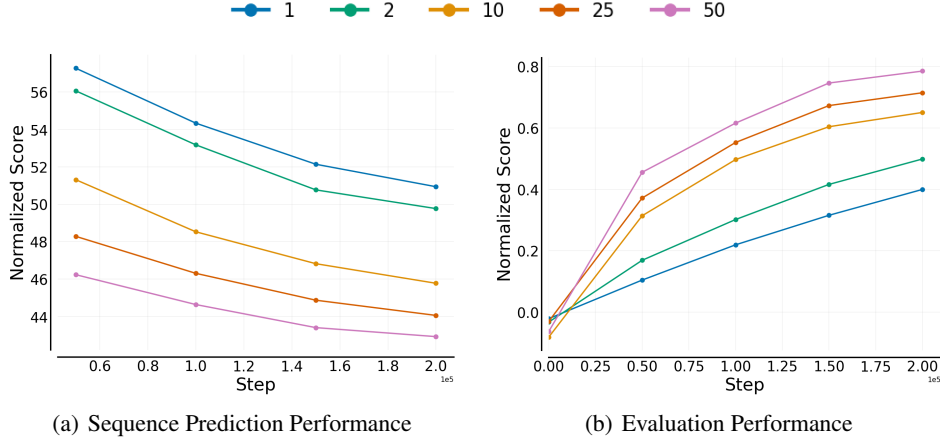


Figure 26. Ablation on the effect of **varying the context length C** for xLSTM. We report (a) validation perplexity and (b) evaluation performance across the 432 training tasks for xLSTM [1:0]. Without actions in the context, the performance of DT improves with increasing C .

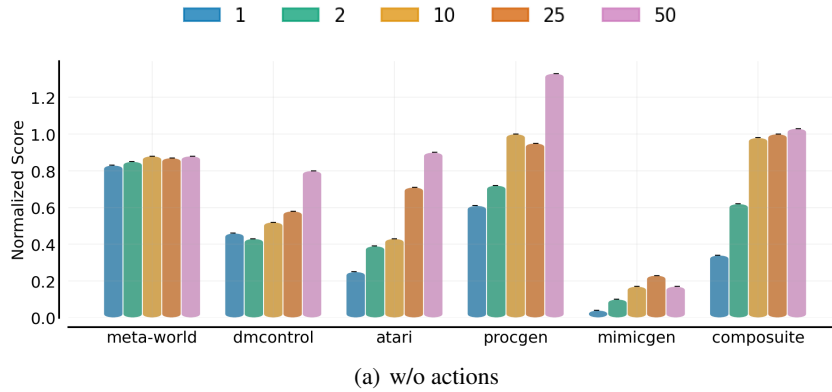


Figure 27. Ablation on the effect of varying the context length C for xLSTM. We show the normalized scores **per domain** for all context lengths.

the number of layer blocks in xLSTM by half. To ensure a fair comparison, we consequently adjust the hidden size of xLSTM to match the number of parameters of the Transformer baseline. In this section, we investigate the effect of these modifications of the xLSTM architecture on the model performance.

In Figure 33, report the validation perplexities and evaluation performance for the *regular* xLSTM with twice the number of layer blocks as DT, and an xLSTM with *half* the number of blocks. Reducing the number of layer blocks results in a slight decrease in performance on both metrics. However, xLSTM still outperforms the Transformer baseline (see Figure 2).

F. Embedding Space Analysis

In Figure 5, we analyze the representations learned by our models using UMAP (McInnes et al., 2018). Here, we explain the clustering procedure in more detail. For every task, we sample 32 sub-trajectories containing 50 timesteps (150 tokens) and encode them using our sequence models. Then, we extract the hidden states at the last layer of our model and aggregate them via mean pooling. We cluster all vectors using the default hyperparameters of UMAP into a two-dimensional space. Finally, we color the resulting points by their domain.

The purpose of this analysis is to examine how the models organize their representations of different environments. In general, tasks within the same domain tend to share similar input characteristics, such as visual inputs (e.g., image frames), possible actions to perform, and reward structures. Therefore, they are more likely to be “grouped” together in the embedding

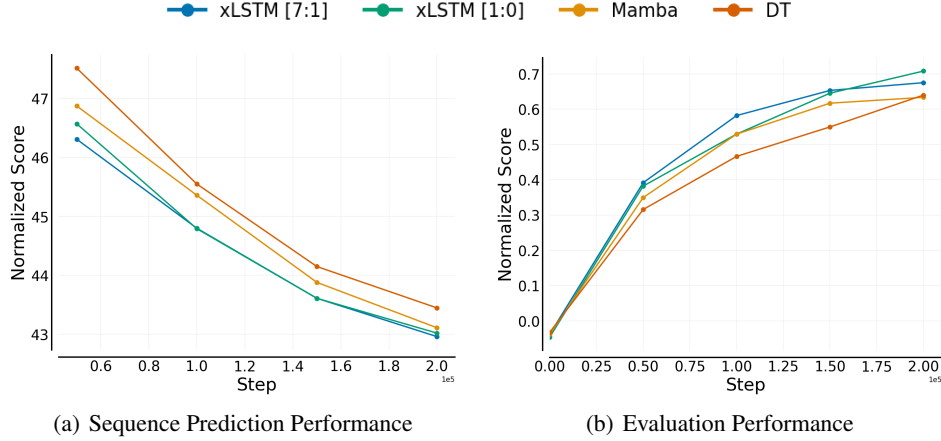


Figure 28. Ablation on the effect of **omitting the RTG condition**. We report the learning curves for (a) validation perplexity and (b) evaluation performance across the 432 training tasks for 206M parameter models. We observe similar performance trends as when including the RTG in the sequence.

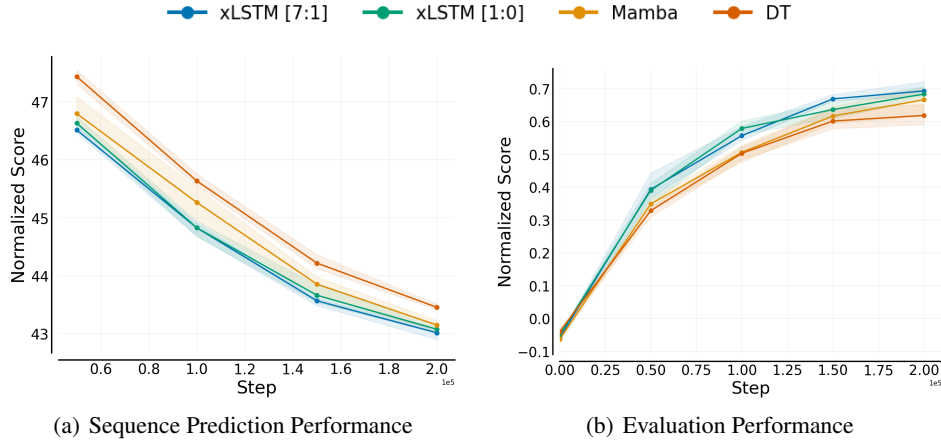


Figure 29. Ablation on the effect of **omitting the RTG condition and the reward condition**. We report the learning curves for (a) validation perplexity and (b) evaluation performance across the 432 training tasks for 206M parameter models. We observe similar performance trends as when including the RTG in the sequence.

space. For example, when embeddings of Atari games are closer to each other than to Procgen games, it indicates that Atari games share more similar underlying dynamics or input structures compared to Procgen. We indeed find that tasks from the same domain cluster together. A more refined and better-separated embedding space may result in better final performance, potentially because it facilitates task identification at inference time. This may, however, be specific to the mixture of training tasks at hand. Therefore, we believe that studying the learned embedding spaces of multi-task agents in a wide range of environments is interesting for future work.

Analogous to Figure 5 for DT and xLSTM, we show the UMAP clustering for Mamba 16M in Figure 34. In comparison to DT, Mamba exhibits a slightly stronger grouping of the embedding space.

G. Raw Scores

In this section, we report the raw scores for all 432 training tasks for the 206M parameter scale. See Tables 8, 9, 10, 11, 12 for Procgen, Atari, Meta-World, DMControl, and Mimicgen, respectively. The raw scores for Composuite are available in Tables 13, 14, 15, and 16.

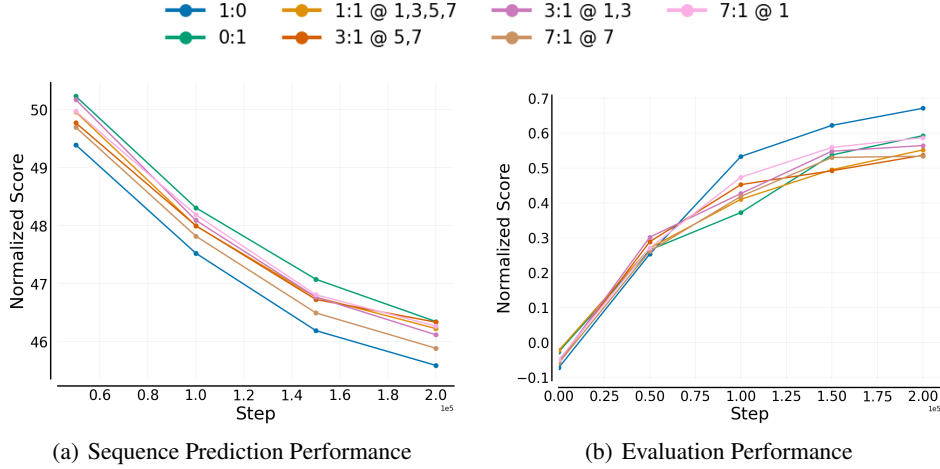


Figure 30. Ablation on the effect of the **mLSTM-to-sLSTM** ratio. We report the learning curves for (a) validation perplexity and (b) evaluation performance across the 432 training tasks for 206M parameter models with varying ratios.

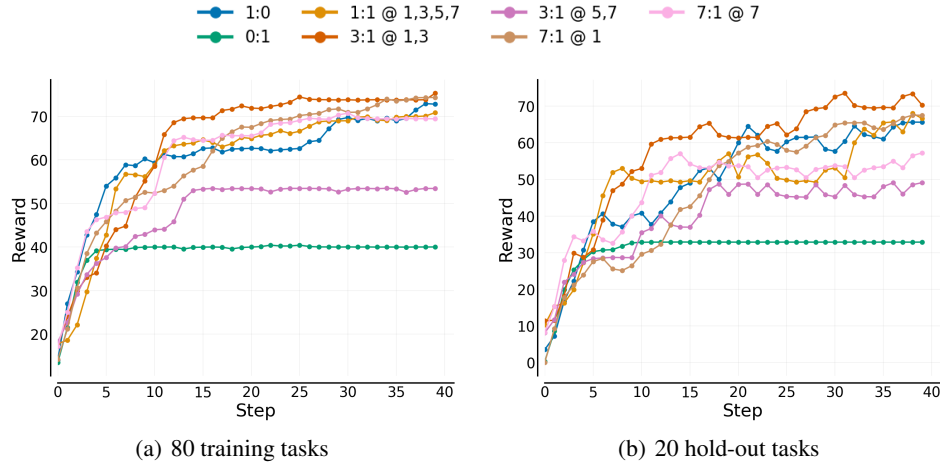


Figure 31. In-context Learning on Dark-Room 10×10 for varying **mLSTM-to-sLSTM** ratios.

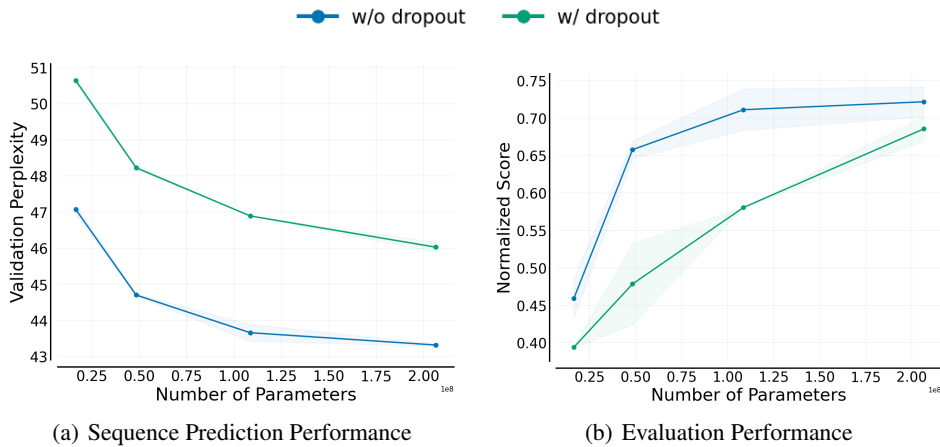


Figure 32. Ablation on the **effect of dropout on DT** performance. We show the (a) validation perplexity and (b) evaluation performance on the training tasks. DT performance drops considerably if training with dropout.

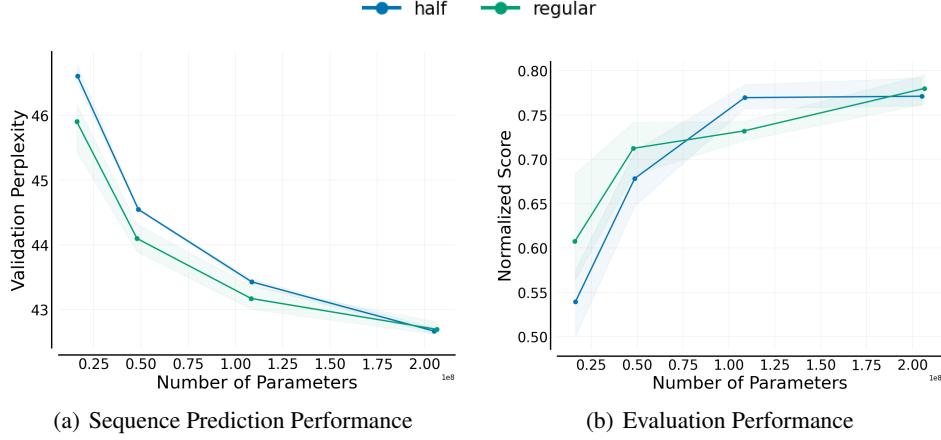


Figure 33. Ablation on the effect of reducing the **number of layer blocks** in xLSTM. We show the (a) validation perplexity and (b) evaluation performance on the training tasks for the layer regular and layer-matched xLSTM models. Reducing the number of layer blocks in xLSTM results in a slight performance decrease.

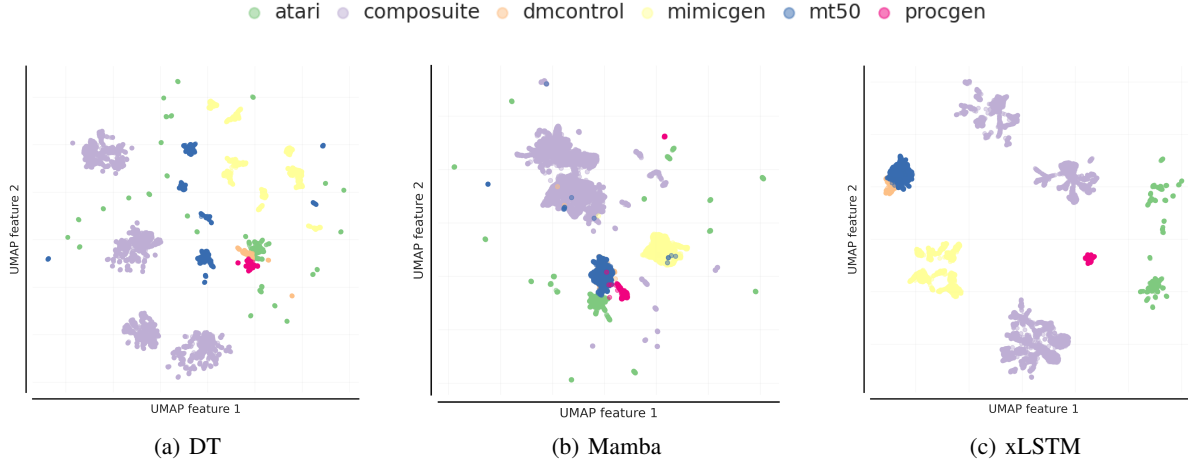


Figure 34. UMAP clustering of hidden states for 432 tasks produced by (a) DT, (b) Mamba, and (c) xLSTM with 16M parameters, colored by domain. We again depict the embedding spaces for DT and xLSTM from Figure 5 for better readability.

Table 8. Raw Scores for Procgen.

Task	DT	Mamba	xLSTM [1:0]	xLSTM [7:1]
bigfish	2.53	2.0	4.6	5.13
bossfight	6.73	4.1	9.27	2.0
caveflyer	6.67	6.3	6.67	4.87
chaser	3.41	3.91	4.92	4.2
coinrun	10.0	9.0	10.0	10.0
dodgeball	2.8	3.4	4.27	3.87
fruitbot	13.33	19.8	19.73	19.27
heist	7.33	7.0	6.67	6.67
leaper	5.33	4.0	8.67	5.33
maze	8.67	10.0	7.33	7.33
miner	8.07	11.0	9.0	8.27
starpilot	24.93	10.1	21.8	28.2
Avg. Reward	8.32	7.55	8.73	8.76

Table 9. Raw Scores for Atari.

Task	DT	Mamba	xLSTM [1:0]	xLSTM [7:1]
Amidar	82.27	30.8	71.07	26.73
Assault	438.2	224.7	410.2	494.13
Asterix	573.33	540.0	763.33	583.33
Atlantis	42573.33	97240.0	83760.0	76973.33
BankHeist	2.67	9.0	0.0	8.67
BattleZone	2000.0	2400.0	2600.0	1733.33
BeamRider	126.13	61.6	176.0	243.47
Boxing	80.8	77.7	83.8	84.93
Breakout	68.13	136.6	92.93	93.73
Carnival	618.67	424.0	697.33	484.0
Centipede	1802.13	1238.2	2416.73	1806.6
ChopperCommand	813.33	800.0	813.33	766.67
CrazyClimber	96853.33	65960.0	106606.67	79873.33
DemonAttack	100.0	65.0	181.33	130.67
DoubleDunk	-2.53	-3.0	-2.93	-3.87
Enduro	34.53	65.5	98.73	48.53
FishingDerby	-72.47	-68.2	-72.07	-71.0
Freeway	29.0	29.8	30.0	28.6
Frostbite	774.67	1248.0	1162.67	1049.33
Gopher	314.67	34.0	132.0	12.0
Gravitar	116.67	175.0	176.67	136.67
Hero	14004.67	11381.0	14688.67	16522.0
IceHockey	-4.8	-6.3	-7.6	-5.93
Jamesbond	490.0	540.0	603.33	510.0
Kangaroo	1426.67	2880.0	2620.0	2653.33
Krull	8880.67	10090.0	8918.0	9569.33
KungFuMaster	8866.67	12700.0	8120.0	11233.33
NameThisGame	7976.67	7967.0	7789.33	7232.0
Phoenix	592.0	1600.0	1807.33	1052.67
Pooyan	283.33	87.5	371.67	406.67
Qbert	4306.67	1700.0	805.0	2613.33
Riverraid	2888.67	6923.0	6688.0	7446.67
RoadRunner	1320.0	350.0	1340.0	213.33
Robotank	18.67	13.2	23.07	25.13
Seaquest	182.67	396.0	448.0	209.33
TimePilot	2533.33	3520.0	3200.0	2966.67
UpNDown	10598.0	12043.0	15340.67	12815.33
VideoPinball	1669.07	0.0	220.4	140.6
WizardOfWor	113.33	160.0	160.0	206.67
YarsRevenge	14356.27	14499.0	16815.0	21403.67
Zaxxon	0.0	0.0	20.0	0.0
Avg. Reward	5556.81	6281.27	6705.61	6383.35

Table 10. Raw Scores for Meta-World.

Task	DT	Mamba	xLSTM [1:0]	xLSTM [7:1]
reach	1860.69 ± 12.51	1859.3 ± 5.79	1859.17 ± 12.62	1864.37 ± 6.57
push	1588.19 ± 207.0	1605.03 ± 107.81	1493.31 ± 238.01	1759.33 ± 3.89
pick-place	137.85 ± 99.18	161.74 ± 153.95	389.81 ± 37.36	296.21 ± 43.77
door-open	1552.95 ± 6.51	1562.39 ± 6.79	1569.35 ± 6.71	1570.16 ± 14.83
drawer-open	1735.13 ± 21.76	1714.4 ± 19.3	1740.48 ± 9.2	1747.33 ± 3.88
drawer-close	1856.67 ± 3.06	1858.05 ± 2.75	1858.7 ± 2.34	1859.33 ± 1.15
button-press-topdown	1322.3 ± 3.12	1326.55 ± 19.93	1341.5 ± 3.15	1322.83 ± 7.25
peg-insert-side	1557.59 ± 98.52	1607.59 ± 9.1	1640.43 ± 13.1	1574.75 ± 90.34
window-open	1594.16 ± 34.13	1568.55 ± 14.38	1576.82 ± 10.21	1578.18 ± 70.3
window-close	1474.26 ± 16.88	1443.94 ± 18.99	1459.83 ± 18.79	1452.21 ± 26.56
door-close	1538.02 ± 14.64	1544.31 ± 3.63	1546.0 ± 9.69	1541.64 ± 10.5
reach-wall	1837.64 ± 1.6	1845.12 ± 3.06	1837.76 ± 3.39	1777.17 ± 94.47
pick-place-wall	1041.54 ± 219.67	843.51 ± 224.6	206.88 ± 184.28	385.57 ± 151.52
push-wall	1689.67 ± 12.74	1701.7 ± 1.54	1599.63 ± 189.06	1487.69 ± 195.8
button-press	1512.08 ± 9.54	1488.1 ± 38.83	1541.77 ± 5.48	1527.3 ± 10.16
button-press-topdown-wall	1314.49 ± 62.73	1295.2 ± 6.62	1321.26 ± 17.59	1328.74 ± 24.16
button-press-wall	1359.83 ± 173.51	1547.14 ± 13.84	1326.57 ± 109.09	1267.11 ± 8.78
peg-unplug-side	1415.68 ± 162.54	1517.49 ± 25.27	1393.98 ± 173.0	1422.64 ± 192.05
disassemble	1452.0 ± 44.54	1441.18 ± 29.15	1220.27 ± 441.51	1072.31 ± 374.95
hammer	1446.68 ± 169.03	1683.04 ± 4.82	1669.54 ± 32.0	1642.34 ± 72.23
plate-slide	1673.66 ± 1.72	1676.83 ± 3.0	1682.41 ± 5.02	1677.52 ± 5.46
plate-slide-side	1719.4 ± 7.85	1694.35 ± 46.29	1686.38 ± 61.27	1690.72 ± 12.97
plate-slide-back	1790.96 ± 6.39	1787.65 ± 5.99	1797.78 ± 1.17	1797.17 ± 0.43
plate-slide-back-side	1773.26 ± 9.72	1763.24 ± 5.59	1785.11 ± 7.42	1788.61 ± 6.67
handle-press	1734.75 ± 220.82	1829.07 ± 29.91	1881.23 ± 15.62	1881.92 ± 10.56
handle-pull	1590.74 ± 35.98	1627.4 ± 34.18	1616.62 ± 52.0	1627.6 ± 21.86
handle-press-side	1852.25 ± 7.0	1857.4 ± 10.13	1847.95 ± 5.61	1857.36 ± 5.57
handle-pull-side	1651.05 ± 3.48	1607.3 ± 22.56	1655.75 ± 4.6	1651.77 ± 7.53
stick-push	1595.45 ± 6.88	1585.22 ± 5.17	1595.35 ± 3.29	1595.21 ± 0.88
stick-pull	1377.41 ± 108.31	1401.91 ± 32.79	1460.27 ± 57.13	1442.68 ± 43.23
basketball	1529.79 ± 11.41	1528.22 ± 18.23	1543.02 ± 2.49	1542.8 ± 17.81
soccer	649.69 ± 160.32	929.06 ± 64.35	792.21 ± 139.63	732.44 ± 290.49
faucet-open	1676.95 ± 121.6	1703.83 ± 41.97	1727.05 ± 45.15	1744.83 ± 15.93
faucet-close	1772.91 ± 9.23	1772.13 ± 2.35	1778.25 ± 3.96	1775.25 ± 0.79
coffee-push	340.21 ± 276.9	232.01 ± 225.2	61.35 ± 51.79	41.79 ± 40.9
coffee-pull	1346.29 ± 101.93	1261.39 ± 195.18	1409.68 ± 34.66	1293.92 ± 129.94
coffee-button	1595.94 ± 16.57	1592.77 ± 2.23	1593.15 ± 49.98	1562.92 ± 36.79
sweep	1485.79 ± 12.17	1452.38 ± 13.74	1508.58 ± 14.96	1471.73 ± 29.08
sweep-into	1796.25 ± 7.64	1472.64 ± 455.9	1804.27 ± 2.38	1786.27 ± 14.64
pick-out-of-hole	1437.38 ± 181.15	1499.35 ± 35.73	1529.83 ± 8.09	1415.91 ± 176.44
assembly	1229.39 ± 16.96	1216.34 ± 22.21	1236.68 ± 21.77	1227.81 ± 7.67
shelf-place	1446.07 ± 30.41	1448.75 ± 39.73	1485.4 ± 12.31	1463.53 ± 9.04
push-back	1226.32 ± 172.59	1022.98 ± 158.35	1011.25 ± 396.65	1027.48 ± 303.73
lever-pull	1604.74 ± 3.32	1634.06 ± 6.08	1639.31 ± 10.11	1626.09 ± 23.72
dial-turn	1688.33 ± 22.94	1667.37 ± 41.45	1713.38 ± 35.16	1686.59 ± 55.09
Avg. Reward	1486.05	1486.18	1455.15	1464.16

Table 11. Raw Scores for DMControl.

Task	DT	Mamba	xLSTM [1:0]	xLSTM [7:1]
finger-turn-easy	121.27 \pm 104.6	396.4 \pm 122.47	449.8 \pm 186.65	640.13 \pm 82.48
fish-upright	181.14 \pm 70.82	154.59 \pm 34.64	277.23 \pm 105.37	241.73 \pm 257.01
hopper-stand	296.15 \pm 141.83	304.78 \pm 32.65	413.95 \pm 35.83	392.34 \pm 152.75
point_mass-easy	342.26 \pm 37.42	720.11 \pm 42.95	734.95 \pm 114.17	823.74 \pm 57.3
walker-stand	911.72 \pm 38.16	785.21 \pm 23.53	947.31 \pm 22.13	864.14 \pm 181.56
walker-run	155.91 \pm 73.84	274.83 \pm 0.44	201.34 \pm 34.77	145.01 \pm 31.71
ball.in.cup-catch	976.93 \pm 0.83	970.9 \pm 4.67	977.33 \pm 0.5	975.93 \pm 0.42
cartpole-swingup	688.5 \pm 42.6	762.4 \pm 63.93	800.14 \pm 13.64	591.08 \pm 86.49
cheetah-run	81.21 \pm 96.85	482.39 \pm 17.23	358.52 \pm 127.92	389.04 \pm 4.11
finger-spin	209.27 \pm 20.57	430.8 \pm 61.66	673.47 \pm 94.37	626.93 \pm 29.21
reacher-easy	45.4 \pm 5.21	180.7 \pm 133.64	78.73 \pm 20.59	58.0 \pm 13.91
Avg. Reward	364.52	496.65	505.06	522.55

Table 12. Raw Scores for Mimicgen.

Task	DT	Mamba	xLSTM [1:0]	xLSTM [7:1]
Panda.CoffeePreparation_D0	0.0 ± 0.0	0.0 ± 0.0	0.0 ± 0.0	0.13 ± 0.12
Panda.CoffeePreparation_D1	0.0 ± 0.0	0.0 ± 0.0	0.0 ± 0.0	0.0 ± 0.0
Panda.Coffee_D0	0.4 ± 0.2	0.0 ± 0.0	0.2 ± 0.2	0.07 ± 0.12
Panda.Coffee_D1	0.2 ± 0.2	0.0 ± 0.0	0.2 ± 0.2	0.07 ± 0.12
Panda.Coffee_D2	0.07 ± 0.12	0.0 ± 0.0	0.07 ± 0.12	0.0 ± 0.0
Panda.HammerCleanup_D0	1.0 ± 0.0	0.9 ± 0.14	1.0 ± 0.0	1.0 ± 0.0
Panda.HammerCleanup_D1	0.47 ± 0.5	0.1 ± 0.14	0.47 ± 0.23	0.47 ± 0.31
Panda.Kitchen_D0	0.87 ± 0.23	0.6 ± 0.0	1.0 ± 0.0	1.0 ± 0.0
Panda.Kitchen_D1	0.0 ± 0.0	0.0 ± 0.0	0.0 ± 0.0	0.0 ± 0.0
Panda.MugCleanup_D0	0.13 ± 0.12	0.1 ± 0.14	0.6 ± 0.2	0.27 ± 0.12
Panda.MugCleanup_D1	0.07 ± 0.12	0.0 ± 0.0	0.2 ± 0.2	0.07 ± 0.12
Sawyer.NutAssembly_D0	0.07 ± 0.12	0.0 ± 0.0	0.0 ± 0.0	0.07 ± 0.12
Sawyer.PickPlace_D0	0.0 ± 0.0	0.0 ± 0.0	0.0 ± 0.0	0.0 ± 0.0
Panda.Square_D0	0.2 ± 0.2	0.0 ± 0.0	0.53 ± 0.12	0.53 ± 0.12
Panda.Square_D1	0.0 ± 0.0	0.0 ± 0.0	0.2 ± 0.2	0.07 ± 0.12
Panda.Square_D2	0.13 ± 0.12	0.0 ± 0.0	0.07 ± 0.12	0.07 ± 0.12
Panda.StackThree_D0	0.0 ± 0.0	0.0 ± 0.0	0.07 ± 0.12	0.0 ± 0.0
Panda.StackThree_D1	0.0 ± 0.0	0.0 ± 0.0	0.07 ± 0.12	0.0 ± 0.0
Panda.Stack_D0	0.47 ± 0.12	0.2 ± 0.0	0.67 ± 0.31	0.73 ± 0.12
Panda.Stack_D1	0.4 ± 0.2	0.0 ± 0.0	0.27 ± 0.12	0.4 ± 0.2
Panda.Threading_D0	0.27 ± 0.12	0.2 ± 0.0	0.27 ± 0.12	0.2 ± 0.2
Panda.Threading_D1	0.2 ± 0.35	0.0 ± 0.0	0.07 ± 0.12	0.07 ± 0.12
Panda.ThreePieceAssembly_D0	0.0 ± 0.0	0.0 ± 0.0	0.0 ± 0.0	0.0 ± 0.0
Panda.ThreePieceAssembly_D1	0.0 ± 0.0	0.0 ± 0.0	0.0 ± 0.0	0.0 ± 0.0
IIWA.Coffee_D0	0.0 ± 0.0	0.0 ± 0.0	0.0 ± 0.0	0.0 ± 0.0
Sawyer.Coffee_D0	0.27 ± 0.31	0.0 ± 0.0	0.13 ± 0.12	0.2 ± 0.2
UR5e.Coffee_D0	0.33 ± 0.12	0.2 ± 0.0	0.47 ± 0.31	0.4 ± 0.2
IIWA.Coffee_D1	0.0 ± 0.0	0.0 ± 0.0	0.0 ± 0.0	0.0 ± 0.0
Sawyer.Coffee_D1	0.07 ± 0.12	0.0 ± 0.0	0.07 ± 0.12	0.0 ± 0.0
UR5e.Coffee_D1	0.13 ± 0.12	0.0 ± 0.0	0.2 ± 0.2	0.33 ± 0.31
IIWA.Coffee_D2	0.0 ± 0.0	0.0 ± 0.0	0.0 ± 0.0	0.0 ± 0.0
UR5e.Coffee_D2	0.0 ± 0.0	0.1 ± 0.14	0.2 ± 0.0	0.07 ± 0.12
IIWA.HammerCleanup_D0	0.0 ± 0.0	0.0 ± 0.0	0.0 ± 0.0	0.0 ± 0.0
Sawyer.HammerCleanup_D0	0.73 ± 0.12	0.9 ± 0.14	0.93 ± 0.12	0.87 ± 0.23
UR5e.HammerCleanup_D0	1.0 ± 0.0	0.9 ± 0.14	1.0 ± 0.0	0.93 ± 0.12
IIWA.HammerCleanup_D1	0.0 ± 0.0	0.0 ± 0.0	0.0 ± 0.0	0.0 ± 0.0
Sawyer.HammerCleanup_D1	0.2 ± 0.2	0.2 ± 0.0	0.27 ± 0.23	0.4 ± 0.35
UR5e.HammerCleanup_D1	0.47 ± 0.12	0.4 ± 0.28	0.8 ± 0.2	0.6 ± 0.0
IIWA.Kitchen_D0	0.0 ± 0.0	0.0 ± 0.0	0.0 ± 0.0	0.0 ± 0.0
UR5e.Kitchen_D0	0.93 ± 0.12	0.8 ± 0.0	1.0 ± 0.0	1.0 ± 0.0
UR5e.Kitchen_D1	0.0 ± 0.0	0.0 ± 0.0	0.0 ± 0.0	0.07 ± 0.12
IIWA.MugCleanup_D0	0.0 ± 0.0	0.0 ± 0.0	0.0 ± 0.0	0.0 ± 0.0
IIWA.MugCleanup_D1	0.0 ± 0.0	0.0 ± 0.0	0.0 ± 0.0	0.0 ± 0.0
UR5e.MugCleanup_D1	0.07 ± 0.12	0.0 ± 0.0	0.13 ± 0.12	0.13 ± 0.12
IIWA.NutAssembly_D0	0.0 ± 0.0	0.0 ± 0.0	0.0 ± 0.0	0.0 ± 0.0
Sawyer.NutAssembly_D0	0.0 ± 0.0	0.0 ± 0.0	0.07 ± 0.12	0.0 ± 0.0
UR5e.NutAssembly_D0	0.0 ± 0.0	0.0 ± 0.0	0.0 ± 0.0	0.07 ± 0.12
IIWA.PickPlace_D0	0.0 ± 0.0	0.0 ± 0.0	0.0 ± 0.0	0.0 ± 0.0
Sawyer.PickPlace_D0	0.0 ± 0.0	0.0 ± 0.0	0.0 ± 0.0	0.0 ± 0.0
UR5e.PickPlace_D0	0.0 ± 0.0	0.0 ± 0.0	0.0 ± 0.0	0.0 ± 0.0
IIWA.Square_D0	0.0 ± 0.0	0.0 ± 0.0	0.0 ± 0.0	0.0 ± 0.0
Sawyer.Square_D0	0.2 ± 0.2	0.4 ± 0.28	0.33 ± 0.12	0.53 ± 0.23
UR5e.Square_D0	0.13 ± 0.23	0.3 ± 0.42	0.27 ± 0.12	0.53 ± 0.23
IIWA.Square_D1	0.0 ± 0.0	0.0 ± 0.0	0.0 ± 0.0	0.0 ± 0.0
Sawyer.Square_D1	0.0 ± 0.0	0.0 ± 0.0	0.0 ± 0.0	0.0 ± 0.0
UR5e.Square_D1	0.0 ± 0.0	0.0 ± 0.0	0.0 ± 0.0	0.0 ± 0.0
IIWA.StackThree_D0	0.0 ± 0.0	0.0 ± 0.0	0.0 ± 0.0	0.0 ± 0.0
Sawyer.StackThree_D0	0.0 ± 0.0	0.0 ± 0.0	0.0 ± 0.0	0.0 ± 0.0
UR5e.StackThree_D0	0.0 ± 0.0	0.0 ± 0.0	0.0 ± 0.0	0.0 ± 0.0
IIWA.StackThree_D1	0.0 ± 0.0	0.0 ± 0.0	0.0 ± 0.0	0.0 ± 0.0
Sawyer.StackThree_D1	0.0 ± 0.0	0.0 ± 0.0	0.0 ± 0.0	0.07 ± 0.12
UR5e.StackThree_D1	0.0 ± 0.0	0.0 ± 0.0	0.0 ± 0.0	0.0 ± 0.0
IIWA.Stack_D0	0.0 ± 0.0	0.0 ± 0.0	0.0 ± 0.0	0.0 ± 0.0
Sawyer.Stack_D0	0.47 ± 0.31	0.2 ± 0.0	0.6 ± 0.2	0.4 ± 0.2
UR5e.Stack_D0	0.4 ± 0.2	0.3 ± 0.14	0.87 ± 0.12	0.67 ± 0.12
IIWA.Stack_D1	0.0 ± 0.0	0.0 ± 0.0	0.0 ± 0.0	0.0 ± 0.0
Sawyer.Stack_D1	0.2 ± 0.2	0.0 ± 0.0	0.4 ± 0.2	0.27 ± 0.12
UR5e.Stack_D1	0.6 ± 0.0	0.1 ± 0.14	0.73 ± 0.12	0.4 ± 0.2
IIWA.Threading_D0	0.0 ± 0.0	0.0 ± 0.0	0.0 ± 0.0	0.0 ± 0.0
Sawyer.Threading_D0	0.13 ± 0.12	0.0 ± 0.0	0.07 ± 0.12	0.13 ± 0.12
UR5e.Threading_D0	0.27 ± 0.31	0.1 ± 0.14	0.4 ± 0.2	0.4 ± 0.2
IIWA.Threading_D1	0.0 ± 0.0	0.0 ± 0.0	0.0 ± 0.0	0.0 ± 0.0
Sawyer.Threading_D1	0.0 ± 0.0	0.0 ± 0.0	0.13 ± 0.12	0.0 ± 0.0
UR5e.Threading_D1	0.07 ± 0.12	0.0 ± 0.0	0.0 ± 0.0	0.0 ± 0.0
IIWA.ThreePieceAssembly_D0	0.0 ± 0.0	0.0 ± 0.0	0.0 ± 0.0	0.0 ± 0.0
Sawyer.ThreePieceAssembly_D0	0.0 ± 0.0	0.0 ± 0.0	0.0 ± 0.0	0.0 ± 0.0
UR5e.ThreePieceAssembly_D0	0.0 ± 0.0	0.0 ± 0.0	0.13 ± 0.12	0.0 ± 0.0
IIWA.ThreePieceAssembly_D1	0.0 ± 0.0	0.0 ± 0.0	0.0 ± 0.0	0.0 ± 0.0
Sawyer.ThreePieceAssembly_D1	0.0 ± 0.0	0.0 ± 0.0	0.0 ± 0.0	0.0 ± 0.0
UR5e.ThreePieceAssembly_D1	0.0 ± 0.0	0.0 ± 0.0	0.0 ± 0.0	0.0 ± 0.0
IIWA.ThreePieceAssembly_D2	0.0 ± 0.0	0.0 ± 0.0	0.0 ± 0.0	0.0 ± 0.0
Sawyer.ThreePieceAssembly_D2	0.0 ± 0.0	0.0 ± 0.0	0.0 ± 0.0	0.0 ± 0.0
UR5e.ThreePieceAssembly_D2	0.0 ± 0.0	0.0 ± 0.0	0.0 ± 0.0	0.0 ± 0.0

Table 13. Raw Scores for Composuite, Part1.

Task	DT	Mamba	xLSTM [1:0]	xLSTM [7:1]
IIWA.Box.None.PickPlace	402.74 ± 14.4	414.73 ± 10.49	424.35 ± 12.95	421.33 ± 11.39
IIWA.Box.None.Push	388.61 ± 35.63	427.0 ± 2.03	424.4 ± 4.63	427.0 ± 0.68
IIWA.Box.None.Shelf	370.3 ± 80.53	417.61 ± 1.44	417.78 ± 0.96	416.41 ± 1.87
IIWA.Box.None.Trashcan	329.27 ± 113.43	424.39 ± 1.04	429.54 ± 1.57	426.07 ± 3.98
IIWA.Box.GoalWall.PickPlace	367.68 ± 81.93	428.6 ± 4.11	428.0 ± 2.32	429.29 ± 1.97
IIWA.Box.GoalWall.Push	299.69 ± 77.03	337.81 ± 88.42	344.59 ± 28.19	318.19 ± 50.76
IIWA.Box.GoalWall.Shelf	360.92 ± 48.29	405.81 ± 9.82	408.1 ± 5.92	402.31 ± 3.08
IIWA.Box.GoalWall.Trashcan	376.45 ± 83.64	422.34 ± 3.61	429.15 ± 2.72	425.64 ± 3.88
IIWA.Box.ObjectDoor.PickPlace	389.21 ± 47.22	417.89 ± 0.92	413.82 ± 4.06	414.08 ± 3.83
IIWA.Box.ObjectDoor.Push	406.51 ± 0.32	403.59 ± 5.82	373.61 ± 40.95	397.45 ± 1.89
IIWA.Box.ObjectDoor.Shelf	329.42 ± 67.73	353.67 ± 56.2	367.47 ± 43.7	396.33 ± 2.67
IIWA.Box.ObjectDoor.Trashcan	325.45 ± 72.77	372.51 ± 41.55	358.72 ± 76.22	391.58 ± 16.76
IIWA.Box.ObjectWall.PickPlace	393.52 ± 51.47	425.76 ± 2.29	420.61 ± 2.99	421.61 ± 1.06
IIWA.Box.ObjectWall.Push	420.21 ± 3.5	412.76 ± 1.67	410.19 ± 1.62	411.5 ± 3.13
IIWA.Box.ObjectWall.Shelf	400.86 ± 3.66	408.22 ± 1.63	401.42 ± 3.93	396.64 ± 10.55
IIWA.Box.ObjectWall.Trashcan	414.43 ± 2.93	413.71 ± 3.47	417.11 ± 1.69	414.46 ± 0.8
IIWA.Dumbbell.None.PickPlace	386.95 ± 51.87	422.35 ± 2.94	421.32 ± 2.03	421.94 ± 1.48
IIWA.Dumbbell.None.Push	360.62 ± 90.94	413.39 ± 6.13	414.23 ± 6.04	393.34 ± 36.66
IIWA.Dumbbell.None.Shelf	310.45 ± 73.45	344.81 ± 53.72	380.51 ± 5.34	350.8 ± 52.16
IIWA.Dumbbell.None.Trashcan	386.09 ± 40.69	396.08 ± 0.7	414.03 ± 3.78	412.34 ± 3.36
IIWA.Dumbbell.GoalWall.PickPlace	413.6 ± 1.16	415.64 ± 3.28	410.7 ± 7.64	413.51 ± 1.23
IIWA.Dumbbell.GoalWall.Push	316.49 ± 38.69	367.45 ± 4.81	336.67 ± 82.13	371.92 ± 5.91
IIWA.Dumbbell.GoalWall.Shelf	395.63 ± 3.19	372.77 ± 30.32	376.75 ± 8.62	372.77 ± 4.25
IIWA.Dumbbell.GoalWall.Trashcan	379.45 ± 58.51	374.31 ± 55.11	412.22 ± 4.09	406.03 ± 5.03
IIWA.Dumbbell.ObjectDoor.PickPlace	358.13 ± 26.76	364.62 ± 40.18	393.83 ± 2.05	347.28 ± 39.81
IIWA.Dumbbell.ObjectDoor.Push	400.9 ± 8.95	383.81 ± 8.46	382.93 ± 0.7	364.06 ± 35.78
IIWA.Dumbbell.ObjectDoor.Shelf	369.75 ± 14.29	325.7 ± 30.94	350.7 ± 21.76	335.84 ± 40.36
IIWA.Dumbbell.ObjectDoor.Trashcan	393.05 ± 3.92	358.77 ± 36.88	397.23 ± 1.73	389.54 ± 9.14
IIWA.Dumbbell.ObjectWall.PickPlace	403.51 ± 12.08	407.37 ± 0.09	404.28 ± 1.23	401.15 ± 10.64
IIWA.Dumbbell.ObjectWall.Push	330.77 ± 30.29	296.98 ± 68.18	334.41 ± 22.28	307.4 ± 33.85
IIWA.Dumbbell.ObjectWall.Shelf	353.9 ± 29.5	374.39 ± 6.58	358.29 ± 33.75	358.76 ± 18.87
IIWA.Dumbbell.ObjectWall.Trashcan	394.48 ± 4.39	361.99 ± 39.17	398.06 ± 0.59	383.43 ± 32.4
IIWA.Plate.None.PickPlace	427.3 ± 0.59	424.44 ± 1.82	424.59 ± 2.01	425.99 ± 1.2
IIWA.Plate.None.Push	424.25 ± 1.13	419.86 ± 3.96	418.13 ± 3.55	418.42 ± 1.3
IIWA.Plate.None.Shelf	408.07 ± 0.95	397.02 ± 6.49	396.55 ± 10.03	394.93 ± 10.81
IIWA.Plate.None.Trashcan	419.62 ± 1.81	420.24 ± 0.33	420.37 ± 0.91	419.42 ± 2.61
IIWA.Plate.GoalWall.PickPlace	424.69 ± 2.67	423.93 ± 1.77	421.83 ± 1.01	420.13 ± 8.21
IIWA.Plate.GoalWall.Push	409.69 ± 3.55	397.97 ± 13.41	390.46 ± 14.79	388.89 ± 3.01
IIWA.Plate.GoalWall.Shelf	404.92 ± 0.82	396.09 ± 4.6	393.01 ± 5.77	401.81 ± 8.93
IIWA.Plate.GoalWall.Trashcan	420.47 ± 1.88	420.68 ± 2.82	420.29 ± 1.48	421.31 ± 1.93
IIWA.Plate.ObjectDoor.PickPlace	408.48 ± 1.12	403.23 ± 7.83	397.51 ± 1.65	401.53 ± 1.76
IIWA.Plate.ObjectDoor.Push	404.34 ± 4.45	395.97 ± 16.84	389.33 ± 7.78	385.77 ± 1.21
IIWA.Plate.ObjectDoor.Shelf	377.91 ± 21.42	373.43 ± 5.34	369.41 ± 4.97	374.16 ± 13.75
IIWA.Plate.ObjectDoor.Trashcan	400.27 ± 3.16	400.74 ± 0.53	399.28 ± 1.63	400.23 ± 0.63
IIWA.Plate.ObjectWall.PickPlace	417.35 ± 3.15	416.76 ± 6.18	409.31 ± 1.26	411.62 ± 0.97
IIWA.Plate.ObjectWall.Push	413.47 ± 3.92	408.16 ± 6.53	405.51 ± 3.71	405.27 ± 1.34
IIWA.Plate.ObjectWall.Shelf	393.23 ± 1.39	376.64 ± 12.49	386.41 ± 8.65	382.81 ± 6.78
IIWA.Plate.ObjectWall.Trashcan	410.85 ± 1.07	408.87 ± 3.95	408.98 ± 0.82	409.35 ± 2.6
IIWA.Hollowbox.None.PickPlace	378.13 ± 94.18	427.5 ± 6.93	428.62 ± 3.62	426.38 ± 3.26
IIWA.Hollowbox.None.Push	386.22 ± 36.15	422.49 ± 8.01	427.73 ± 1.97	426.12 ± 2.3
IIWA.Hollowbox.None.Shelf	416.65 ± 6.66	419.89 ± 11.03	418.34 ± 6.49	415.11 ± 0.89
IIWA.Hollowbox.None.Trashcan	424.38 ± 2.77	421.62 ± 1.4	426.9 ± 2.35	425.99 ± 1.81
IIWA.Hollowbox.GoalWall.PickPlace	430.17 ± 3.37	427.76 ± 0.48	427.91 ± 0.76	426.47 ± 1.62
IIWA.Hollowbox.GoalWall.Push	401.33 ± 3.96	373.0 ± 41.02	390.09 ± 9.46	394.35 ± 14.43
IIWA.Hollowbox.GoalWall.Shelf	424.55 ± 2.3	379.05 ± 64.32	423.51 ± 1.31	419.69 ± 3.38
IIWA.Hollowbox.GoalWall.Trashcan	425.95 ± 0.73	425.27 ± 0.66	424.8 ± 1.0	420.68 ± 3.33
IIWA.Hollowbox.ObjectDoor.PickPlace	276.87 ± 109.64	369.45 ± 57.47	374.76 ± 45.83	301.41 ± 112.33
IIWA.Hollowbox.ObjectDoor.Push	326.56 ± 109.6	352.22 ± 53.97	390.78 ± 6.35	324.09 ± 55.59
IIWA.Hollowbox.ObjectDoor.Shelf	339.03 ± 43.75	370.75 ± 8.36	362.72 ± 30.31	353.98 ± 38.19
IIWA.Hollowbox.ObjectDoor.Trashcan	395.18 ± 8.7	370.39 ± 35.98	387.21 ± 14.61	387.99 ± 21.95
IIWA.Hollowbox.ObjectWall.PickPlace	364.95 ± 27.07	355.61 ± 76.66	356.01 ± 8.3	369.47 ± 24.62
IIWA.Hollowbox.ObjectWall.Push	422.04 ± 2.08	414.47 ± 8.08	414.39 ± 5.5	408.53 ± 8.05
IIWA.Hollowbox.ObjectWall.Shelf	400.82 ± 2.4	400.31 ± 1.28	403.69 ± 2.06	401.27 ± 1.97
IIWA.Hollowbox.ObjectWall.Trashcan	415.82 ± 0.9	416.68 ± 0.14	392.79 ± 44.13	417.34 ± 0.77

Table 14. Raw Scores for Composuite, Part 2.

Task	DT	Mamba	xLSTM [1:0]	xLSTM [7:1]
Jaco.Box.None.PickPlace	401.38 ± 3.88	400.41 ± 0.63	399.74 ± 5.35	396.54 ± 4.99
Jaco.Box.None.Push	399.84 ± 3.29	397.79 ± 1.71	392.77 ± 1.12	397.31 ± 1.39
Jaco.Box.None.Shelf	383.53 ± 0.31	384.65 ± 5.31	385.85 ± 1.1	386.34 ± 3.47
Jaco.Box.None.Trashcan	374.88 ± 43.66	398.46 ± 2.69	397.66 ± 4.99	398.21 ± 0.91
Jaco.Box.GoalWall.PickPlace	394.75 ± 2.52	395.12 ± 0.38	392.3 ± 5.3	389.93 ± 3.83
Jaco.Box.GoalWall.Push	317.78 ± 67.67	343.43 ± 7.49	351.67 ± 20.65	336.02 ± 8.59
Jaco.Box.GoalWall.Shelf	374.62 ± 20.35	387.0 ± 1.42	387.73 ± 2.11	384.74 ± 1.19
Jaco.Box.GoalWall.Trashcan	374.07 ± 30.72	393.81 ± 0.68	395.49 ± 1.23	392.53 ± 3.46
Jaco.Box.ObjectDoor.PickPlace	396.05 ± 1.12	391.81 ± 4.67	388.37 ± 1.26	383.39 ± 9.07
Jaco.Box.ObjectDoor.Push	364.64 ± 38.39	383.07 ± 5.73	366.91 ± 33.04	387.51 ± 2.93
Jaco.Box.ObjectDoor.Shelf	373.8 ± 2.81	379.75 ± 1.45	375.38 ± 6.27	376.86 ± 1.37
Jaco.Box.ObjectDoor.Trashcan	388.4 ± 1.28	353.97 ± 52.06	389.38 ± 2.0	389.81 ± 2.89
Jaco.Box.ObjectWall.PickPlace	394.31 ± 2.66	385.33 ± 5.43	388.54 ± 7.62	387.82 ± 2.26
Jaco.Box.ObjectWall.Push	387.4 ± 9.34	384.75 ± 4.29	383.61 ± 7.58	383.32 ± 7.73
Jaco.Box.ObjectWall.Shelf	364.38 ± 2.57	361.28 ± 8.2	367.38 ± 2.04	369.22 ± 2.79
Jaco.Box.ObjectWall.Trashcan	385.73 ± 6.85	385.9 ± 1.13	385.34 ± 0.74	380.01 ± 5.08
Jaco.Dumbbell.None.PickPlace	319.87 ± 1.83	334.2 ± 1.93	376.46 ± 9.19	334.95 ± 68.5
Jaco.Dumbbell.None.Push	388.29 ± 1.98	372.13 ± 5.46	373.3 ± 6.88	369.49 ± 4.36
Jaco.Dumbbell.None.Shelf	300.81 ± 61.26	344.47 ± 15.49	361.77 ± 6.21	362.88 ± 8.22
Jaco.Dumbbell.None.Trashcan	369.52 ± 11.5	369.83 ± 13.39	387.28 ± 1.88	377.27 ± 9.7
Jaco.Dumbbell.GoalWall.PickPlace	306.12 ± 40.29	306.26 ± 32.85	349.04 ± 18.3	348.42 ± 37.3
Jaco.Dumbbell.GoalWall.Push	107.91 ± 29.9	136.11 ± 9.04	245.71 ± 30.15	188.19 ± 58.09
Jaco.Dumbbell.GoalWall.Shelf	300.97 ± 114.65	368.99 ± 0.5	363.58 ± 9.74	346.57 ± 27.41
Jaco.Dumbbell.GoalWall.Trashcan	321.81 ± 87.58	317.94 ± 23.15	376.09 ± 2.22	378.49 ± 4.52
Jaco.Dumbbell.ObjectDoor.PickPlace	382.35 ± 1.62	380.2 ± 5.17	349.1 ± 32.92	372.44 ± 7.6
Jaco.Dumbbell.ObjectDoor.Push	382.32 ± 1.08	353.42 ± 7.17	353.85 ± 6.83	338.66 ± 19.03
Jaco.Dumbbell.ObjectDoor.Shelf	312.14 ± 64.22	330.22 ± 47.38	343.51 ± 30.97	331.5 ± 37.18
Jaco.Dumbbell.ObjectDoor.Trashcan	371.06 ± 8.48	375.34 ± 4.07	373.78 ± 6.05	370.06 ± 8.94
Jaco.Dumbbell.ObjectWall.PickPlace	279.55 ± 111.58	314.05 ± 21.02	360.29 ± 15.75	360.38 ± 12.02
Jaco.Dumbbell.ObjectWall.Push	381.11 ± 3.7	351.38 ± 1.82	349.16 ± 2.93	352.64 ± 11.94
Jaco.Dumbbell.ObjectWall.Shelf	354.95 ± 1.59	316.33 ± 42.6	342.43 ± 7.94	332.97 ± 15.33
Jaco.Dumbbell.ObjectWall.Trashcan	367.01 ± 8.38	354.32 ± 22.23	365.47 ± 7.45	363.25 ± 3.18
Jaco.Plate.None.PickPlace	397.25 ± 0.77	389.99 ± 6.44	384.38 ± 5.92	380.69 ± 2.55
Jaco.Plate.None.Push	395.18 ± 1.01	390.69 ± 9.12	381.68 ± 6.86	380.2 ± 3.48
Jaco.Plate.None.Shelf	380.49 ± 0.75	381.62 ± 0.09	356.49 ± 41.25	380.99 ± 2.43
Jaco.Plate.None.Trashcan	391.97 ± 0.76	390.62 ± 0.57	391.2 ± 1.38	390.3 ± 1.83
Jaco.Plate.GoalWall.PickPlace	379.45 ± 24.14	378.13 ± 6.34	377.33 ± 11.32	376.12 ± 4.31
Jaco.Plate.GoalWall.Push	293.6 ± 38.38	319.4 ± 24.13	320.49 ± 24.25	320.5 ± 31.85
Jaco.Plate.GoalWall.Shelf	358.04 ± 22.32	369.8 ± 15.11	367.73 ± 12.97	362.35 ± 3.32
Jaco.Plate.GoalWall.Trashcan	383.53 ± 7.45	387.55 ± 1.56	389.51 ± 2.03	388.57 ± 1.98
Jaco.Plate.ObjectDoor.PickPlace	390.4 ± 1.3	381.92 ± 15.09	376.2 ± 7.51	380.34 ± 9.73
Jaco.Plate.ObjectDoor.Push	372.01 ± 4.07	366.41 ± 16.51	359.43 ± 10.46	355.71 ± 3.99
Jaco.Plate.ObjectDoor.Shelf	366.15 ± 6.61	357.96 ± 8.35	368.82 ± 4.35	362.39 ± 7.11
Jaco.Plate.ObjectDoor.Trashcan	382.66 ± 0.58	384.3 ± 0.38	384.0 ± 1.92	383.57 ± 1.1
Jaco.Plate.ObjectWall.PickPlace	390.73 ± 1.55	378.98 ± 6.95	376.76 ± 8.54	373.98 ± 5.41
Jaco.Plate.ObjectWall.Push	378.3 ± 4.49	372.47 ± 10.13	364.42 ± 8.12	360.69 ± 3.82
Jaco.Plate.ObjectWall.Shelf	364.2 ± 3.52	364.64 ± 3.01	368.33 ± 1.95	360.73 ± 6.42
Jaco.Plate.ObjectWall.Trashcan	374.17 ± 3.76	375.68 ± 1.54	382.5 ± 2.76	373.86 ± 4.91
Jaco.Hollowbox.None.PickPlace	402.23 ± 2.04	386.75 ± 25.35	396.5 ± 1.04	398.48 ± 3.76
Jaco.Hollowbox.None.Push	392.65 ± 9.62	396.56 ± 4.13	397.09 ± 7.5	396.63 ± 0.38
Jaco.Hollowbox.None.Shelf	377.5 ± 2.78	382.06 ± 6.3	384.26 ± 5.2	381.68 ± 4.82
Jaco.Hollowbox.None.Trashcan	394.85 ± 1.28	394.82 ± 3.27	393.68 ± 3.67	392.87 ± 1.71
Jaco.Hollowbox.GoalWall.PickPlace	395.2 ± 1.44	385.82 ± 13.41	378.92 ± 9.41	379.34 ± 7.17
Jaco.Hollowbox.GoalWall.Push	349.5 ± 34.56	337.43 ± 15.64	348.44 ± 11.76	340.9 ± 2.77
Jaco.Hollowbox.GoalWall.Shelf	357.89 ± 19.58	349.29 ± 10.1	344.53 ± 6.27	333.97 ± 12.22
Jaco.Hollowbox.GoalWall.Trashcan	385.01 ± 1.04	385.4 ± 1.7	386.58 ± 0.37	384.52 ± 0.05
Jaco.Hollowbox.ObjectDoor.PickPlace	335.16 ± 76.71	387.66 ± 8.98	375.68 ± 4.01	344.62 ± 44.5
Jaco.Hollowbox.ObjectDoor.Push	356.64 ± 41.54	386.82 ± 11.07	383.4 ± 9.21	385.73 ± 7.74
Jaco.Hollowbox.ObjectDoor.Shelf	371.32 ± 0.65	362.29 ± 13.12	366.72 ± 4.12	360.22 ± 15.51
Jaco.Hollowbox.ObjectDoor.Trashcan	358.07 ± 46.79	385.01 ± 1.12	383.6 ± 2.35	385.17 ± 0.42
Jaco.Hollowbox.ObjectWall.PickPlace	393.5 ± 2.63	377.85 ± 3.53	378.61 ± 8.16	375.96 ± 5.55
Jaco.Hollowbox.ObjectWall.Push	391.74 ± 4.74	382.69 ± 12.26	387.67 ± 9.52	379.01 ± 6.44
Jaco.Hollowbox.ObjectWall.Shelf	371.33 ± 3.41	367.26 ± 11.73	365.73 ± 7.59	356.39 ± 16.14
Jaco.Hollowbox.ObjectWall.Trashcan	382.6 ± 1.63	385.72 ± 2.03	382.62 ± 1.19	382.01 ± 4.22

Table 15. Raw Scores for Composuite, Part 3.

Task	DT	Mamba	xLSTM [1:0]	xLSTM [7:1]
Kinova3_Box_None_PickPlace	432.49 ± 3.69	432.11 ± 7.68	432.28 ± 3.45	431.06 ± 2.67
Kinova3_Box_None_Push	398.81 ± 44.71	416.96 ± 17.33	428.52 ± 1.83	416.41 ± 18.69
Kinova3_Box_None_Shelf	411.22 ± 3.9	413.65 ± 0.42	415.58 ± 4.21	411.67 ± 3.98
Kinova3_Box_None_Trashcan	378.21 ± 81.97	426.67 ± 2.1	431.01 ± 0.89	427.82 ± 1.12
Kinova3_Box_GoalWall_PickPlace	347.29 ± 145.33	430.92 ± 1.73	431.3 ± 2.19	408.26 ± 40.64
Kinova3_Box_GoalWall_Push	325.78 ± 131.68	390.05 ± 6.59	382.78 ± 2.17	388.29 ± 6.07
Kinova3_Box_GoalWall_Shelf	357.79 ± 96.22	395.77 ± 28.11	418.95 ± 2.7	417.37 ± 1.02
Kinova3_Box_GoalWall_Trashcan	373.8 ± 80.27	424.09 ± 0.02	428.12 ± 3.66	427.05 ± 0.87
Kinova3_Box_ObjectDoor_PickPlace	425.72 ± 1.7	427.38 ± 0.43	424.25 ± 2.86	424.5 ± 3.45
Kinova3_Box_ObjectDoor_Push	395.44 ± 30.77	414.0 ± 5.47	406.02 ± 0.61	410.58 ± 8.15
Kinova3_Box_ObjectDoor_Shelf	381.62 ± 37.98	326.93 ± 2.6	408.55 ± 2.3	381.75 ± 45.62
Kinova3_Box_ObjectDoor_Trashcan	392.17 ± 40.87	415.87 ± 2.48	419.24 ± 0.61	416.46 ± 1.78
Kinova3_Box_ObjectWall_PickPlace	405.45 ± 21.25	387.27 ± 50.08	425.83 ± 2.68	423.06 ± 3.66
Kinova3_Box_ObjectWall_Push	419.98 ± 2.8	414.6 ± 1.04	412.82 ± 1.07	415.16 ± 7.28
Kinova3_Box_ObjectWall_Shelf	399.47 ± 4.56	399.51 ± 1.29	402.37 ± 2.66	402.42 ± 1.48
Kinova3_Box_ObjectWall_Trashcan	416.15 ± 4.57	412.41 ± 0.4	399.87 ± 31.99	394.97 ± 36.15
Kinova3_Dumbbell_None_PickPlace	380.36 ± 55.46	418.88 ± 5.8	419.3 ± 7.37	416.89 ± 2.86
Kinova3_Dumbbell_None_Push	394.84 ± 25.64	396.29 ± 13.63	367.03 ± 53.29	390.74 ± 22.17
Kinova3_Dumbbell_None_Shelf	290.98 ± 123.89	394.73 ± 4.82	386.09 ± 19.99	397.38 ± 2.93
Kinova3_Dumbbell_None_Trashcan	358.26 ± 43.32	377.36 ± 53.06	413.01 ± 6.02	414.39 ± 1.97
Kinova3_Dumbbell_GoalWall_PickPlace	408.52 ± 19.13	392.63 ± 23.38	404.51 ± 4.31	412.68 ± 11.05
Kinova3_Dumbbell_GoalWall_Push	294.63 ± 35.99	358.66 ± 10.09	321.72 ± 41.37	310.79 ± 67.84
Kinova3_Dumbbell_GoalWall_Shelf	384.01 ± 20.53	383.06 ± 15.17	395.02 ± 0.83	377.15 ± 28.52
Kinova3_Dumbbell_GoalWall_Trashcan	377.28 ± 51.33	370.59 ± 31.83	413.63 ± 2.06	378.76 ± 27.34
Kinova3_Dumbbell_ObjectDoor_PickPlace	415.58 ± 5.38	404.89 ± 11.83	405.77 ± 7.4	410.95 ± 8.75
Kinova3_Dumbbell_ObjectDoor_Push	359.17 ± 15.53	265.44 ± 62.94	367.39 ± 23.91	311.57 ± 45.56
Kinova3_Dumbbell_ObjectDoor_Shelf	360.34 ± 28.19	379.36 ± 6.7	385.26 ± 2.74	363.99 ± 37.65
Kinova3_Dumbbell_ObjectDoor_Trashcan	409.92 ± 1.78	407.09 ± 1.26	407.79 ± 0.71	407.57 ± 2.85
Kinova3_Dumbbell_ObjectWall_PickPlace	404.63 ± 16.95	409.29 ± 4.6	406.14 ± 2.11	411.69 ± 6.71
Kinova3_Dumbbell_ObjectWall_Push	311.79 ± 94.94	285.81 ± 62.32	342.04 ± 22.98	244.56 ± 16.32
Kinova3_Dumbbell_ObjectWall_Shelf	378.68 ± 3.03	378.63 ± 0.91	376.92 ± 0.76	361.79 ± 25.06
Kinova3_Dumbbell_ObjectWall_Trashcan	400.98 ± 4.19	398.65 ± 3.89	401.96 ± 1.45	395.81 ± 3.51
Kinova3_Plate_None_PickPlace	424.09 ± 4.78	427.36 ± 4.29	424.82 ± 1.31	425.02 ± 2.92
Kinova3_Plate_None_Push	412.25 ± 19.8	422.75 ± 2.79	417.63 ± 6.13	416.41 ± 4.33
Kinova3_Plate_None_Shelf	409.96 ± 0.2	409.11 ± 0.52	410.28 ± 0.65	409.52 ± 1.61
Kinova3_Plate_None_Trashcan	422.54 ± 2.13	422.07 ± 1.15	421.73 ± 1.36	422.97 ± 0.74
Kinova3_Plate_GoalWall_PickPlace	427.74 ± 0.81	421.23 ± 6.67	416.44 ± 1.6	416.35 ± 15.86
Kinova3_Plate_GoalWall_Push	401.46 ± 2.17	385.01 ± 15.39	377.6 ± 3.14	386.87 ± 12.31
Kinova3_Plate_GoalWall_Shelf	410.49 ± 0.77	409.46 ± 0.15	409.63 ± 0.65	407.67 ± 3.33
Kinova3_Plate_GoalWall_Trashcan	421.05 ± 0.88	421.19 ± 0.48	422.63 ± 0.81	423.21 ± 1.16
Kinova3_Plate_ObjectDoor_PickPlace	423.26 ± 0.3	407.55 ± 0.81	406.43 ± 2.07	414.11 ± 7.32
Kinova3_Plate_ObjectDoor_Push	258.58 ± 18.57	278.08 ± 34.02	300.72 ± 90.5	257.79 ± 48.13
Kinova3_Plate_ObjectDoor_Shelf	404.4 ± 0.95	403.82 ± 0.86	405.9 ± 0.31	401.09 ± 2.61
Kinova3_Plate_ObjectDoor_Trashcan	415.34 ± 1.08	415.81 ± 0.35	416.09 ± 0.31	414.34 ± 1.85
Kinova3_Plate_ObjectWall_PickPlace	420.16 ± 2.07	413.68 ± 5.5	408.0 ± 2.29	411.83 ± 4.11
Kinova3_Plate_ObjectWall_Push	400.11 ± 16.39	403.95 ± 3.67	406.48 ± 5.73	403.65 ± 6.23
Kinova3_Plate_ObjectWall_Shelf	391.09 ± 3.65	391.99 ± 6.62	386.25 ± 16.53	391.7 ± 5.14
Kinova3_Plate_ObjectWall_Trashcan	413.36 ± 1.11	413.44 ± 3.93	413.82 ± 2.45	415.14 ± 1.46
Kinova3_Hollowbox_None_PickPlace	424.86 ± 6.23	433.78 ± 0.13	430.43 ± 1.11	430.84 ± 1.55
Kinova3_Hollowbox_None_Push	361.99 ± 40.33	369.17 ± 8.0	396.28 ± 28.04	380.94 ± 28.74
Kinova3_Hollowbox_None_Shelf	417.73 ± 13.43	417.46 ± 0.36	423.26 ± 3.53	424.02 ± 2.62
Kinova3_Hollowbox_None_Trashcan	424.65 ± 1.15	409.34 ± 12.4	425.0 ± 2.72	416.0 ± 15.33
Kinova3_Hollowbox_GoalWall_PickPlace	386.68 ± 49.29	425.24 ± 0.83	421.85 ± 8.69	420.32 ± 9.71
Kinova3_Hollowbox_GoalWall_Push	403.57 ± 0.96	383.09 ± 8.37	384.13 ± 10.01	381.43 ± 8.58
Kinova3_Hollowbox_GoalWall_Shelf	385.7 ± 36.06	395.01 ± 4.51	423.93 ± 5.1	417.05 ± 13.43
Kinova3_Hollowbox_GoalWall_Trashcan	406.37 ± 27.44	404.11 ± 3.64	405.09 ± 22.54	389.36 ± 32.05
Kinova3_Hollowbox_ObjectDoor_PickPlace	344.01 ± 63.38	364.3 ± 13.82	387.53 ± 20.66	324.36 ± 55.48
Kinova3_Hollowbox_ObjectDoor_Push	390.98 ± 46.38	416.05 ± 8.96	405.41 ± 5.34	406.76 ± 16.92
Kinova3_Hollowbox_ObjectDoor_Shelf	359.0 ± 25.63	381.87 ± 12.39	390.42 ± 6.21	357.94 ± 48.51
Kinova3_Hollowbox_ObjectDoor_Trashcan	405.87 ± 4.17	411.24 ± 1.26	414.92 ± 3.6	408.73 ± 5.66
Kinova3_Hollowbox_ObjectWall_PickPlace	424.57 ± 0.92	408.98 ± 6.4	417.83 ± 5.67	419.63 ± 9.2
Kinova3_Hollowbox_ObjectWall_Push	249.37 ± 176.18	319.13 ± 111.09	324.39 ± 76.09	335.61 ± 74.98
Kinova3_Hollowbox_ObjectWall_Shelf	394.7 ± 9.3	328.52 ± 61.08	357.89 ± 37.75	362.16 ± 40.05
Kinova3_Hollowbox_ObjectWall_Trashcan	354.65 ± 48.89	353.43 ± 78.59	407.99 ± 1.96	408.29 ± 4.94

Table 16. Raw Scores for Composuite, Part 4.

Task	DT	Mamba	xLSTM [1:0]	xLSTM [7:1]
Panda_Box_None.PickPlace	409.21 ± 5.27	408.66 ± 7.81	409.83 ± 1.87	405.46 ± 3.84
Panda_Box_None.Push	402.52 ± 2.55	373.74 ± 49.95	400.35 ± 2.32	399.37 ± 9.95
Panda_Box_None.Shelf	383.69 ± 4.34	381.42 ± 3.66	383.55 ± 5.74	386.01 ± 1.29
Panda_Box_None.Trashcan	400.37 ± 5.64	395.77 ± 2.77	407.95 ± 1.92	406.17 ± 3.36
Panda_Box_GoalWall.PickPlace	401.53 ± 6.39	389.57 ± 18.4	397.12 ± 4.39	401.64 ± 9.81
Panda_Box_GoalWall.Push	272.61 ± 79.58	257.61 ± 57.4	263.72 ± 45.71	281.71 ± 31.21
Panda_Box_GoalWall.Shelf	384.43 ± 1.66	389.06 ± 3.69	388.59 ± 3.9	383.94 ± 2.0
Panda_Box_GoalWall.Trashcan	400.68 ± 4.51	400.18 ± 6.03	403.24 ± 5.65	392.28 ± 16.82
Panda_Box_ObjectDoor.PickPlace	359.01 ± 12.2	365.3 ± 5.97	359.63 ± 0.79	359.27 ± 10.88
Panda_Box_ObjectDoor.Push	363.07 ± 3.13	352.85 ± 13.71	340.37 ± 6.06	340.5 ± 4.97
Panda_Box_ObjectDoor.Shelf	346.29 ± 2.53	345.8 ± 4.91	349.82 ± 6.46	341.44 ± 11.05
Panda_Box_ObjectDoor.Trashcan	361.19 ± 1.65	356.77 ± 3.24	356.66 ± 5.73	337.69 ± 32.63
Panda_Dumbbell_None.PickPlace	342.62 ± 39.18	310.15 ± 24.64	318.76 ± 2.7	342.02 ± 31.28
Panda_Dumbbell_None.Push	299.34 ± 78.28	341.64 ± 42.57	359.06 ± 42.88	263.35 ± 154.81
Panda_Dumbbell_None.Shelf	264.01 ± 101.29	362.15 ± 0.87	319.71 ± 33.9	297.54 ± 67.67
Panda_Dumbbell_None.Trashcan	174.45 ± 64.43	329.06 ± 43.08	373.77 ± 16.73	327.93 ± 68.84
Panda_Dumbbell_GoalWall.PickPlace	310.61 ± 42.65	268.34 ± 147.91	329.02 ± 62.28	360.39 ± 5.25
Panda_Dumbbell_GoalWall.Push	249.21 ± 43.29	282.01 ± 4.89	270.81 ± 11.98	285.28 ± 5.25
Panda_Dumbbell_GoalWall.Shelf	319.5 ± 68.89	347.34 ± 20.01	364.15 ± 2.6	318.6 ± 33.85
Panda_Dumbbell_GoalWall.Trashcan	377.5 ± 5.27	360.98 ± 9.73	379.05 ± 7.52	337.19 ± 40.73
Panda_Dumbbell_ObjectDoor.PickPlace	344.54 ± 5.77	346.57 ± 0.33	340.15 ± 8.5	338.46 ± 10.42
Panda_Dumbbell_ObjectDoor.Push	289.31 ± 11.14	308.25 ± 9.24	309.4 ± 5.02	304.1 ± 8.06
Panda_Dumbbell_ObjectDoor.Shelf	323.26 ± 3.52	279.85 ± 18.84	313.19 ± 17.79	323.49 ± 0.27
Panda_Dumbbell_ObjectDoor.Trashcan	334.05 ± 5.55	337.49 ± 0.68	341.0 ± 3.14	333.06 ± 7.77
Panda_Plate_None.PickPlace	384.37 ± 30.37	404.77 ± 5.27	397.34 ± 1.3	398.41 ± 2.51
Panda_Plate_None.Push	397.95 ± 1.05	398.1 ± 4.91	397.42 ± 3.32	397.64 ± 2.7
Panda_Plate_None.Shelf	352.29 ± 37.8	372.12 ± 13.92	370.46 ± 3.11	367.5 ± 6.03
Panda_Plate_None.Trashcan	392.99 ± 1.41	393.63 ± 2.91	394.05 ± 3.74	393.71 ± 1.27
Panda_Plate_GoalWall.PickPlace	398.36 ± 3.95	398.24 ± 4.51	393.0 ± 1.9	399.02 ± 4.53
Panda_Plate_GoalWall.Push	387.68 ± 0.49	377.79 ± 11.92	355.01 ± 34.01	350.1 ± 22.72
Panda_Plate_GoalWall.Shelf	380.05 ± 0.52	367.67 ± 22.6	339.46 ± 40.63	359.76 ± 5.67
Panda_Plate_GoalWall.Trashcan	391.41 ± 3.83	389.44 ± 3.8	395.4 ± 2.49	393.96 ± 2.68
Panda_Plate_ObjectDoor.PickPlace	350.33 ± 18.2	348.67 ± 8.14	329.35 ± 4.62	336.64 ± 16.61
Panda_Plate_ObjectDoor.Push	346.4 ± 9.33	337.36 ± 17.06	326.32 ± 7.92	323.51 ± 2.24
Panda_Plate_ObjectDoor.Shelf	290.68 ± 11.21	321.54 ± 17.89	326.04 ± 18.76	305.25 ± 20.96
Panda_Plate_ObjectDoor.Trashcan	348.09 ± 3.63	349.43 ± 4.05	351.8 ± 0.25	349.29 ± 1.91
Panda_Hollowbox_None.PickPlace	410.32 ± 6.76	412.25 ± 3.0	408.01 ± 1.93	405.29 ± 5.3
Panda_Hollowbox_None.Push	404.95 ± 1.07	406.74 ± 4.03	401.61 ± 6.16	402.46 ± 4.04
Panda_Hollowbox_None.Shelf	387.59 ± 5.19	380.86 ± 10.45	369.22 ± 14.85	369.57 ± 4.84
Panda_Hollowbox_None.Trashcan	399.09 ± 2.01	400.52 ± 5.27	401.03 ± 5.27	392.82 ± 7.37
Panda_Hollowbox_GoalWall.PickPlace	406.02 ± 10.18	403.47 ± 0.97	405.96 ± 0.39	407.16 ± 3.77
Panda_Hollowbox_GoalWall.Push	259.87 ± 75.12	293.02 ± 117.06	341.55 ± 23.29	281.79 ± 42.98
Panda_Hollowbox_GoalWall.Shelf	387.38 ± 3.45	369.01 ± 6.14	365.26 ± 6.74	316.46 ± 81.46
Panda_Hollowbox_GoalWall.Trashcan	377.54 ± 44.77	395.3 ± 4.85	396.82 ± 4.17	401.54 ± 5.21
Panda_Hollowbox_ObjectDoor.PickPlace	334.94 ± 35.48	341.18 ± 32.31	342.71 ± 7.54	353.64 ± 2.45
Panda_Hollowbox_ObjectDoor.Push	192.69 ± 6.49	294.01 ± 57.68	257.48 ± 13.16	230.54 ± 8.56
Panda_Hollowbox_ObjectDoor.Shelf	343.92 ± 10.22	202.17 ± 4.87	328.01 ± 42.52	285.35 ± 64.92
Panda_Hollowbox_ObjectDoor.Trashcan	338.02 ± 36.48	363.04 ± 2.59	360.88 ± 2.45	363.04 ± 1.29